Improving data-oriented light use efficiency models of gross primary productivity with remotely sensed spectral indices

Dissertation

zur Erlangung des akademischen Grades doctor rerum naturalium (Dr. rer. nat.)

vorgelegt dem

Rat der Chemisch-Geowissenschaftlichen Fakultät der Friedrich-Schiller-Universitaet Jena

von

Anna Goerner

Dipl.-Geooekol.
geboren am 11.03.1983 in Pirna

2011

Gutachter:

1: Prof. Dr. Christiane Schmullius, Friedrich Schiller Universität Jena

2: Dr. Markus Reichstein, Max-Planck-Institut für Biogeochemie, Jena

Tag der öffentlichen Verteidigung: 01. Juli 2011

Acknowledgments

I am grateful for discussions with many colleagues at the MPI for Biogeochemistry about and beyond the subject of this thesis. I especially wish to thank Markus Reichstein for his trustful supervision. He was always efficient in sorting out my scientific confusions when help was needed and otherwise enabled and encouraged me to shape this thesis work according to my own interests. Likewise, I am grateful to Christiane Schmullius for her guidance regarding many aspects of this thesis and for integrating me in her Earth Observation group as much as possible. I also appreciate the discussions on surface anisotropy with François-Marie Bréon.

Parts of this thesis have—in modified form—been published in peer reviewed journals (Goerner et al., 2009, 2011). I wish to thank my coauthors Markus Reichstein, Serge Rambal, Enrico Tomelleri, Niall Hanan, Dario Papale, Danilo Dragoni, Christiane Schmullius as well as the anonymous referees, John Gamon and the editors Georg Wohlfahrt and Marvin Bauer for their constructive comments on these two manuscripts.

I gratefully acknowledge the financial and logistic support by the Max Planck Society.

Contents

CHAPTER 1

Background and motivation

Contents

Understanding the continuous exchange of elements among the land, the oceans, and the atmosphere is one of the big research questions in Earth system science. Comprehending how these so called biogeochemical cycles function and interact—including their responses to changes in climate and other perturbations—is crucial for a sustainable future of mankind on planet Earth. To arrive at this understanding biotic, biochemical, geochemical and physical aspects have to be taken into account.

Studies of the carbon cycle are driven by this basic human desire to unravel how our environment functions and to understand the role of ecosystems in and human influence on the Earth System. Besides pure curiosity, research in this field is also stimulated by the realisation that anthropogenic emissions of carbon dioxide can lead to significant and lasting changes in the climate system (Solomon et al., 2007).

In the past decades, Earth system science has significantly advanced due to increased availability of observations on various spatial and temporal scales. For example, the assessment of spatio-temporal ecosystem-atmosphere interaction has greatly benefited from improved availability of various kinds of Earth observation data from space. The establishment and expansion of measurement networks for atmospheric concentrations and ecosystem-atmosphere fluxes of greenhouse gases has also been crucial for the advancement of scientific understanding.

1.1 Carbon assimilation in terrestrial ecosystems

The overarching topic of this thesis is the quantification of carbon uptake by terrestrial ecosystems. Before going into the details, let me place carbon uptake in the conceptual framework of the terrestrial carbon cycle (c.f. Fig. 1.1).

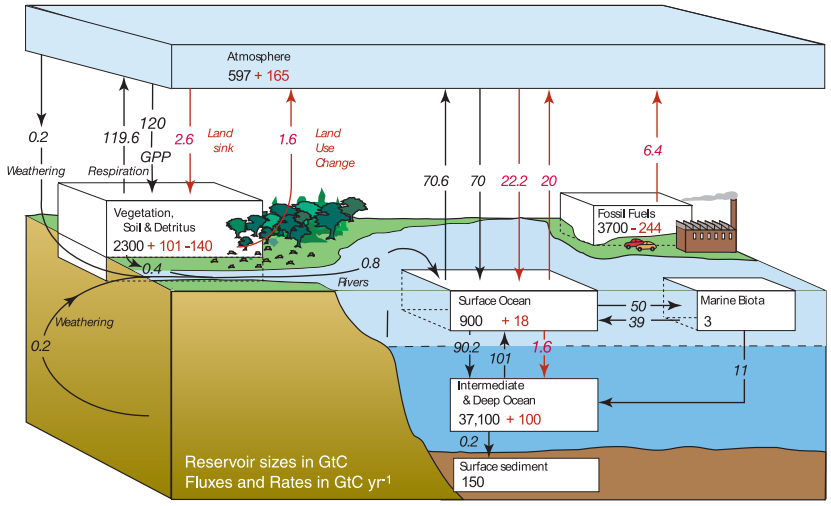

Fig. 1.1: *The global carbon cycle for the 1990s, showing the main annual fluxes in GtC yr—1: pre-industrial 'natural' fluxes in black and 'anthropogenic' fluxes in red. Denman et al. (Reprinted from 2007, (Fig. 7.3)).*

As outlined by Canadell et al. (2000), the metabolism of the terrestrial biosphere is highly complex and subject to variability at all temporal scales (seasonal to decadal and beyond). The dominant pathway by which carbon enters an ecosystem—and hence the principal control of carbon input—is photosynthesis, a process that converts carbon dioxide into organic compounds using the energy of light. The total carbon uptake by plants per unit ground and and time is termed GPP.

About half of it is respired by the plants themselves (Schulze et al., 2005), a component flux called autotrophic respiration (R_a). The imbalance of assimilation and respiration by living parts of primary producers is called net primary productivity (NPP) (Chapin III et al., 2009). If NPP is positive, carbon is allocated to an increase in structural biomass or to the plant's pool of reserves.

In natural ecosystems, eventually all parts of the vegetation are decomposed and mineralised, so carbon dioxide (CO_2) returns to the atmosphere via heterotrophic respiration (R_h). The difference between GPP and total ecosystem respiration (R_{eco}) is termed net ecosystem productivity (NEP) or—when viewed as input into the atmosphere—as net ecosystem exchange (NEE = -NEP). The relationships between the components of ecosystem fluxes can be summarised like this (Luyssaert et al., 2009):

$$
\begin{aligned}
R_{eco} &= R_a + R_h && (1.1)\\
NPP &= GPP - R_a && (1.2)\\
NEP &= NPP - R_h && (1.3)\\
&= GPP - R_{eco} && (1.4)
\end{aligned}
$$

For an ultimate quantification of an ecosystem's carbon budget—and hence the ecosystem's ability to partially offset anthropogenic CO_2 emissions—disturbances such as fire, harvest, soil degradation need to be considered, as well as lateral fluxes of carbon, besides fluxes of volatile organic compounds (VOCs) and methane (Chapin et al., 2006).

The terrestrial carbon cycle is tightly coupled to the cycling of other elements and substances (Lohse et al., 2009), first of all to the hydrologic cycle (Nobel, 2005). A fundamental trade-off for plants is the evaporative loss of water during CO_2 acquisition for photosynthesis. Many approaches to model GPP thus take into account the limits set by plant water availability.

This study focusses on GPP because it is the largest global CO_2-flux and driver of several ecosystem functions (Beer et al., 2010).

1.2 What determines gross primary productivity?

A major determinant of canopy photosynthesis—and thus GPP—is the amount of light intercepted by the leaves, i.e. the available energy (Schulze et al., 2005). Apart from geographic location and season, light interception is influenced by the angular relationship between leaves and Earth—sun geometry as well as by the way plants modify their own light climate (Baldocchi and Amthor, 2001).

Further influences on canopy photosynthesis include temperature, wind speed, humidity, availability of soil moisture and nutrients, especially nitrogen, as an essential component of photosynthetic enzymes (Baldocchi and Amthor, 2001). Along with the environmental constraints listed above, the specific photosynthetic pathway of the plant and the life history of the leaves are also important (Schulze et al., 2005). Furthermore, stress caused by salt, heavy metals, oxygen deficiency or

herbivory result in reduced photosynthetic capacity. Many of the above factors influence photosynthetic capacity twofold: by affecting the canopy's ability to absorb photochemically active radiation (PAR), and by directly or indirectly changing the conductivity of the stomates—and thus regulating the influx of CO_2 and the efflux of water vapour, i.e. transpiration.

1.2.1 Mechanistic basis of carbon input into ecosystems

Photosynthesis consists of two types of reactions: light harvesting reactions and carbon fixing reactions. In most plants they occur at the same time within chloroplasts, i.e. organelles within mesophylic cells of green leaves (Chapin et al., 2002).

Upon entering the leaf, visible light can be absorbed by two types of photosynthetic pigments: chlorophylls (a and b) and several carotenoid pigments (e.g. xanthophylls, carotenes). Carotenoids pass on the light energy they absorb to the chlorophylls, until it reaches a reaction center (Robinson, 2001). This absorbed radiation is transformed into chemical energy in the compounds ATP and NADPH. The carbon fixing reactions of the Calvin cycle then shift the energy contained in the temporary products ATP and NADPH into relatively stable sugars that can be stored, transported and metabolized. The first and rate-limiting step of these reactions is the attachment CO_2 to preexisting carbon skeletons by the enzyme ribulose-bisphosphate carboxylase-oxygenase (Rubisco), a protein that accounts for 25% of leaf nitrogen. The availability of CO_2 and ATP and NADPH also constrains the carbon fixing reactions.

When the oxygen concentration is high relative to CO_2 concentration in the chloroplasts of C3-plants Rubisco adds oxygen to Ribulose-1,5-bisphosphate (RuBP), a 5-carbon compound in the Calvin cycle, instead of CO_2. This initiates the conversion of RuBP to CO_2, a process called photorespiration that results in a net carbon loss of 20-40 %. The reason for this 'waste' is not clear, but it could be a mechanism of photoprotection (Chapin et al., 2002).

Due to a sudden increase in irradiance or a decrease in photosynthesis at constant irradiance (for example during drought, chilling or other stress factors) plants absorb energy beyond their current photosynthetic capacity. This excess energy can be transferred to the omnipresent oxygen, thereby creating reactive oxygen species that can damage cell components including photosynthetic pigments (Demmig-Adams and Adams, 2006).

Photorespiration provides a supply of reactants (ADP and NADP) to the light reaction under circumstances in which inadequate supply of CO_2 limits the rate at which these reactants can be regenerated by carbon fixation reactions.

Plants have other lines of defense against excess radiation (Robinson, 2001). In continuous high-light environments, plants protect themselves by reducing the amount of energy that gets absorbed. This can be achieved by reducing the total leaf surface area, by vertical orientation of the leaves and by increasing reflectance

for example by having waxes or hair on the surface. An internal protective mechanism is the dissipation of excess energy as heat. This process involves the xanthophyll cycle pigments violaxanthin, antheraxanthin and zeaxanthin, which are all carotenoids. Under excess light conditions most of the xanthophyll pigments are de-epoxized into zeaxanthin (Demmig et al., 1987; Demmig-Adams, 1990). This reaction is favored by the low pH values and the presence of ascorbate, which can be expected under excess radiation (Robinson, 2001). It has been observed that increased levels of zeaxanthin go along with increased heat dissipation, although the exact mechanism is still unknown. The de-epoxidation of violaxanthin and antheraxanthin is reversed under low-light conditions.

1.2.2 Focus: water limitation

1.2.2.1 The importance of water stress

Among the biotic and abiotic constraints of primary productivity listed above, water availability is especially important on a global scale. Zhao and Running (2010) found large-scale periodic regional droughts and a general drying trend over the southern hemisphere to be the cause of a reduction of global terrestrial NPP over the past 10 years.

From the simple diagnostic model Biome-BGC Nemani et al. (2003) estimated that water limitation is the most important constraint for vegetation growth on 40% of Earth's vegetated surface, while temperature and radiation limit growth over 33% and 27% of the Earth's vegetated surface. Beer et al. (2010) corroborate these results. Their study, too, indicates that water availability is the dominating constraint on primary production in over 40% of the vegetated land and in up to 70% of savannas, shrublands, grasslands, and agricultural areas. The findings of Beer et al. (2010) imply that the productivity of these ecosystems is highly susceptible to projected changes of precipitation over the 21^{st} century, whereas tropical and boreal forests seem more robust.

It is likely that large scale droughts have reduced regional and global primary productivity already (Zhao and Running, 2010). Apart from affecting NPP directly, heat and drought can also cause ecosystem disturbances that result in a release of carbon to the atmosphere:

- Since climate regulates the amount of dry fuel available for ignition, it has a significant influence on the spatial and temporal distribution of fire activity. A study by van der Werf et al. (2008) found that fire activity in arid ecosystems is constrained by the availability of fuel, which in turn is driven by the amount of precipitation in the preceding wet season. In wet ecosystems fire occurrence seems to depend on the extend of the dry season that determines the dryness of the fuel. Increased frequencies of large fires will affect forest composition and diminish tree densities and thus influence carbon pools (Westerling et al., 2006).

- Drought can also lead to higher tree mortality, caused either by carbon starvation due to stomatal closure, by cavitation, by limitations of the cellular metabolism, by a higher susceptibility to pathogens or by a combination of the above Allen et al. (2010).

1.2.2.2 Global change—increased risk of drought

Global patterns of air temperature and precipitation are changing. The increase in global temperatures resulting from increasing atmospheric CO_2 concentrations leads to more water vapor in the atmosphere, so changes in precipitation patterns can be expected (Solomon et al., 2009). The poleward expansion of the Hadley cells in a warmer climate will lead to a further drying of the already dry subtropics. According to the 4th Assessment report of the IPCC (Christensen et al., 2007), a substantial part of the world will be affected by a decrease in precipitation. An analysis with 22 Atmosphere–Ocean General Circulation Models (AOGCM)s by (Solomon et al., 2009) identified the following areas that are expected to undergo reductions in precipitation in the dry season (see also Fig. 1.2): Mexico and South-Western United States, North Africa and Southern Europe, South Africa, Eastern South America, West Australia, and Southeast Asia The Mediterranean region, Central America, and some areas in southern South America, South Africa and South-West Australia are also likely to experience precipitation reductions in the wet season and in the annual mean Solomon et al. (2009).

1.3 Measuring productivity

1.3.1 Direct measurement

There are significant uncertainties related to measuring primary productivity directly, especially below ground (Gower et al., 1999). The largest part of NPP is allocated to biomass of different plant tissues such as stem and branches, leaves, coarse and fine roots (Luyssaert et al., 2009). To quantify NPP, biomass changes of all plant tissues need to be known as well as the amount of biomass lost to herbivory (Gower et al., 1999). To complete the balance, organic material both lost and produced between samplings such as root exudates and volatile organic compounds also need to be taken into account (Clark et al., 2001). According to Gower et al. (1999), biomass increments can be determined in two ways. The first option is harvesting. This approach is most suitable for ecosystems where the growth is bigger than the local spatial variability of biomass, e.g. crops, herbaceous ecosystems and tundra. The alternative is to use allometric relationships on permanent plots. This method involves measuring radial increments of the stems in permanent plots and relating these increments to the growth of all tissues by statistical relationships. Measuring below ground productivity is costly, laborious and the accuracy is disputed. One problem is due to the difficulties in determining the amount

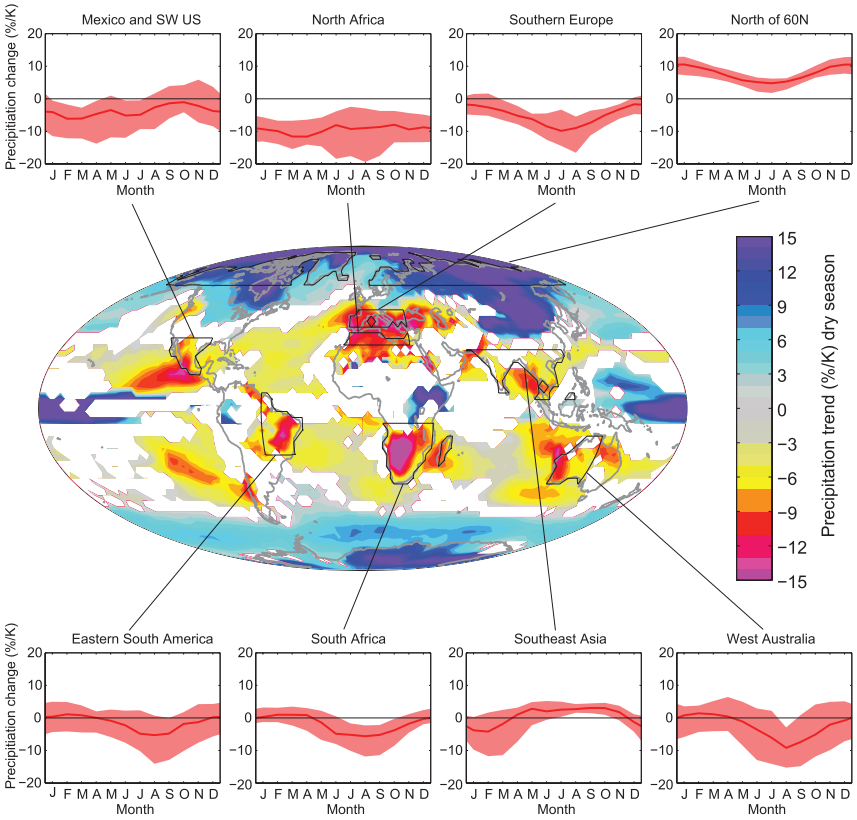

Fig. 1.2: *Expected decadally averaged changes in the global distribution of precipitation per degree of warming (percentage of change in precipitation per degree of warming, relative to 1900—1950 as the baseline period) in the dry season at each grid point, based upon a suite of 22 AOGCMs for a midrange future scenario (A1B, see Meehl et al. (2007)). White is used where fewer than 16 of 22 models agree on the sign of the change. Data are monthly averaged over several broad regions in Inset plots. Red lines show the best estimate (median) of the changes in these regions, while the red shading indicates the ±1-Σ likely range (i.e., 2 of 3 chances) across the models. (Figure and caption are a reproduction of Fig. 3 in Solomon et al., 2009).*

and turn-over time of fine roots and mycorrhiza (Trumbore and Gaudinski, 2003). This fraction constitutes a relatively small part of below ground biomass but, due to a high turn-over, might contribute much to below-ground primary productivity. For an overview of measurement methods, their advantages and drawbacks see (Gower et al., 1999; Majdi et al., 2005; Gaudinski et al., 2010).

1.3.2 Measurement with eddy covariance

Measuring NEP with eddy covariance technique has several advantages over other methods (Baldocchi, 2003). The method enables us to measure gas and energy exchange at the right scale, i.e. at ecosystem level, since the longitudinal extension of the measurement footprint ranges from hundreds of meters to kilometers (Schmid, 1994). The eddy covariance technique enables direct measurements of

the net gas exchange over the canopy-atmosphere interface without disturbing the ecosystem over a wide spectrum of time scales (from hours to years).

Fluxes of CO_2, water vapour and other trace gasses as well as heat can be quantified by determining the covariance between fluctuations in vertical velocity (ω) and concentrations (or mixing ratios) of the gases of interest (Aubinet et al., 2000; Baldocchi, 2008). Gas concentrations are measured with a fast response infrared gas analyser at high frequency (10-20 Hz), synchronous to 3-dimensional measurements of wind speed taken by a three-axis sonic anemometer (Aubinet et al., 2000, 2003b; Papale et al., 2006)

The physical basis for the eddy covariance method is a three-dimensional mass conservation equation. Baldocchi et al. (1988) state that

> " the time rate of change of the mean mixing ratio (concentration) of a chemical constituent at a fixed point in space (I) is balanced by the mean horizontal and vertical advection (II), by the mean horizontal and vertical divergence or convergence of the turbulent flux (III), by molecular diffusion (D), and by any source or sink (S) "

$$\underset{(I)}{\frac{\delta\overline{\chi}}{\delta t}} = \underbrace{-\overline{u}\frac{\delta\overline{\chi}}{\delta x} - \overline{\nu}\frac{\delta\bar{\chi}}{\delta y} - \bar{\omega}\frac{\delta\overline{\chi}}{\delta z}}_{(\cdots\cdots\cdots II\cdots\cdots\cdots)} \underbrace{- \frac{\delta\overline{u'x'}}{x} - \frac{\delta\overline{\nu'y'}}{y} - \frac{\delta\overline{\omega'z'}}{z}}_{(\cdots\cdots\cdots III\cdots\cdots\cdots)} + D + S \quad (1.5)$$

$\chi \ldots$	*mixing ratio of a chemical constituent*
$u, \nu, \omega \ldots$	*streamwise, lateral, and vertical wind velocity components, respectively, that operate in the respective longitudinal (x), lateral (y), and vertical (z) directions. The mean covariances between wind velocity components and χ represent turbulent fluxes.*
$D \ldots$	*molecular diffusion*
$S \ldots$	*source/sink term*
	Overbars denote time averaging and primes (') denote fluctuations from the mean

Under ideal conditions (horizontally uniform and level surface, enough turbulence, no significant changes in concentrations during measurement interval) equation 1.5 can be simplified, and the mean vertical turbulent flux under steady state conditions is

$$F = -\overline{\rho_a}\overline{\omega'\chi'} \quad (1.6)$$

where ρ_a is the density of dry air.

The foundations for this theoretical framework have already been laid in the late 19^{th} century (Reynolds, 1985). However, it was only in the 1990s that commercial anemometers, gas analysers and data storage systems became available to measure continuously, with sufficient accuracy. The first yearlong study of CO_2

exchange was done by Wofsy et al. (1993). After this, regional networks (e.g. CarboEuroflux, AmeriFlux) were established quickly (Aubinet et al., 2000; Valentini et al., 2000; Running, 1999) and collaborate since 1997 in the FLUXNET project. At present, more than 500 sites with longterm measurements of CO_2, water vapour fluxes, and many ancillary meteorological, soil and plant variables are organised in the global network FLUXNET (*FLUXNET project*, 2010).

The site data combined by FLUXNET are processed according to standard methodologies including averaging to half-hourly values, filtering for insufficient friction velocity (u*), partitioning of the net ecosystem exchange flux into productivity and respiration components as well as filling of gaps caused by interrupted measurements or quality filtering. Section 2.1 explains these processing steps in more detail.

1.4 Ecosystem light use efficiency — How is it constrained?

The influence of light levels on photosynthesis was not explicitly considered until the 1950s, in forest ecosystems (Monsi and Saeki, 2005) as well as for crops (De Wit, 1959). Since the studies by Monteith (1972); Monteith and Moss (1977) the term LUE, also called radiation use efficiency (RUE) or conversion efficiency, became a convenient way to summarize how efficiently ecosystems can use light energy to produce photosynthates at any given time.

LUE is a quotient where the numerator is a measure of production and the denominator quantifies irradiance (Schwalm et al., 2006). However, in the scientific literature the same name is used to describe slightly different processes on different scales. A study by Grace et al. (2007) notes that some articles express LUE as mols of CO_2 per mols photons of absorbed light, while others express it in units of energy (in Joules) captured in chemical bonds of photosynthates per Joule of solar energy absorbed. Some authors deviate from the physical meaning of 'efficiency' as a unit-less ratio by relating accumulated biomass (which was comparatively easy to measure in the past) to energy. There are also variations in the meaning of the denominator: sometimes authors use energy absorbed by the vegetation, others use incident energy. While some studies refer only to PAR, others refer to the full solar spectrum.

Carbon and biomass have both been used to describe the carbon dynamics of ecosystems because the carbon and energy content is relatively constant for organic matter (Chapin et al., 2002).

1.4.1 How is LUE determined (on a local scale)?

Since LUE is a derived quantity, it cannot be measured directly. It is either quantified as the ratio of a measure of production and a measure of irradiance (see

above) or by proxy (e.g. certain radiation measurements).

Historically, in crop science radiation use efficiency is a derived quantity based on accumulated crop mass and absorbed radiation (Monteith, 1972; Monteith and Moss, 1977; Sinclair and Muchow, 1999).

1.4.2 Constraints of ecosystem light use efficiency

There is considerable scatter in LUE within each vegetation type (Ruimy and Saugier, 1994; Gower et al., 1999).

A comprehensive review by Garbulsky et al. (2010) lists two main influences on spatial and longterm variability in LUE:

- Forest age and management practices on annual scale (Landsberg and Waring, 1997)
- Nutritional status such as nitrogen availability (Mäkelä et al., 2008; Ollinger et al., 2008) on local scales, because of the scatter in the data on the relationship between maximum photosynthetic rate and and foliar nitrogen concentrations (Woodward et al., 1995)

Some studies (Turner, 2003; Still et al., 2004) report little evidence for relationships between climatic or biogeochemical controls and spatial variability of LUE. However, in their meta-analysis Garbulsky et al. (2010) found that the spatial and long-term variability of LUE is controlled firstly by precipitation, and secondly by the vegetation type. Annual and maximum LUE has been primarily related to mean annual precipitation.

The meta-analyis by Garbulsky et al. (2010) concluded that intra-annual variation of LUE is mainly linked to the energy balance and water availability along the climatic gradient. They also showed that intra-annual variation of LUE is only weakly influenced by VPD and tem-perature, contrary to what is frequently assumed. For annual crops a positive relationship between LUE and temperature (Andrade et al., 1993) and a negative relationship to VPD (Kiniry et al., 1998) has been found. The LUE of Great Plain grasslands seems to depend on potential evapotranspiration and precipitation (Polley et al., 2010).LUE of forests has been shown to be positively related to temperature (Landsberg and Waring, 1997). For other vegetation types (e.g. shrublands) only few studies exist (Sims et al., 2005; Turner et al., 2005) and the biophysical controls are not yet well understood.

Apart from LUE, (annual) GPP is also controlled by the leaf area, which is closely related to faPAR.

1.5 Estimating primary productivity on regional and global scales

Terrestrial GPP deserves special attention because it is the largest global carbon flux (Denman et al., 2007) and drives other ecosystem functions such as respiration and vegetation growth (Ciais et al., 2005; Reichstein et al., 2007).

On the leaf and canopy scale, photosynthesis is quite well understood and can be easily measured (e.g. Baldocchi and Amthor, 2001), see also section 1.3. On the regional to global scale, however, there is no way to measure ecosystem gas exchange directly. To estimate primary productivity on this scale, one of the following approaches must be taken (Beer et al., 2010):

(1) Use of local information to build and calibrate process-based, prognostic models, which can then be applied at global scale,

(2) Data-oriented, so called diagnostic modeling establishes general relationships between GPP data and sets of descriptive variables at site level. These relationships are then applied to global spatial fields of the explanatory variables ("upscaling"),

(3) Combination of point measurements of atmospheric CO_2 concentrations (flask samples, or continuous observations on tall towers, or column averaged CO_2 concentrations derived from satellite data (Heimann, 2009) or ground based solar absorption measurements (Macatangay et al., 2008)) with atmospheric transport models (Rödenbeck et al., 2003; Lauvaux et al., 2009) ("top down" approach),

(4) Estimation of NPP from biomass inventories (Poorter et al., 1990; Roy and Saugier, 2001).

These techniques are complementary to each other (Canadell et al., 2000, 2004). Approach (4) is the most uncertain way to estimate primary productivity (DeLucia et al., 2007), and mainly mentioned for historic reasons and sake of completeness. Process models are useful tools to check our mechanistic understanding of ecosystems. Their main purpose is the extrapolation into the future. Data oriented models are a useful tools to constrain and test these process models (Beer et al., 2010), as they rely on very few theoretical assumptions. Diagnostic models do not allow for extrapolations into the future. Their strength is the assessment of the status quo and of historic trajectories, depending on the availability of sufficient input and training data.

1.5.1 Prognostic modelling of gross primary productivity

Prognostic models of primary productivity or other components of the carbon balance are not a subject of this thesis.

1.5.2 Diagnostic modelling of gross primary productivity—Overview

Diagnostic models of GPP relate site level measurements of GPP to a set of explanatory variables, e.g. meteorology, vegetation type, remotely sensed vegetation indices (Beer et al., 2010) at daily, monthly or annual time scales. Examples are given in Table 1.1.

Tab. 1.1: *Categories of diagnostic GPP (after Beer et al., 2010)*

Type of model	short description	References
LUE approach	GPP is the product of LUE and aPAR; LUE is a function of a maximum LUE and certain environmental constraints	Monteith (1972); Running et al. (2000)
water use efficiency (WUE) approach	GPP of whole river catchments, combines recently derived global WUE fields with long-term averaged evapotranspiration at the watershed scale	Beer et al. (2007, 2009)
Koeppen-Geiger cross biome (KGB) approach	Look-up table of mean GPP per climate class and biome type	Beer et al. (2010)
MIAMI model	relates primary productivity to mean annual temperature and precipitation	Lieth and Whittaker (1975); Beer et al. (2010)
machine learning techniques		
artificial neural networks (ANN)	prediction of GPP by an empirical model in which the weights associated to the nodes of the model are determined in a training process (by back-propagation of the error in the output)	Papale and Valentini (2003)
model tree ensemble (MTE)	prediction of GPP by a set of multiple linear regressions from explanatory variables (faPAR, faPAR$\times$ potential radiation, precipitation, temperature)	Jung et al. (2009)

Developing and using different flavors of models ultimately leads to more robust estimates of primary productivity (Beer et al., 2010). Each type of diagnostic modeling is associated with uncertainty—propagated from the input data but also due to the representativity of the model structure. Comparing and combining results from diverse approaches helps to understand how big these uncertainties are.

Terrestrial models of photosynthetic uptake that use LUE as an input (Haxeltine and Prentice, 1996; Ruimy et al., 1999) deserve special attention because of several promising options to improve them by deriving LUE directly from remotely sensed data.

1.5.3 LUE models of primary productivity—focus on MOD17

A number of GPP models set a maximum (or potential) LUE as a constant and downregulate it by minimum temperature and one or several estimators of water

stress (Potter et al., 1999; Running et al., 2004; Yuan et al., 2007; Mäkelä et al., 2008). The way in which the maximum LUE and the coefficients accounting for stress effects are set differs between models. The maximum LUE is often set as a constant across sites and biomes or it is defined for each vegetation type. Assuming maximum LUE to be constant for different locations within one biome is an oversimplification possibly causing the poor performance of global models of GPP (Heinsch et al., 2006).

A frequently chosen indicator of water stress is VPD (Granger and Gray, 1989; Running and Nemani, 1988), also in LUE-based models of photosynthetic uptake. This practice is supported by several studies that suggest atmospheric conditions reflect surface parameters (Bouchet, 1963; Morton, 1983). In certain places (most of China, conterminous U.S.) VPD has been shown to capture the interannual variability of water stress, though it may fail to capture the full seasonal water stress in dry regions experiencing strong summer monsoons (Mu et al., 2007a,b).

This study uses the MOD17 model of primary productivity as an example because it is used operationally to produce global datasets of GPP and NPP, products that are freely and easily accessible in near-real time since March 2000 (`http://modis.gsfc.nasa.gov/data`) and are thus rather influential.

1.5.3.1 Algorithm of the MOD17 model of primary productivity

The MOD17 model of primary productivity is a classic example of a LUE model (c.f. section 1.5.3). A maximum LUE is reduced by simple ramp functions of daily Tmin and VPD (see Fig. 1.3). The resulting actual LUE is multiplied by the available energy (Heinsch et al., 2003):

$$LUE = LUE_{max} * f(Tmin) * f(VPD) \tag{1.7}$$

$$GPP = LUE * aPAR \tag{1.8}$$

$$= LUE * faPAR * PAR \tag{1.9}$$

A minimum temperature scalar (Tmin) reduces the conversion efficiency when cold temperatures limit plant function (Heinsch et al., 2003, 2006). Another scalar reduces LUE when VPD increases beyond a threshold (VPD_{min}) that is considered high enough to limit photosynthesis. The effect of soil water availability on photosynthetic assimilation is not included in the MOD17 algorithm (Heinsch et al., 2006). To partially account for this issue, sensitivity to VPD is increased in the model as a surrogate for drought effects (McCallum et al., 2009).

Both scalars range from 1 (implicating no inhibition of photosynthesis by environmental conditions) to 0 (total inhibition). The five parameters of the model (LUE_{max}, $Tmin_{min}$, $Tmin_{max}$, VPD_{min}, VPD_{max}) have been defined for 11 biome types and are stored in a biome property look-up table (BPLUT) (c.f. Table A.1). The algo-

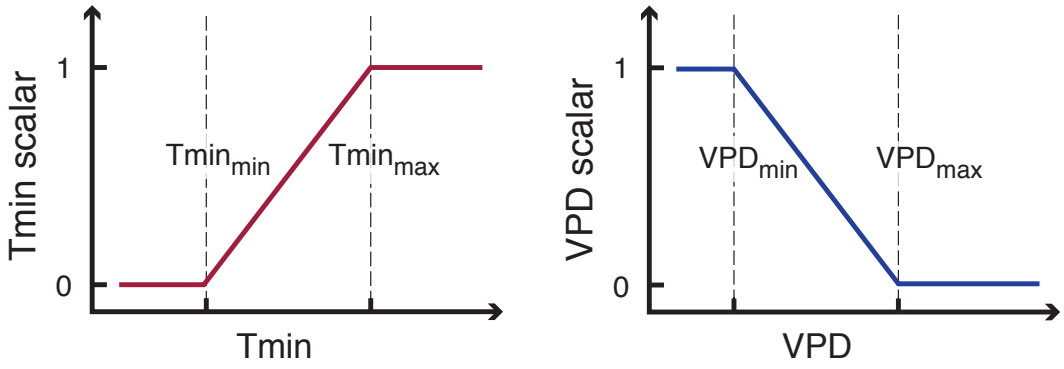

Fig. 1.3: *The MOD17 Tmin and VPD attenuation scalars are simple linear ramp functions of daily Tmin and VPD. Adapted from Heinsch et al. (2003).*

rithm used to map these 11 biome types employs the University of Maryland (UMD) classification scheme (Hansen et al., 2000; Heinsch et al., 2003). The BPLUT has originally been parameterised using a global simulation of the general ecosystem model BIOME-BGC (Running et al., 2000; Zhao et al., 2005) and was later on adjusted using updated meteorological and faPAR data compared to data from 12 North American FLUXNET sites (Zhao et al., 2005; Heinsch et al., 2006).

A second product of the MOD17 algorithm is NPP. Daily maintenance and growth respiration are estimated using biome-specific allometric relationships based on leaf area index (LAI) and faPAR and subsequently subtracted from GPP (Heinsch et al., 2003). However, the final NPP-product is only available at annual timescale (Running et al., 2000).

In the following, only GPP is considered because it is available at a daily resolution from the NASA data portal and—given the availability of suitable input data—it can be calculated at even higher temporal resolution.

1.5.3.2 Operational input into the MOD17 GPP model

There are three sources of input into the MOD17 model: land cover and faPAR data (both are derived at 1 km spatial resolution from the MODIS sensors), and meteorological data.

Biome type information originates from two MODIS land cover classification schemes (Heinsch et al., 2006). Besides the UMD land cover classification (i.e. land cover classification type 2 of the MOD12Q1 product) used by the core MOD17 algorithm (Hansen et al., 2000), the MOD15 algorithm for deriving LAI and faPAR relies on the land cover classification type 3 (LAI/fPAR biome scheme) with 6 biome types (Myneni et al., 2002).

Apart from the land cover classification that defines the basic vegetation architecture and characteristics, MOD15 algorithm inputs include atmospherically corrected bidirectional reflectance values in a red and and a near-infrared spectral

band, as well as the sun and viewing geometry for the reflectance data (Huemmrich et al., 2005).

The faPAR retrievals are performed by comparing observed and modeled surface directional reflectances for a suite of canopy structures and soil patterns that covers a range of expected natural conditions (Myneni et al., 2002; King et al., 2004). The resulting probability distributions are then checked for energy conservation, which limits the number of acceptable solutions (Myneni et al., 2002). If no acceptable solutions were found, a backup algorithm derives faPAR as biome-specific linear functions of normalised difference vegetation index (NDVI). For each day, faPAR is calculated as the mean of all possible solutions for a given pixel (Huemmrich et al., 2005). The final product reports the maximum clear-sky daily value of an 8 day aggregation period (Plummer, 2006).

Meteorological data are provided by the NASA Global Modeling and Assimilation Office (GMAO) (used to be Data Assimilation Office (DAO)) at a resolution of 1° x 1.25° and 3 h (Heinsch et al., 2003; Zhao et al., 2005). These data are generated by the Goddard EOS Data Assimilation System (GEOS-DAS) based on general circulation model outputs, boundary conditions (sea surface temperature, terrain, etc.) and surface observations to form a regular gridded meteorological data set (Zhao et al., 2005; Bloom et al., 2005; Atlas and Lucchesi, 2000). From these original data, the the current version of the MOD17 algorithm (collection 5) derives average daily VPD, daily minimum temperature Tmin and total shortwave radiation and interpolates them to the 1 km resolution of the MODIS pixels.

1.5.3.3 Assessment of the MOD17 model

There is general agreement that the MODIS algorithm captures the seasonality of site GPP quite well across a wide array of climates under non-drought conditions (Plummer, 2006). However, the MOD17 GPP product does have a number of weaknesses caused by the choice of input data (meteorologic, radiometric, biophysical), model parameterization and the algorithm itself (Plummer, 2006; Heinsch et al., 2006).

Uncertainties propagated from input data

The classification accuracy of the MOD12Q1 land cover product, which is reported to be 65-80% (Cohen et al., 2003), influences the MOD17 GPP twofold: through the biome-specific model parameters and indirectly through the MODIS faPAR algorithm. During land cover classification, most problems occur while trying to differentiate between different forest classes. According to (Plummer, 2006), parameter differences between forest classes are small, thus the net effect is small. However, validation of remote-sensing-based biophysical products is complicated by a underrepresentation of validation sites with grass and evergreen broad leaves (Baret et al., 2006).

The representativeness of the MOD15 fraction of absorbed photosynthetically active radiation (faPAR) is not clear. Plummer (2006) states that the "use of the maximum eight-day absorption may undervalue the impact of this canopy structure (Heinsch et al., 2006; Ritts et al., 2006; Leuning et al., 2005). In addition, it is unclear whether the maximum is truly representative of the situation over eight days due to variation in atmospheric conditions and cloud".

The coarse resolution of the assimilated meteorology can result in site specific mismatches (Turner et al., 2005). As long as there is no accurate reanalysis product available with a higher spatial resolution, this problem cannot be overcome on a global scale. Collection 6 of the MOD17 product will be fed by a more recent version of GMAO data with higher spatial resolution (MODIS Land Team, 2009; Rienecker et al., 2008).

Problems resulting from model structure

While global models, especially if they are to be operated in near-real time, need to be simple (Heinsch et al., 2003), the appropriateness of the MOD17 model structure for certain conditions has been questioned. Most of all, the performance of MOD17 in drought conditions is criticised (Turner et al., 2005; Leuning et al., 2005; Plummer, 2006; Hwang et al., 2008). The inclusion of a parameter describing soil water availability in stead of or in addition to the VPD control in the photosynthesis model was suggested (Reichstein et al., 2004), and a better representation of GPP has indeed been demonstrated in site-level studies (Leuning et al., 2005; Kanniah et al., 2009a). However, an accurate proxy of plant available soil water content does not yet seem to exist on a global scale. Soil moisture estimates derived from microwave remote sensing are only available for the uppermost centimeters and especially uncertain in densely vegetated areas. Proxies based on a ratio of precipitation and evapotranspiration (Leuning et al., 2005)are not readily applicable on a global scale, because global precipitation data, either from reanalysis (Ruiz-Barradas and Nigam, 2005) or from remote sensing, are not yet considered reliable enough.

There is also concern that assuming a constant LUE_{max} for each land cover class is an oversimplification (Turner et al., 2005; Leuning et al., 2005). During cloudy conditions, when radiation is more uniformly distributed, i.e mostly diffuse, LUE is known to be higher compared to cloud-free days (Knohl and Baldocchi, 2008). LUE also changes seasonally due to changes in leaf pigment content (Turner, 2003). Same-biome variability of LUE as well as mixing of different classes within one pixel are additional sources of error (Plummer, 2006).

1.6 Estimating light use efficiency from space

Many problems of the LUE-based models of photosynthetic assimilation discussed in section 1.5.3.3 would become irrelevant if actual LUE could be derived from remotely sensed data with reasonable uncertainty. The two most promising buzzwords for a direct, remote estimation of LUE are chlorophyll fluoresence and PRI. Both are based on the fact that light energy, after having being passed to reaction center chlorophylls (see section 1.2.1), is utilized by one of three competitive processes (Robinson, 2001):

- assimilatory and nonassimilatory photochemistry (photochemical quenching),
- dissipation as heat (nonphotochemical quenching, photoprotection), see section 1.2.1
- dissipation as chlorophyll fluorescence (re-emission of light at longer wavelength than the excitation energy).

Since the energy balance between light harvesting and photosynthetic use plus dissipation must be kept, quantification of the dissipation processes allows inference about photosynthesis.

1.6.1 Estimating LUE with fluorescence measurements

The competition of fluorescence with photosynthesis for the use of absorbed light energy has enabled generations of plant physiologists to use it as a tool for assessing the vitality of the photosynthetic system (Papageorgiou and Govindjee, 2005; Baker, 2008; Meroni et al., 2009b).

The chlorophyll in leaves has a fluorescence emission spectrum in the waveband between 650 and 800 nm, peaking at ca. 690 nm and 740 nm (Grace et al., 2007).

In field or laboratory assessments of plant stress is often inferred from changes in fluorescence during several minutes following artificial illumination (active fluorescence). These saturating light pulses are impractical at the canopy scale (Rascher and Pieruschka, 2008), therefore LASER-induced spot or scanning methods are being tested (Kolber et al., 1998, 2005; Ananyev et al., 2005; Rascher and Pieruschka, 2008)

Alternatively, the 'passive' fluorescence triggered by sunlight can be used as an indicator for LUE (Flexas et al., 2002). The radiation emitted as fluorescence is added as a weak signal to the reflected solar radiation (Meroni et al., 2009b). This solar-induced fluorescence is 2-3% or less of the reflectance signal (Grace et al., 2007). This implies that great care must be taken to separate the two signals. One strategy to achieve this involves measuring the emitted radiation in 'dark lines' of the solar spectrum. Little incident energy and thus little reflected radiation in these spectral wavebands increases the relative contribution of fluorescence. Several

of those 'dark lines' result from absorption in the sun's atmosphere (Frauenhofer lines). These features are numerous, but only one coincides with the fluorescence emission spectrum (Grace et al., 2007): the H_α feature centered at 656.4 nm. They are also very narrow (0.04-0.4 nm), so a high spectral resolution is necessary to use these features for fluorescence measurements. Wider absorption features result from absorption by gasses in the Earth's atmosphere, most notably the O_2-B (687.0 nm) and O_2-A (760.4 nm) absorption bands. These absorption lines can be easily used for ground-based measurements. Measuring within these telluric absorption bands using air-borne or space-borne sensors requires a very accurate atmospheric correction, since absorption acts two-way: both incident and outgoing radiation are affected (Davidson, Malcolm et al., 2003; Guanter et al., 2007).

In their review on remote sensing of sun-induced chlorophyll fluorescence Meroni et al. (2009b) conclude "that today ground-based estimation of [fluorescence] can be achieved by several commercially available field spectrometers while there is still a need for technical development in airborne and spaceborne sensors to better fit the spectral requirements for precise [fluorescence] retrieval".

Before satellite-based fluorescence measurements can be used to estimate GPP for large regions, several issues need to be addressed (Damm et al., 2010):

- Atmospheric effects must be corrected precisely (Guanter et al., 2007).
- The influence of canopy structure on the fluorescence signal must be better understood.
- The contribution of different surface elements to one measurement by the remote fluorescence sensor (i.e. mixed pixel effects) needs to be considered.
- The impact of changing sun-sensor geometry on the fluorescence signal (Meroni et al., 2008) requires further studies.
- The understanding of physiological relationship between fluorescence and photosynthesis needs to be developed further.

1.6.2 photochemical reflectance index (PRI) as proxy for LUE

Physiological background & formulation of PRI

The changes in pigment composition induced by the photo-protective mechanism of xanthophyll-de-epoxidation (c.f. section 1.2.1) result in a change of reflectance near 531 nm (Bilger et al., 1989; Gamon et al., 1992, 1997; Peñuelas et al., 1995, c.f. Fig. 1.4). Gamon et al. (1993a) found this reflectance change at approximately 531 nm in 20 species representing a wide range of habitats, phenologies and photosynthetic pathways. The exact spectral position might vary depending on the relative contribution of the component caused by xanthophyll pigment interconversion and a component caused by chloroplast conformational changes.

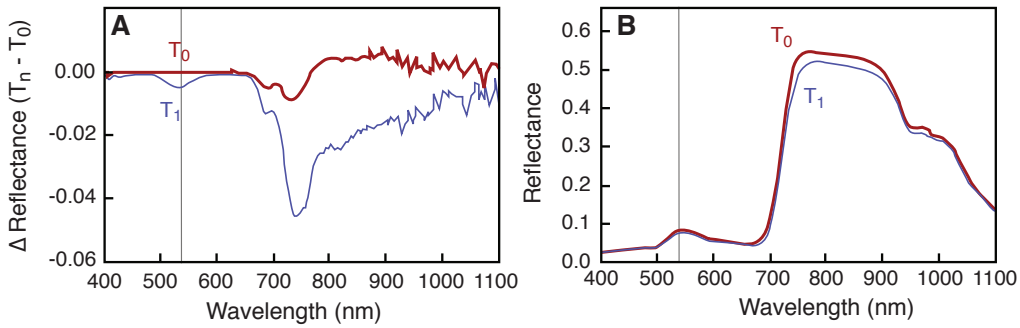

Fig. 1.4: *A) Difference in reflectance as a function of stress level; T_0: Unstressed sunflower leaves at time zero; T_1: light-stressed leaves after 40 minutes B) Observed change in leaf reflectance. Adapted from Gamon et al. (1990); Hall et al. (2008).*

Normalising reflectance at this wavelength (R_{531}) by reflectance at a reference wavelength (R_{ref}) helps to correct for changes in 'background' reflectance that might be caused by a number of optical effects, including changes in illumination angle and chloroplast movements (Gamon et al., 1993a, , see also the change in 'background reflectance for *Zea sp.* in Fig. 1.5):

$$PRI_{ref} = \frac{R_{531} - R_{ref}}{R_{531} + R_{ref}} \tag{1.10}$$

Gamon et al. (1993a) suggest 570 nm as an optimal reference wavelength at leaf level because it is situated near the right shoulder of the xanthophyll-de-epoxidation reflectance feature. The suitability of this (R_{570}) and other reference bands have been tested based on statistical correlations (e.g. Gamon et al., 1992; Inoue et al., 2008). The scientific literature does not agree on a single best reference wavelength for PRI, which makes cross-study comparisons difficult (Garbulsky et al., 2011). Garbulsky et al. (2011) summarise that "it is not entirely clear if the best wavelengths for measuring this feature at the leaf scale (531 and 570 nm) are necessarily the best wavelengths at progressively larger scales, where multiple scattering and other confounding effects may alter the spectral response of the xanthophyll cycle feature, much in the way that pigment absorption peaks can vary depending upon their chemical and scattering medium."

More work is needed to determine a PRI-formulation that can be applied on large areas based remote sensing data.

Successful studies of PRI as indicator of photosynthetic efficiency

PRI has been effective in detecting changes in photosynthetic efficiency in single leaves (Peñuelas et al., 1995; Gamon et al., 1997; Méthy, 2000; Guo and Trotter, 2004) and in small canopies of sunflower (Gamon et al., 1992), barley (Filella et al., 1996), chaparral (Stylinski et al., 2002) and other species (Trotter et al., 2002) as

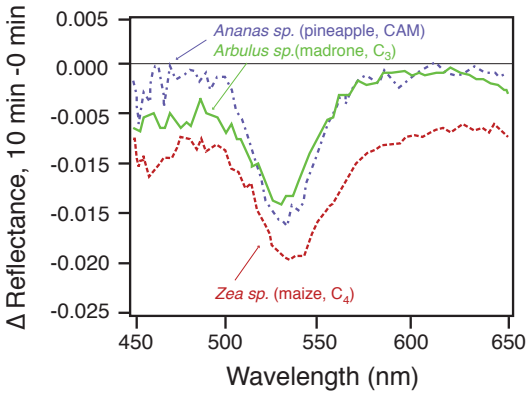

Fig. 1.5: *Reflectance changes as a function of wavelength 10 minutes after sudden high light exposure of dark-adapted leaves representing three photosynthetic pathways (C_3, C_4, CAM). Reflectance has been normalised to reflectance at time zero. Each spectrum represents the mean of measurements on three leaves. Adapted from Gamon et al. (1993a).*

well as at the ecosystem scale (Peñuelas and Inoue, 2000; Rahman et al., 2001; Nichol et al., 2000, 2002).

By tracking the xanthophyll de-epoxidation state and thus LUE, PRI becomes complementary to spectral indices such as normalised difference vegetation index (NDVI) and enhanced vegetation index (EVI) that are good indicators of canopy greenness but are no proxy of fluctuations in photosynthetic activity unrelated to changes of greenness and leaf area (Running and Nemani, 1988; Gamon et al., 1993b; Asner et al., 2004).

In particular, PRI has been successfully applied in detecting changes of photosynthetic activity caused by water stress (Tambussi et al., 2002; Thenot et al., 2002; Asner et al., 2004; Sun et al., 2008; Suárez et al., 2008; Peguero-Pina et al., 2008; Suárez et al., 2010), ozone-induced stress (Meroni et al., 2009a; Panigada et al., 2009), salinity stress (Naumann et al., 2008a,b), as well as nutrient enrichment and eutrophication (Siciliano et al., 2008).

Challenges

In some studies at canopy and ecosystem level no statistically significant correlation between PRI and LUE was observed (Méthy, 2000). These difficulties to upscale the PRI-LUE-relationship have several roots. One issue are the different footprints of the PRI-sensor and the set-up used for assessing ecosystem LUE—usually an eddy covariance tower (Méthy, 2000). Often this spatial mismatch goes along with a temporal mismatch: while the PRI measurements are instantaneous, the eddy covariance technique averages measurements over half-hourly intervals. Observing different subsets of the land surface with the two methods has a 3-dimensional, structural aspect. While eddy covariance flux measurements integrate vertically over the footprint, any type of PRI sensor only records

what is in its 'line of sight', including some scattered photons. It does not 'see' photosynthetically active surface obstructed by leaves and branches. A discrepancy between the two measurement methods is unavoidable as soon as the relative contributions of plant materials with different LUEs to the overall signal recorded the PRI-sensor differs from the proportions within the flux-tower footprint. Photosynthetic efficiency is known to vary between species (Guo and Trotter, 2004), between shaded and sunlit leaves of the same species (Peñuelas et al., 1995) and with age. In addition, the PRI is influenced by the contribution of photosynthetically inactive plant material and soil to the reflectance signal. Especially for sparse canopies with LAI $<$3, variations in soil background reflectance strongly influence the PRI signal (Barton and North, 2001; Filella et al., 2004).

An emergent property at the canopy level is that LUE increases on cloudy days, even if the total incident energy decreases to 70-80% of the value on a clear day (Gu et al., 1999). This property arises from the saturation of leaf photosynthesis at a certain illumination intensity. On cloudy days, the fraction of diffuse light increases: light does not arrive as a beam from only one direction, but from many directions. Hence a large number of leaves receive a moderate amount of light which can result in a larger overall LUE compared to cloud-free days on which only the top leaves are illuminated (often beyond their photosynthetic capacity) while a large fraction of leaves remains in deep shade (Gu, 2002; Farquhar and Roderick, 2003).

The limitations imposed by the inherent heterogeneity of ecosystems additionally affect radiation measurements when the position of sensor and/ or the sun relative to the land surface changes in between acquisitions (Louis et al., 2005). Apart from these effects of viewing and illumination geometry—often summarized as the bidirectional reflectance distribution function (BRDF)-effect on PRI (Suárez et al., 2008)—the ecosystem itself changes diurnally and seasonally. Leaves might change their orientation and leaf area varies—differently for different species within an ecosystem (Barton and North, 2001; Hilker et al., 2008b).

Also, the total pool of photosynthetic pigments and the relative contributions of carotenoids and chlorophylls to it vary; these changes show up in PRI measured over seasons or years (Stylinski et al., 2002; Sims and Gamon, 2002; Filella et al., 2009).

The PRIs sensitivity to carotenoid/ chlorophyll ration actually seems to be an advantage for tracking ecosystem LUE (Filella et al., 2009). Carotenoid pigments other then xanthophylls, for example b-carotene or lutein, are also involved in photoprotective processes (Frank and Brudvig, 2004; Telfer, 2005; Dall'Osto et al., 2006).

Under stress or during leaf senescence—while photosynthetic efficiency decreases—chlorophyll degrades faster than carotenoids (Gitelson and Merzlyak, 1994; Peñuelas et al., 1995). Therefore, environmental stress often increases the carotenoid/chlorophyll ratio, which correlates with PRI.

Based on these considerations, Filella et al. (2009) conclude that PRI "may provide

an integrated remote sensing assessment of photoprotective and accessory pigments and, therefore, of photosynthetic radiation-use efficiency to the extent that this is correlated with carotenoid/chlorophyll ratio." They found that "over the long term (weeks), PRI tracked the variations in the carotenoids/chlorophyll-a+b ratio and, over the short term (minutes), the changes in the de-epoxidation state."

PRI from space-borne sensors

While there have been several successful studies with air-borne PRI-sensors (e.g. Nichol et al., 2000, 2002; Asner et al., 2004, 2005), only few studies have attempted an investigation of the PRI-LUE relationship with satellite data so far. Limiting factors are probably the number of space-borne sensors with the necessary narrow spectral bands, the pre-processing required for PRI calculation (correction for atmospheric disturbances and BRDF effects) and other challenges detailed above. However, some studies on boreal, temperate, and Mediterranean type ecosystems have successfully tested MODIS-derived PRI as a proxy for ecosystem LUE (Drolet et al., 2005, 2008; Rahman et al., 2004; Garbulsky et al., 2008; Xie et al., 2009).

MODIS seems to be the most appropriate sensor currently available to test space-borne PRI because one of its 10 nm wide "ocean bands" is centred at 531 nm. The not too narrow spectral bands might actually be an advantage, given that Gamon et al. (1992, 1993a) found that the optimum wavelength for LUE tracking varies in between species and canopy types. The temporal resolution of MODIS data is comparatively high. Since both the Terra and the Aqua satellites have a roughly identical MODIS sensor aboard, two or more data acquisitions per day can take place under cloud free conditions. The MODIS observation footprint for the required spectral bands is about 1 km^2 if the sensor view zenith angle is limited to no more than 40° (Wolfe et al., 1998). This is in the same order of magnitude as the footprint of eddy covariance towers, although the fetch of eddy covariance systems depends on measurement height, the surface roughness, and the characteristics of the boundary layer as well as the atmospheric stability (Rebmann et al., 2005). We can assume comparable conditions in the remotely sensed area and the flux tower source area when restricting the analysis to towers located in a large enough homogeneous area. Hence, for some carefully selected eddy covariance sites a comparison to ground based estimates of light use efficiency is possible. At a homogeneous site the results will not be compromised if some of the 1 km MODIS pixel are not properly centered on the eddy covariance tower and do only partially coincide with the flux-tower footprint area.

The quality flags associated with every MODIS pixel allow for screening according to cloud cover and the general usefulness of the data. Given an ideally homogeneous study site the following issues need to be taken into account when interpreting PRI values in 1 km MODIS pixels:

1. The sensor lacks a spectral band at 570 nm (c.f. Table 1.2), hence another

reference band needs to be chosen.

2. Changes in viewing and illumination geometry in between measurements are likely to influence PRI (Barton and North, 2001).

3. A stringent atmospheric correction should be performed in order to avoid variations simply due to differences in atmospheric composition (Grace et al., 2007).

4. In addition to these difficulties, studies at a regional scale (or larger) would ultimately need to deal with sub-pixel heterogeneity.

Tab. 1.2: *Bandwidth of the MODIS' spectral bands used in this study.*

Band	Bandwidth (nm)	Use in this study
1	620-670	PRI, NDVI, EVI
2	841-876	NDVI, EVI
3	459-479	EVI
4	545-565	PRI
11	526-536	PRI
12	546-556	PRI
13	662-672	PRI
14	673-683	PRI

Hardly any space-borne LUE estimation has been undertaken so far for more water limited ecosystems. Garbulsky et al. (2008) estimated LUE for an evergreen Mediterranean oak forest in Castelporziano, Italy. However, the trees there do have access to groundwater (Damm et al., 2002), thus water limitation is not severe. It is important to bridge this gap because the area affected by drought is about to increase: According to Christensen et al. (2007), it is likely that annual precipitation will decrease in several regions, among them Central Europe, the Mediterranean, the south-western US, Central America and Southern Australia (c.f. section 1.2.2.2). For the Mediterranean this goes along with an increased risk of summer drought (Giorgi, 2006). It is crucial to improve the performance of diagnostic models with respect to drought events. Upgraded data-oriented models can then serve as benchmarks to improve current process models.

It is crucial to find out if spaceborne PRI can help to improve assessments of carbon uptake for many of the world's ecosystems.

1.7 Aims of this study

To improve MOD17-type-models of gross primary productivity it is attractive to derive LUE directly from just one kind of satellite data, without relying on estimates of different meteorological variables. This study will help to find out if photochemical reflectance index (PRI) can function as a proxy of LUE in global models.

This study will be based on radiances recorded by the MODIS on board the Terra and Aqua satellites because this configuration provides a useful temporal resolution and a spectral band around 531 nm. However, MODIS does not have the usual PRI reference band at 570 nm. Thus, the MODIS PRI needs to be based on several alternative reference bands. One goal of this study is to identify the most suitable among all possible reference bands, first of all for a test site.

Changes of LUE in drought-tolerant evergreen species are often not paralleled by changes in NDVI,LAI or canopy structure (Gamon et al., 1992; Running and Nemani, 1988).

Due to negligible changes in radiation interception in these Mediterranean evergreen fortests, it is of great importance to have accurate measurements of short-term changes in radiation-use efficiency (Filella et al., 2009). Thus sclerophyll dominated ecosystems are a good starting point for testing the performance of satellite-based PRI as LUE proxy. A pilot study within this thesis will therefore concentrate on a Mediterranean *Quercus ilex* forest. Special emphasis will be placed on the capability of satellite-based PRI to estimate LUE during drought events because this is where current diagnostic models of GPP have deficiencies. Specifically, it will be assessed which reference band is most suitable for this application. The influence of different methods of atmospheric correction on the PRI-LUE relationship will also be tested in this pilot study. Though, for reasons detailed above, a relationship between LUE and NDVI or enhanced vegetation index (EVI) is not expected for this ecosystem, these indices are included in the analysis as benchmarks.

Despite the fluctuations in illumination geometry, dimension of the surface area sensed by each instantaneous field-of-view and background reflectance at every site, the site level models based on MODIS PRI published so far yielded good agreement with observed LUE. That considerable potential exists for mapping LUE with a common model has also been shown by Drolet et al. (2008), who found a unifying model for eight sites in central Saskatchewan. These boreal sites are close to each other (within the confines of one satellite scene), hence they can be simultaneously monitored instead of by comparing data from different image acquisitions. The viewing geometry and atmospheric disturbance of the satellite signal is therefore similar. Consequentially, the next step is to evaluate PRI based models across sites and satellite scenes.

Therefore, in a second stage following the pilot study on the Mediterranean holm oak forest, the analysis will be expanded from one ecosystem to sites representing a diversity of plant functional types and different vegetation densities. The objective of this study is to discover if the known limitations of PRI can be overcome and a single PRI-based model of LUE (i.e. based on the same reference band, with the same parameterisation) can be applied under a wide range of conditions. So far it is unclear if—using satellite data with rather coarse spatial resolution—the same empirical model can be applied at multiple sites or if different reference bands have to be used depending on for example plant functional type and vegetation density.

A secondary objective of this study is to learn how different frequently used faPAR products affect the in-situ LUE estimates that are used as ground truth.

CHAPTER 2

Data, data preparation and methodology

Contents

The main types of data used in this study are local eddy covariance measurements (plus associated meteorological variables) and MODIS satellite data, which are available globally. The relationship of MODIS-PRI to LUE is tested at site level. If a universally applicable relationship between MODIS-PRI and LUE can be found, this would provide an opportunity to upscale LUE to larger areas.

2.1 Flux data from eddy covariance measurements

2.1.1 Processing of flux measurements according to FLUXNET standards

For this study, flux and micro-meteorological data were extracted from the FLUXNET LaThuile database (http://www.fluxdata.org/DataInfo/default.aspx). The data of that data base were recorded at 253 individual research sites encompassing 7 climate types and 11 plant functional types, following network-specific protocols (Aubinet et al., 2000).

The assumptions on which the simplified equation 1.6 in section 1.3.2 is based are often not fulfilled. Horizontal turbulent transport and advection do occur, advection, for example, results from patchy vegetation or uneven terrain (Lee, 1998; Finnigan

et al., 2003; Finnigan, 2008). There is no technique available to correct fully for advection effects. However, some first-order corrections can be made for moderate effects of topography. These corrections aim to re-align a coordinate system in a way that the mean vertical flux that is zero so that hence equation 1.6 can be applied again (Baldocchi et al., 1988; McMillen, 1988; Baldocchi, 2008). Several different techniques are available and can be chosen according to the particularities of the measurement footprint (Finnigan et al., 2003; Finnigan, 2004). In some cases this correction is not sufficient and the magnitude of the bias due to advection remains unknown unless measured (Feigenwinter et al., 2008; Yi et al., 2008). However, measuring advection directly is difficult, because it involves multiple sets of eddy covariance towers to measure flux divergence or horizontal gradients in fluxes and scalars (Aubinet et al., 2003a; Feigenwinter et al., 2004).

Another correction needs to be introduced to avoid that the flux measurements are biased by insufficient turbulent mixing, which is measured as friction velocity (u*) (Goulden et al., 1996; Aubinet et al., 2000; Barford et al., 2001; Gu et al., 2005). At nighttime, the atmospheres thermal stratification stabilises. This can cause an isolation of the air around the vegetation from the air moving in the atmosphere above (Baldocchi, 2008). Under these circumstances, the CO_2 fluxes measured by the eddy covariance system would not represent the gas exchange of the ecosystem (Aubinet et al., 2005; Sun et al., 2007). The u* threshold for this decoupling ranges between 0.1 and 0.5 m s^{-1}, depending on topography and canopy height (Aubinet et al., 2000; Loescher et al., 2006). To correct the data for advective transport measurements acquired at low-turbulence conditions are discarded (u* filtering) (Aubinet et al., 2005).

To validate and calibrate ecosystem models it is necessary to partition the measured net ecosystem exchange (NEE) into its gross primary productivity (GPP) and total ecosystem respiration (R_{eco}) components. The flux partitioning is essentially an extrapolation of R_{eco} data from night- to day-time, based on short-term relationships between temperature and R_{eco} (Reichstein et al., 2005). Using short-term sensitivities instead of long-term dependencies reduces the influence of other confounding factors, such as soil moisture or growth dynamics. The daytime R_{eco} resulting from this extrapolation is subsequently subtracted from NEE to calculate GPP. The validity of this flux separation has been corroborated by a new method using a light response curve approach, independent of night-time data (Lasslop et al., 2010).

To come up with long, uninterrupted series of flux data for creating carbon budgets on daily, weekly, monthly or yearly time steps, gap filling is an essential processing step (Falge, 2001; Moffat et al., 2007). It is also necessary for cross-site comparisons, validation of satellite products, model inversions or synthesis studies. Incomplete records result from u*-filtering and other data rejections under certain climatic conditions (e.g. precipitation, dew), but also from malfunctioning, maintenance and calibration of the sensors (Luyssaert et al., 2009). The uncertainty associated with the gap filling (i.e. interpolation) becomes larger with increasing gap length (Moffat et al., 2007), especially during periods of rapid change such as

green-up and senescence.

The LaThuile data collection contains—besides NEE, GPP and R_{eco} fluxes—radiation measurements (photosynthetic photon flux density (PPFD), global radiation (R_g), net radiation (R_n), for some sites shortwave and longwave incoming and outgoing radiation, below canopy or reflected PPFD), precipitation and temperature records, sensible and latent heat fluxes, for some sites soil water content data and in-situ faPAR measurements, as well as some derived quantities such as surface conductance, soil water storage and evapotranspiration. The data are available at half-hourly and daily temporal resolution.

2.1.2 A note on uncertainty

Many studies have addressed the robustness of eddy flux measurements, also with regard to differences between sites. Uncertainties in eddy-covariance derived ecosystem GPP values result from measurement uncertainties, gap-filling and flux partitioning. Reichstein et al. (2005) and Papale et al. (2006) provide an extensive summary of the uncertainties related to eddy flux data and present a standardized processing method including spike detection, storage correction, u* filtering, gap-filling and partitioning methods that has been applied to all net ecosystem exchange data within the FLUXNET LaThuille data collection. Uncertainties due to different processing of site data are thus minimised. Given a homogeneous site, the largest uncertainty results from the so-called u*-correction (Papale et al., 2006).

Another potentially big source of uncertainty, the partitioning of net ecosystem flux into ecosystem respiration and gross primary productivity, has been addressed by Lasslop et al. (2010). Their comparison of two partitioning methods shows a strong correlation and no significant biases for gross primary productivity and ecosystem respiration. Although the overall agreement of the two partitioning methods is good, there can be large deviations for specific sites or years. Therefore, the influence of the partitioning method on the relationship between LUE and PRI has been checked for the sites used in this study. The mean difference between GPP derived with either flux partitioning method was calculated for each site-year. By dividing this GPP-uncertainty-measure by daily aPAR, the resulting uncertainty in LUE was calculated and subsequently added to/ subtracted from each daily LUE value to visualise the range of possible LUEs(c.f. Fig. 4.6). Including this uncertainty did neither change the observed patterns nor the conclusions. In fact, since GPP is a gross flux, the relative error is quite small, while for NEE (not considered here) the error can be relatively larger.

The high frequency site data are aggregated to half-hourly data by the principal investigators of the individual sites with different software, which presents another source of uncertainty. A comparison of different techniques performed by Mauder et al. (2008) indicates a good agreement among the software within 5–10% difference for 30-min CO_2 flux values. Considering this uncertainty does not change the

results presented in this thesis. The quality evaluation by Göckede et al. (2008) for the CarboEurope-IP network demonstrated a high average data quality, and good representativeness of the measurement data for the specified target land cover types.

2.1.3 Study-specific preparation of eddy covariance data and associated measurements

The half-hourly GPP extracted from the FLUXNET LaThulle collection were quality-checked with the flags included in the data set. Data points where NEE or PPFD measurements were not original or high quality gap filled were discarded. As a result of the standardised partitioning of the net CO_2 flux GPP values can become negative. When the 'true' value is close to zero, the statistical random error might induce negative GPP values. In the pilot study, only 0.46 % of the night time GPP values (with photosynthetic photon flux density $< 100\mu$mol m^2 s^{-1}) are lower than zero. Records associated with negative GPP were excluded from the analysis.

To ensure that the data recorded by MODIS are representative and not contaminated by clouds, it is crucial to know if a satellite image was taken during clear-sky conditions. Thus, for each day and each study site diurnal curves of incident PPFD (as a measure of PAR) were plotted. The deviation of the actual PPFD-curve from the typical diurnal course on a cloud-free day during the same time of year was visually inspected and used to label days as 'cloud-free', 'cloud-free during a interval' (start and end of that interval were recorded), or 'cloudy', Fig. 2.1 shows exemplary PAR curves for both a cloudy day and a day with clear-sky. The measurements were taken within one week.

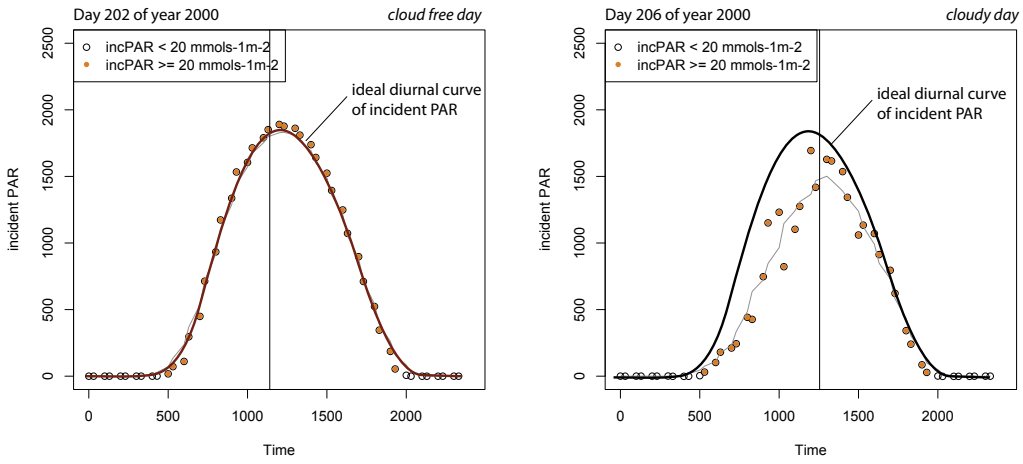

Fig. 2.1: *Incoming photosynthetically active radiation at a site in southern France on a cloud free and a cloudy day, along with the curve that represents the diurnal course of incident PAR on a cloud free day for that particular site and time of year. These curves were used to identify cloud-free days for all sites.*

2.2 Remotely sensed data

2.2.1 MODIS data for calculating PRI

To process the MODIS data for this study the procedure described by Drolet et al. (2005) was modified. Five MODIS products were downloaded from the Level 1 and Atmosphere Archive and Distribution System (http://ladsweb.nascom.nasa.gov) and the Earth Observing System data gateway http://redhook.gsfc.nasa.gov/~imswww/pub/imswelcome/). Of those products, from both the Terra (product name starts with 'MOD') and Aqua (product name starts with 'MYD') satellite, all scenes containing the tower locations of the study sites were selected.

The MOD/MYD021KM product contains calibrated digital signals measured by the MODIS sensor, from which at-sensor reflectances and radiances at 1 km spatial resolution can be calculated from two pairs of scale and offset terms included in the product (Toller et al., 2005). We calculated top-of-atmosphere reflectances for the spectral bands listed in Table 1.2.

The MOD/MYD03 product has the same spatial extent and resolution and provides the geographic coordinates as well as the solar and sensor zenith and azimuth angles of each pixel. These geolocation data were used to extract the spectral information of the pixel closest to each tower location. For the same location aerosol optical thickness was extracted from the MOD04 product and satellite-based estimates of cloud coverage were obtained from the MOD35 product.

Prior to further processing those acquisition dates were discarded

- where the quality flags attached to the MODIS products indicated saturation of a detector,
- where cloud cover is likely,
- where the quality of the atmospheric optical thickness estimation in the MOD04 product is poor or
- where the sensor viewing angle at the tower site is more than 40° (otherwise the MODIS pixel footprint would get too large, the result being a mixed signal from different land cover classes, c.f. Wolfe et al., 1998).

2.2.2 Effect of correction for surface anisotrophy on photochemical reflectance index

A small preliminary analysis was done to evaluate whether the accuracy of a MODIS-based PRI would be improved by a BRDF-correction based on readily available data.

For this, BRDF parameters derived from reflectance data recorded by the PARASOL instrument aboard the POLDER3 satellite have been used (François-

Marie Bréon., pers. comm.). These BRDF parameters have been derived for each of 4 different NDVI classes per biome type (IGBP-classification Bacour and Bréon, 2005; Vermote et al., 2009). This look-up-table approach was chosen because there are relatively few places available where enough observations could be collected to constrain the BRDF model (Lacaze et al., 2009). The temporal variations in reflectance anisotropy within the BRDF-estimation-period at a given site are assumed to be small.

For the site of the pilot study, MODIS-reflectance data have been corrected with the POLDER/PARASOL BRDF parameters matching the current NDVI observation. A comparison between the corrected and the uncorrected data can be seen in Fig. 2.2. While the BRDF-correction does influence the reflectance of the individual bands, the effects cancel each other out due to the normalisation implicit in the photochemical reflectance index (PRI). Correction the reflectance data for scattering and absorption effects by the atmosphere using a model specifically developed for MODIS data (6S) does influence the PRI-signal (c.f. Fig. 2.3). It can be concluded that correcting MODIS data for surface anisotropy with current globally available correction methods would not improve the accuracy of LUE prediction and is thus not worth doing.

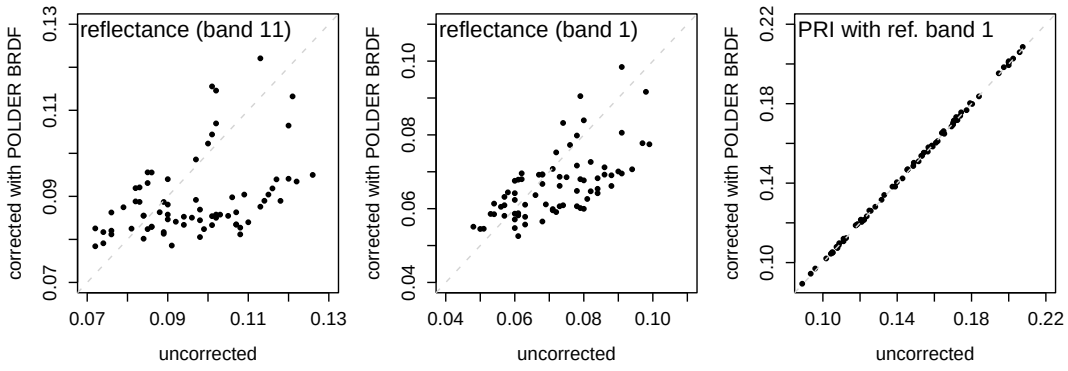

Fig. 2.2: *Attempted correction for surface reflectance anisotropy with POLDER/ PARASOL BRDF parameters (6 × 6 km) for 2002 at FR-Pue without explicit consideration of atmospheric effects. While the correction influences the reflectance of the individual bands that are used to compute PRI, these effects cancel each other out in the vegetation index itself.*

2.2.3 Geolocation

For all satellite scenes used in this study, the orientation of the pixel closest to the tower location has been plotted along with borders of distinct land cover types and other features (such as roads) that are likely to affect the reflectance signal (see Fig. 2.4). All these images were visually inspected. Whenever the tower-pixel included a significant fraction of something other than the ecosystem observed by the flux tower, the respective satellite scene has been discarded.

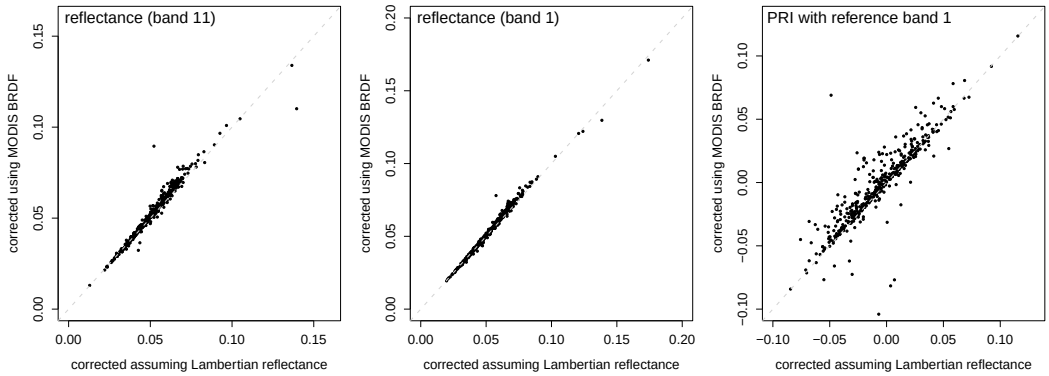

Fig. 2.3: *Surface reflectance corrected for anisotropy with MODIS BRDF parameters versus surface reflection assuming an isotropic surface for 2000-2005 at FR-Pue. In both cases a correction for atmospheric effects has been perfomed using 6S with the same input, so the difference is only due to applying the BRDF correction with 6S. The relatively small changes in reflectance (2.0-3.5%) result in rather large differences in PRI (13-31%).*

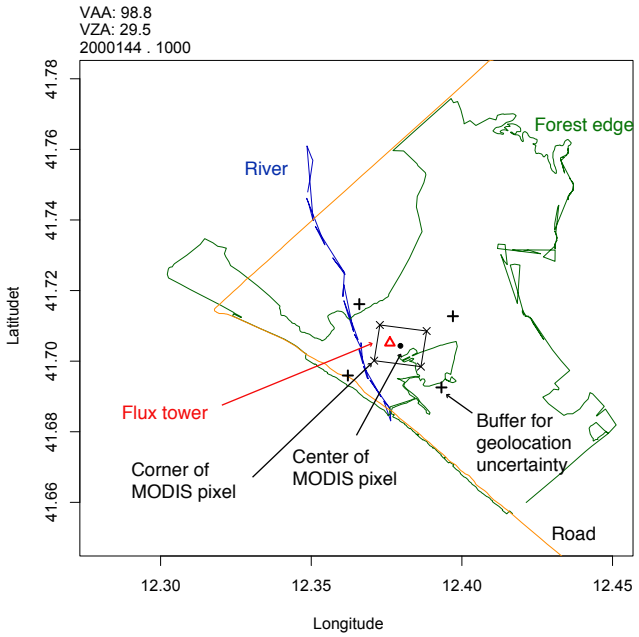

Fig. 2.4: *Example of the location of a MODIS pixel relative to the flux tower. This Italian site (IT-Cpz) is the most heterogeneous site used in this study.*

CHAPTER 3

Pilot study: Tracking seasonal drought effects on ecosystem light use efficiency with satellite-based PRI in a Mediterranean forest

Contents

Chapter summary

Gross primary productivity (GPP) changes occur at different time-scales and due to various mechanisms such as variations in leaf area, chlorophyll content, rubisco

activity, and stomatal conductance. Diagnostic estimates of primary productivity are obviously error prone when these changes are not accounted for. Additional complications arise when factors influencing a biome-specific maximum light use efficiency (LUE) must be estimated over a large area. In these cases a direct estimation of ecosystem LUE could reduce uncertainty of GPP estimates. Here, we analyse whether a MODIS-based photochemical reflectance index (PRI) is a useful proxy for the light use efficiency of a Mediterranean Quercus ilex *forest. As the originally proposed reference band for PRI is not available on MODIS, we tested the reference bands 1 (620-670 nm), 4 (545-565 nm), 12 (546-556 nm), 13 (662-672 nm), and 14 (673-683 nm) using different atmospheric correction algorithms. We repeated the analysis with different temporal resolutions of LUE (half-hourly to daily). The strongest correlation between LUE and PRI was found when considering only a narrow range of viewing angles at a time (especially 0-10° and 30-40°). We found that the MODIS-based PRI was able to track ecosystem LUE even during severe summer time water limitation. For this Mediterranean-type ecosystem we could show that a GPP estimation based on PRI is a huge improvement compared to the MODIS GPP algorithm. In this study, MODIS spectral band 1 turned out to be the most suitable reference band for PRI, followed by the narrow red bands 13 and 14. As to date no universally applicable reference band was identified in MODIS-based PRI studies, we advocate thorough testing for the optimal band combination in future studies.*

3.1 Introduction

Many diagnostic models of terrestrial ecosystem productivity compute gross primary productivity (GPP) as the product of the amount of absorbed photosynthetically active radiation (aPAR) and a light use efficiency term (Monteith, 1972; Monteith and Moss, 1977; Kumar and Monteith, 1981). aPAR can be conceived as the product of photosynthetically active radiation incident on the ground (Incident PAR (incPAR)) and the fraction of incPAR absorbed by the vegetation (faPAR). These entities can be derived from global meteorological fields and satellite products, respectively (e.g. Ruimy and Saugier (1994); Goetz and Prince (1999)).

It follows from the above that light use efficiency (LUE) is the ratio of productivity to aPAR. In this study, we refer more specifically to LUE as mols of CO_2 captured per mol of photons absorbed. LUE is inherently variable as it is determined by the quantum efficiency of photosynthesis (Grace et al., 2007). Photoprotective mechanisms reduce the photosynthetic quantum efficiency at times of environmental stress (such as temperature extremes, water or nutrient deficit, exposure to high light intensities, e.g. Green (2003); Runyon et al. (1994)). In addition, decreased stomatal conductance in times of drought will reduce available CO_2 and thus the rate of photosynthesis (Galmés et al., 2007).

In current diagnostic models, the light use efficiency (LUE) term is implemented either as a constant (sometimes stratified according to plant functional type) or

as a (biome-specific) maximum LUE that is reduced by scalars representing environmental stress (Yuan et al., 2007). It has been shown that this look-up table approach is not able to capture the full range of productivity dynamics, especially at finer temporal scales (Turner, 2002; Turner et al., 2006; Schwalm et al., 2006), primarily due to inaccurate maximum LUE estimates (Martel et al., 2005). Additional uncertainty arises when environmental drivers reducing maximum LUE need to be estimated on a global scale (Heinsch et al., 2006). Also, current remote-sensing based models have difficulties to detect drought stress (Turner et al., 2005) unless soil water content is accounted for (Leuning et al., 2005), which is difficult on a global scale. If we can obtain direct estimations of LUE from remote sensing data, this will lead us to more accurate calculations of GPP. We would need an integrative indicator of how photosynthetic capacity is controlled by environmental stress. Traditional vegetation indices such as the normalised difference vegetation index (NDVI) seem inappropriate for this task because they mainly measure greenness and can only track decreases in photosynthetic activity when they lead to yellowing or shedding of leaves (Gamon et al., 1995).

Another option to estimate LUE employs the mechanisms with which plants protect their chloroplasts from the creation of harmful reactive oxygen species. This danger arises if plants are subject to more light than they can use for photosynthesis. The photoprotection process includes changes in the trans-thylakoid pH-gradient, conformational changes in the chloroplasts, and the de-epoxidation of violaxanthin via antheraxanthin to zeaxanthin (Demmig-Adams and Adams, 2006). The formation of zeaxanthin is necessary to dissipate excess light as heat (Demmig et al., 1987) and at the same time decreases reflectance in a narrow wavelength range centred around 531 nm (Gamon et al., 1990).

The photochemical reflectance index (PRI) combines reflectance at this wavelength (ρ_{531}) with a reference wavelength insensitive to short-term changes in light energy conversion efficiency (usually 570 nm, ρ_{570}) and normalises it (Gamon et al., 1992; Peñuelas et al., 1995):

$$PRI = (\rho_{531} - \rho_{570})/(\rho_{531} + \rho_{570}) \tag{3.1}$$

Many studies have been conducted at the leaf and canopy scale with plants representing different photosynthetic pathways and ecosystems. In these studies PRI was well correlated with the epoxidation state of xanthophylls and LUE (Peñuelas et al., 1995; Stylinski et al., 2002; Sims and Gamon, 2002; Weng et al., 2006). A strong relationship between PRI and LUE could also be shown for plants suffering from environmental stress affecting energy dissipation pathways, namely nitrogen limitation (Gamon et al., 1992), high ozone concentrations (Meroni et al., 2008), water limitation (Suárez et al., 2008), or flooding (Naumann et al., 2008a). Several studies tested the performance of PRI as an indicator of LUE at ecosystem scale. The test was successful for boreal ecosystems, although in these studies LUE was based on incident PAR rather then aPAR (Nichol et al., 2000, 2002). In predominantly water limited ecosystems the applicability of PRI as LUE proxy might be limited to vegetation types that are not subject to strong changes in canopy

structure (Filella et al., 2004; Sims et al., 2006).

3.2 Methods

3.2.1 Study site and data

For this study, we focused on a flux tower site in the Puéchabon state forest (43.7414° N, 3.5958° E) in southern France, 35 km north-west of Montpellier. The *Quercus ilex* forest has been managed as a coppice for centuries, the last cut occurred in 1942. Allard et al. (2008) give a detailed site description, but we cite the most relevant characteristics here. The average tree height is about 5 m, the overstorey leaf area index (LAI) stated as 2.8±0.4). The main species in the shrubby, sparse understorey ($<$ 2 m) are *Buxus sempervirens*, *Phyllirea latifolia*, *Pistacia terebinthus*, and *Juniperus oxycedrus*. The climate is of Mediterranean type, with an annual precipitation of ca. 900 mm (ranging from 550-1550 mm for 1984-2006) of which 80 % occur between September and April. A reason to chose the Puéchabon site for this analysis is the role of *Quercus ilex* as one of the dominant species in Mediterranean type ecosystems (Terradas, 1999), covering about 6.55 x 10^4 km^2 (Quézel and Médail, 2003). Our analysis of the entropy, a quantity describing data homogeneity (Clausi, 2002), of a Landsat scene subset including the flux tower indicates that the site is homogeneous at the MODIS spatial resolution (Fig. 3.1, similar entropy levels in ca. 1 km distance from flux tower). The variations in surface properties observable within ca. 1 km around the flux tower are characteristic for the whole area covered by *Quercus ilex* growing on hard karstic limestones (ca. 4000 km^2) (Lacaze et al., 1994). Moreover, the flux tower footprint reliably represents the targeted land cover type (Göckede et al., 2008). Comparability of remote sensing data and in-situ measurements is therefore granted.

In this study we look at the years 2002 - 2005 because satellite data as well as flux and meteorology data were available for this time span. Processing of the flux data has been performed according to the standard CarboEurope methods (Reichstein et al., 2005; Papale et al., 2006, see section 2.1). In addition to GPP from the LaThuile data set we used half-hourly incident photosynthetically active radiation (included in LaThuile data set) and below canopy photosynthetically active radiation (bcPAR) data (available from principal investigator, i.e. Serge Rambal). bcPAR is calculated as an average of 14 upward looking PAR sensors installed at different places below the canopy. Incident PAR was measured with an upward looking PAR sensor mounted on the eddy covariance tower. We filtered the PAR values for measurement errors (i.e. reject PAR < 0 and standard deviation (bcPAR) > 600 μmol m^{-2} s^{-1}). As faPAR values we used estimates derived from half-hourly incPAR and below canopy PAR as well as the operational MODIS faPAR data.

We used soil moisture data to identify periods of water stress. The daily time course of soil water storage (mm) was simulated with a soil water balance model (Rambal, 1993) and further compared with monthly profiles of soil water con-

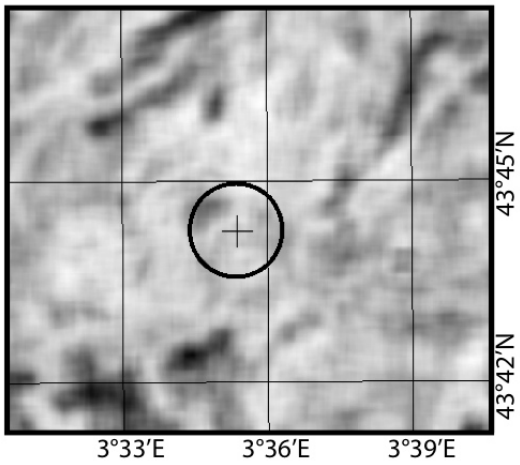

Fig. 3.1: *Entropy calculated for the red band of a Landsat ETM+ scene (13. Aug. 2001). The location of the Puéchabon flux tower is indicated by a cross. The circle marks the relatively uniform area in which a MODIS pixel containing the tower will be positioned (radius 1km + 300 m uncertainty). Light tone: high entropy, dark tone: low entropy.*

tent measured with a neutron probe and integrated over the rooting depth (c.a. 4.5m). The relationships between simulated and observed values showed very close agreement (r^2 = 0.87).

3.2.2 Benchmark ecosystem light use efficiency

In this pilot study, the light use efficiency (LUE) of an ecosystem is defined as the overall production of photosynthates per unit of absorbed photosynthetically active radiation. After Monteith (1972) this can be expressed as

$$GPP = LUE * faPAR * incPAR = LUE * aPAR \tag{3.2}$$

where GPP is gross primary productivity, PAR is incident photosynthetically active radiation, aPAR is the absorbed PAR, and faPAR is the fraction of PAR absorbed by the vegetation. LUE can either be seen as the ratio of GPP and aPAR or as the slope of a—possibly non-linear—function relating GPP to aPAR. To see whether differences arise from these two concepts, we used both as benchmarks to test the performance of several vegetation indices. The GPP values used in this context stem from the half-hourly eddy covariance data.

3.2.2.1 Light Use Efficiency solely based on site data

At the half-hourly scale, the fraction of absorbed photosynthetically active radiation (faPAR) was calculated as

$$faPAR = 1 - \frac{bcPAR}{incPAR} \tag{3.3}$$

We decided to use the more common term faPAR for what strictly speaking is the fraction of intercepted PAR (fIPAR) (Gower et al., 1999). Nighttime values (with incPAR $< 100\mu$mol m^{-1} s^{-1} and outliers were screened out. Outliers were identified within a moving window as

$$X < Q_1 - IQR \qquad \cup \qquad X > Q_3 + IQR \tag{3.4}$$

where X are the data tested for outliers, Q_1 and Q_3 are the first and third quartiles, and IQR is the interquartile range. The standard deviation in below canopy PAR of the discarded observations was three times as high as in the full data set. The filtered half-hourly faPAR was then multiplied with the quality checked half-hourly incident PAR to obtain absorbed photosynthetically active radiation (aPAR). Light use efficiency was subsequently calculated as the ratio of half-hourly GPP and half-hourly aPAR. As the LUE in this study is calculated as $\frac{\mu mol\, CO_2}{\mu mol\, photosynthetic\, photons}$, it is essentially a dimensionless quantity. We also tested whether it is more meaningful to aggregate the half-hourly data and hence minimise noise. Thus we applied moving average filters to the half-hourly GPP, incPAR, and faPAR values, with window sizes of 90, 150, and 210 minutes. LUE was calculated both as ratio of averaged GPP and original half-hourly aPAR and as ratio of averaged GPP and aPAR derived from averaged incPAR and faPAR. Light use efficiencies was also calculated as a daily ratio. Daily averages of the original quality checked GPP, incPAR, and bcPAR data were used to calculate first a daily average faPAR and then aPAR and LUE.

To see whether we can obtain a better grip on the diurnal variations, we calculated LUE as the slope of half-hourly GPP and aPAR. This variety of LUE was defined as the slope of a linear function fitted to the half-hourly GPP and aPAR values of each day. For 37 % of the days the goodness of fit (r^2) was less than 0.6, thus fitting a linear function to the half-hourly GPP and aPAR values of these days is somehow arbitrary. As this occurred predominantly in low LUE conditions we did not reject those slopes in order to avoid biasing the data. In case of negative slopes on some summer days with low midday GPP observations the slope was set to 0.

3.2.2.2 Light Use Efficiency based on site data and MODIS faPAR

Collection 5 MODIS faPAR (Myneni et al., 2002) was downloaded separately for the Terra and Aqua platform as ASCII subsets from the Oak Ridge National Laboratory DAAC website (http://www.modis.ornl.gov/modis/index.cfm). In these data sets each faPAR value is representative of a period of eight consecutive days. To reduce gaps we merged the Terra and Aqua data sets. Preliminary tests with the individual MODIS faPAR time series revealed that the MODIS product is prone to underestimating faPAR for this site compared to bcPAR/incPAR based estimates, especially in winter time. Thus, whenever two MODIS faPAR estimates were available for the same period, we kept the higher one for the combined data set. We calculated another version of LUE through dividing average daily GPP values by the product of the MODIS faPAR values and average daily incPAR.

3.2.2.3 Light Use Efficiency as obtained from the MODIS biome property look-up table (BPLUT)

To assess the performance of vegetation index-based LUE proxies we also calculated the LUE in the way it is operationally used in the MODIS GPP algorithm (Heinsch et al., 2003). In this approach, a biome-specific maximum light use efficiency is reduced by a vapour pressure deficit scalar and a minimum temperature scalar (c.f. section 4.1). These attenuation scalars are calculated from daily VPD and T_{min} based on linear ramp functions, the parameters of which are contained in the biome property look-up table (BPLUT). We used site measurements instead of the 1° by 1.25° NASA Data Assimilation Office (DAO) data routinely fed into the MODIS GPP algorithm to exclude mismatches between DAO and site meteorology as a source of error.

3.2.3 Remote sensing based estimates of light use efficiency

3.2.3.1 Acquisition and atmospheric correction of MODIS data

The processing of MODIS data for this study is based on the procedure described by Drolet et al. (2005). The pre-processing of the MODIS data that is not specific to this chapter is described in section 2.2.1.

To account for the variation in reflectance introduced by the way of processing, we tested 4 different modes of atmospheric correction: With the 6S model (Vermote et al., 1997) atmospheric correction was performed assuming uniform Lambertian reflectance. Moreover, a dark object subtraction (DOS) approach has been taken to correct the spectral data. We also included at-sensor-reflectances in the comparison, i.e. without any correction for atmospheric disturbance and geometric effects.

From preliminary experiments (c.f. 2.2.2) we know that the effect of BRDF correction on PRI is small compared to the effect of atmospheric correction. However, the impact of surface reflectance anisotropy on a MODIS-based PRI is difficult to assess precisely. The standard MOD43 product only contains BRDF-parameters for the "land bands", i.e. the spectral bands 1-7. The theoretical benefit resulting from correcting anisotropy effects is eroded by the additional uncertainties caused by unavailability of BRDF shape parameters from the same day, location, and spectral bands as the radiance data. As considering BRDF effects is known to improve the quality of NDVI (Bacour et al., 2006), we used 6S in the BRDF-correction mode prior to the calculation of NDVI and EVI. The data set with no atmospheric correction applied was subject to the same constraints as for the 6S-approach to arrive at the same number of samples.

In the DOS-case reflectance was calculated as

$$\rho = \frac{\pi(L_{sat} - L_{path})}{E_0 cos(\Theta_z) T_z} \tag{3.5}$$

where L_{sat} is the at-satellite radiance, E_0 is the exoatmospheric solar constant (contained within MOD021km), and Θ_z is the solar zenith angle. T_z is the atmospheric transmittance in the illumination direction, fixed at 1 in this case. The path radiance is estimated separately for each spectral band as

$$L_{path} = L_{sat,min} - 0.01(E_0 cos(\Theta_z) T_z)/\pi \quad (3.6)$$

The first step in retrieving L_{path} consisted in selecting all acquisition times when the pixel containing the tower is flagged as "confident clear", without cirrus clouds, heavy aerosol or shadows, and where the sensor zenith angle was no more than 40°. For scenes with flawless tower pixels the 25000 pixels with the smallest Euclidean distance to the tower-pixel were examined for contamination by cloud cover, shadows, aerosols or bad detectors. $L_{sat,min}$ was then defined as the average of the 500 pixels with the lowest radiance among the good quality pixels neighbouring the tower pixel. A more detailed description of dark object subtraction can be found in (Song et al., 2001).

The MODIS cloud mask does not allow the detection cloud cover or cloud shadows with absolute certainty. To rule these distortions out we only analysed at acquisition times where the diurnal curve of incident PAR (ground-based measurements) was near-perfect (c.f. section 2.1.3). We refer to this approach whenever we talk about cloud-free days in this study. The total screening left 439 acquisition times in case of the 6S approach (and "no correction") and 1145 acquisition times in case of the DOS approaches for further analysis. Due to increased cloud cover in winter the majority of usable image acquisitions occurs during the growing season.

3.2.3.2 Preparation of vegetation indices

In studies using field- or airborne spectrometers with high spectral resolution the PRI is defined as in equation 3.1. It is based on ρ_{531} (reflectance at 531 nm), which is sensitive to the epoxidation state of xanthophyll cycle pigments, and ρ_{570} (reflectance at 570 nm), being largely unaffected by short-term stress (Gamon et al., 1992).

MODIS-band 11 is centred at 531 nm (cf. Table 1.2). As the MODIS-sensor is not equipped with a spectral band centred at 570 nm, we tested bands 1 (620-670 nm), 4 (545-565 nm), 12 (546-556 nm), 13 low gain (662-672 nm), and 14 low gain (673-683 nm) as potential reference bands, in accordance with the proposition of Drolet et al. (2005, 2008). To obtain only positive PRI-values that compare better with the traditional vegetation indices, a sPRI was calculated (Rahman et al., 2004):

$$sPRI = (PRI + 1)/2 \quad (3.7)$$

A modification of sPRI has been computed for each of the 5 reference bands and each of the 3 modes of atmospheric correction. To compare the performance of the PRI as a proxy of LUE against the capability of well known vegetation indices

we calculated the normalised difference vegetation index (NDVI) (Tucker, 1979),

$$NDVI = \frac{\rho_{NIR} - \rho_{red}}{\rho_{NIR} + \rho_{red}} = \frac{\rho_{bd2} - \rho_{bd1}}{\rho_{bd2} + \rho_{bd1}} \tag{3.8}$$

and the enhanced vegetation index (EVI) (Huete et al., 1997),

$$EVI = 2.5 \cdot \frac{\rho_{NIR} - \rho_{red}}{\rho_{NIR} + 6 \cdot \rho_{red} - 7.5 \cdot \rho_{blue} + 1} \quad 2.5 \cdot \frac{\rho_{bd2} - \rho_{bd1}}{\rho_{bd2} + 6 \cdot \rho_{bd1} - 7.5 \cdot \rho_{bd3} + 1} \tag{3.9}$$

from reflectance data that were corrected for atmospheric and BRDF effects.

3.2.4 Modelling GPP

In the end, we would like to know which approach of estimating light use efficiency gives the best results when modelling GPP with equation 3.2. The light use efficiency term will be approximated by (a) the VI that correlates best with LUE and (b) the LUE derived from the MODIS biome parameter look-up table and local temperature and VPD measurements. For (a) we applied leave-one-out cross-validation by fitting a linear model to all but one VI-LUE pairs. This model was then used to calculate a LUE value from the left-over VI value. This LUE estimate was then multiplied with the matching aPAR value: GPP = LUE·faPAR·PAR = (a·VI+b)·faPAR·PAR. The relative difference of this modelled GPP value to the actually measured GPP was recorded. This procedure was repeated for every VI-LUE pair. For (a) we run one batch with reference LUE calculated as daily slope with only site data, for another batch we picked the LUE version with MODIS faPAR. With this cross-validation approach we reduced the risk of overfitting to the specific data available. We compared average values, mean absolute errors, and root mean squared error (RMSE). We used the modelling efficiency measure (ME, Janssen and Heuberger (1995)), which compares the relative improvement of the chosen model over the benchmark situation 'average of observed values':

$$ME = 1 - \frac{\sum_{i=1}^{n}(O_i - M_i)^2}{\sum_{i=1}^{n}(O_i - \bar{O})^2} \tag{3.10}$$

We had a closer look at dry (soil water content $<$ 100 mm) and wet periods (soil water content $>$ 200 mm).

3.3 Results

3.3.1 Comparing LUEs at different time scales

Multiple good quality MODIS image acquisitions rarely occur on the same day for the same location. Even if, any light use efficiency that could be estimated from

optical satellite data would still be a snapshot. The acquisition time can theoretically influence the ability to estimate daily LUE from satellite data. In summer time, the diurnal curve of GPP often displays a depression at midday, or GPP simply declines during midday and afternoon (data not shown). To check the effect of acquisition time on the estimation of daily LUE, we compared LUE calculated as half-hourly ratio against LUE calculated as daily ratio for all cloud-free days of 2002-2005. The potential image acquisition times of the Aqua and Terra satellite in the study area range from 10 a.m. to 2 p.m. For all half-hour time steps within this interval the linear fit between daily and half-hourly LUE yielded a correlation coefficient of at least 0.92 ($p<0.001$, example for 12:00 to 12:30 shown in Fig. 3.2). The linear functions relating the half-hourly and the daily LUE in each time interval are close to the 1:1 line (slope 0.86-0.97, intercept 0.0013-0.0023).

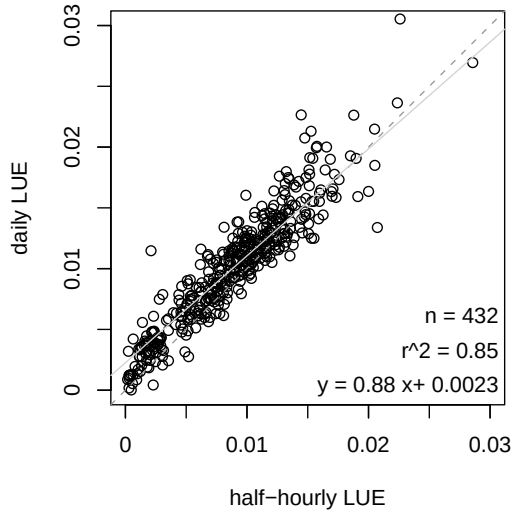

Fig. 3.2: *Comparison of half-hourly and daily light use efficiency (LUE) for 12:00 to 12:30 at cloud free days (i.e. potential satellite acquisition days). Equally good or better relationships are observed for the other half-hour intervals between 10 a.m. and 2 p.m.. The linear function fitted to the observations is shown by the continuous line, the 1:1 line is dashed.*

The relative similarity of half-hourly and daily LUEs is also revealed on an annual basis. While–naturally–some half-hourly LUEs exceed the daily LUE, the annual means are comparable and display the same interannual variations (Fig. 3.3, A). The 90^{th} percentile of daily LUE ranges between 0.0261 (2002) and 0.0230 $\frac{\mu mol\, CO_2}{\mu mol\, photons}$ (2002); this difference is equivalent to 11% of the 2002 value. The 90^{th} percentiles of all years exceed the maximum LUE given in the MODIS BPLUT for evergreen broadleaf forests (0.021 $\frac{\mu mol\, CO_2}{\mu mol\, photons}$). The LUE calculated according to the MODIS GPP algorithm does about represent the average LUE in non-summer months. However, during the summer months, a decline in LUE calculated from site GPP and aPAR can be observed that is not captured by BPLUT-based LUE (Fig. 3.3).

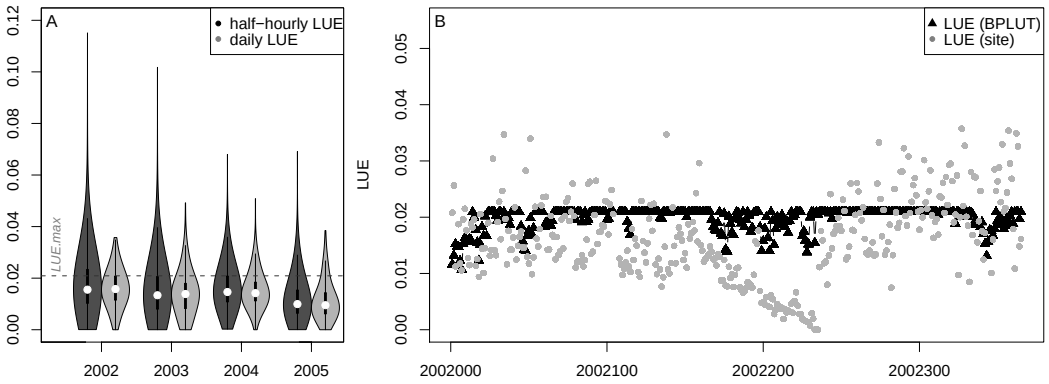

Fig. 3.3: *(A) Annual means and standard deviation of half-hourly and daily light use efficiency; LUE.max: maximum LUE for evergreen broadleaf forests according to MOD17 biome property look-up table (BPLUT) (B) BPLUT-approach does not capture LUE dynamics of the site, similar pattern for all years*

3.3.2 Strength of relationship between VIs and LUE, aPAR, and GPP

We then checked the correlation between 14 varieties of LUE and the vegetation indices, i.e. the sPRI with 5 different reference wavelength and 3 modes of atmospheric correction each, as well as the NDVI, and EVI. For each viewing-geometry constrained subset of observations we made sure that all VIs were available simultaneously. Whether we look at the full data set or constrain to certain sun-sensor geometries: the behaviour of LUE in the family of ratios at daily and sub-daily level is very consistent. Therefore only one representative is displayed in Fig. 3.4 A-E. In our study, the PRI with the broad reference band 1 yielded the best correlation with ecosystem LUE (r up to 0.78). However, we only achieved such a good correlation when constraining the dataset with respect to viewing geometry and when we did not apply atmospheric correction. In the following we will detail the effects of different constraints.

Looking at the whole dataset, only constrained as outlined in section 3.2.2 (Fig. 3.4 A, we find that the scaled PRI with the red reference bands (1, 13, 14) correlate best with the ground based LUE estimates ($r = 0.65$, $p<0.001$ for LUE calculated with MODIS faPAR, $n = 156$ samples). Choosing only observations made by either Terra or Aqua does change neither the strength of the correlation nor the slope of a linear function fitted to the LUE and PRI values (data not shown). The best relationship between a "traditional vegetation index" and LUE is $r \leq 0.43$, for NDVI with atmospheric (Lambertian) correction ($p<0.001$). For all sPRIs analysed, none of the atmospheric correction procedures tested does yield a significantly better correlation with LUE compared to sPRI calculated from top-of-atmosphere reflectances.

As a next step we only look at satellite data that are subject to backscatter conditions, that is to say where sun and sensor have $\leq 10^\circ$ difference in zenith angle and $\leq 60^\circ$ difference in azimuth angle. Because of these constraints and because we made sure that we compared vegetation indices from exactly the same obser-

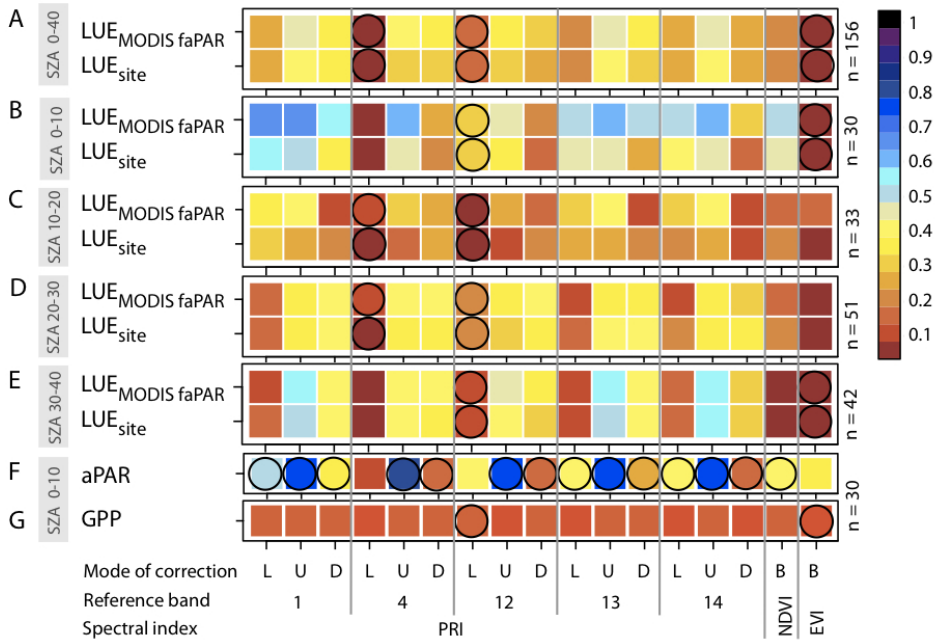

Fig. 3.4: *(A-E) Correlation between ground based light use efficiency estimates (LUE with faPAR from MODIS data and from interception measurements, c.f. section 3.2.2) and MODIS vegetation indices. (A) Sensor zenith angle (SZA) 0-40° (B) SZA 0-10° (C) SZA 10-20°, (D) SZA 20-30°, (E) SZA 30-40° (F) Correlation of aPAR and VI (G) Correlation of GPP and VI (F-G) constraints as for B. Black circles indicate negative correlation. The atmospheric correction modes are abbreviated with L (correction with 6S assuming Lambertian conditions), B (correction with 6S considering BRDF effects), U (uncorrected), and D (dark object subtraction).*

vation times, only six samples remained. For these 6 days, correlation between the remaining sPRI and LUE values does improve a lot (data not shown because of sample size). sPRI with reference band 14 yields the best correlation with LUE (r = 0.91, for LUE based on MODIS faPAR, followed by sPRI with reference band 13 and 1. For observations near backscatter direction atmospheric correction seems to be necessary to obtain a good relationship between the different sPRIs and LUE. Due to the small number of observations in this configuration we must be careful not to attach too much importance to this result. Neither NDVI nor EVI have a correlation with LUE to speak of.

Constraining the satellite data to sensor zenith angles (SZA) of $\leq$ 10°) or 30-40° increases the correlation between LUE and all vegetation indices compared to the complete data set (Fig. 3.4 B, E). The sPRI with reference bands 1, 13, and 14 perform similarly well regarding their correlation with LUE (r up to 0.79 for sPRI with reference band 1 and LUE based on MODIS faPAR, no atmospheric correction, p $<$ 0.001). In the subsets with 10-20° and 20-30° SZA the correlation between vegetation indices and LUE is comparable to the full data set, both in pattern and magnitude. For the viewing angle restricted data sets atmospheric correction does generally not improve the correlation. NDVI and PRI with reference band 1 at near-nadir SZA are the only exceptions.

On the whole, PRI without atmospheric correction correlates best with LUE. This pattern shows up again when correlating the VIs with absorbed PAR. The uncorrected sPRIs show a strong relationship with aPAR, this time negative (example for 0-10° SZA shown in Fig. 3.4 F). The correlation patterns of other LUE variations versus VIs do also correspond to the aPAR correlation patterns, albeit at a lower magnitude and only after selecting for narrow SZA (not all data shown). We observe no correlation between GPP and sPRI or the other VIs (Fig. 3.4 G). This pattern is consistent regardless of the constraints applied to the data set.

3.3.3 Ability of sPRI to track LUE over time

The sPRI with reference band 1(as well as the two narrow red bands) and no atmospheric correction (SZA 0-10°) does well in tracking the seasonal course of light use efficiency (Fig. 3.5 A). Especially, it picks up the decline in LUE during drought periods in the summer (Fig. 3.5 C). The best performing sPRI (reference band 1, no atmospheric correction, SZA 0-10°) yields a somewhat higher correlation with LUE than the best performing traditional vegetation index (NDVI, reflectances corrected with 6S assuming Lambertian behaviour, SZA 0-10°), that is r = 0.78, $p<0.001$ compared to r = 0.70, $p<0.001$ (Fig. 3.4). This relationship deteriorates when all available data in this range of SZA are considered, not only those where all vegetation indices are available simultaneously (Fig. 3.5). EVI is a far worse predictors of LUE. The PRI (and LUE) is minimal during summer droughts. Since the amount of incident PAR is maximum in summer, aPAR and PRI are inversely correlated (r = -0.86, $p <0.001$) for sPRI with reference band 1, no atmospheric correction, SZA 0-10° and daily aPAR; c.f. Fig. 3.4). All of the potential reference bands tested in this study are clearly influenced by the same forcing and show a distinct seasonal cycle. The changes within the ecosystem add to the effects caused for instance by viewing geometry and absorbed PAR and can be visualised as normalised ratios. As band 1 integrates over the wavelength of band 13 and 14 it is not surprising that they show the same temporal variation. The gaps in summertime result from saturation of the narrow red bands. These bands were designed with a higher sensitivity to monitor dark oceanic surfaces and are thus more likely to saturate over relatively bright terrestrial targets, especially when vegetation cover is not dense.

3.3.4 Modelling GPP

The VI selected as LUE-proxy in this analysis is the sPRI with reference band 1 and no atmospheric correction performed (constrained to near nadir viewing angles). PRI with reference band 1 was chosen over the PRIs with reference bands 13 and 14 because band 1 does rarely saturate and thus yields a higher data coverage. As shown in section 3.3.3, the PRIs with red reference bands otherwise behave very similar. Setting up a model with this sPRI and a site-data-only LUE yields a relative difference between modelled and observed GPP of 40.2% (median, n=49, c.f. Fig.

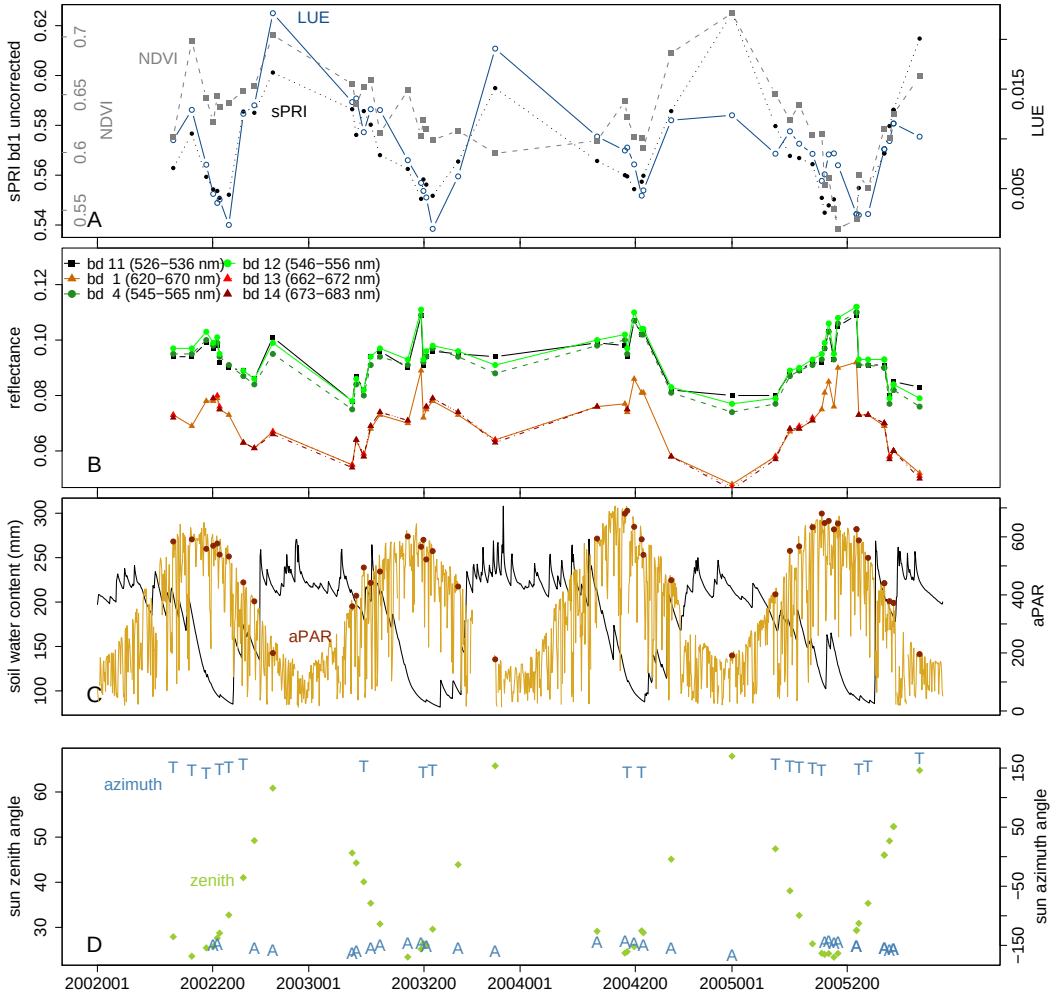

Fig. 3.5: *(A) Timeseries of LUE, best-performing PRI (reference band 1, no radiance correction), and best-performing other vegetation index (NDVI with BRDF correction) (B) Reflectances used for PRI calculation (no atmospheric correction) (A+B) Only observations with near-nadir viewing angles are shown (C) Cumulative water deficit as water stress indicator and daily aPAR averages (D) Sun zenith and azimuth angles during time of image acquisition (A+C) A = Aqua, T = Terra*

3.6, Table 3.1). When the GPP estimation is based on LUE with MODIS faPAR, the difference to the observed GPP is 50.6% (median, n=44). If GPP is modelled with the MODIS algorithm, the difference to the observed GPP is as large as 151% (median). To achieve comparability, we chose the same observation times as in the first set-up (n=49). With the look-up table approach GPP is severely overestimated during all satellite data acquisition times (near nadir viewing angles) and even more so during times of water stress (Table 3.2). In contrast, the discrepancy between observed GPP values and PRI-based GPP estimates during dry periods is not much different from periods with high water availability.

Tab. 3.1: *Comparison of GPP-models (c.f. section 3.3.4). The LUE for the two leftmost models was estimated from sPRI (reference band 1, no atmospheric correction, sensor zenith angle 0-10°), based on a regression of the other n-1 sPRI values against LUE estimates. In the model on the right, LUE is calculated from MODIS biome property look-up table (BPLUT) parameters and site meteorological data. Numbers are dimensionless or in $\mu molCO_2\ m^{-2}s^{-1}$ (*).*

		LUE from	
	site data only	site GPP & MODIS faPAR	BPLUT
number of obs.	49	45	44
avg. modelled GPP*	2.126	3.860	8.747
avg. observed GPP*	3.981	4.051	4.047
Mean absolute error*	2.088	1.390	4.752
RMSE*	2.3208	3.389	27.345
Modelling efficiency	-5.172·10^{32}	-1.034·10^{30}	-3.470·10^{32}

Tab. 3.2: *Average difference between observed and modelled GPP (cf. section 3.3.4, Table 3.1) in dry periods, well-watered periods, and the whole time series with standard deviation (in $\mu mol\ \ CO_2\ m^{-2}\ s^{-1}$). In parentheses: number of observations.*

LUE from:	ΔGPP_{dry}	ΔGPP_{wet}	ΔGPP_{all}
site data only	1.602±1.239 (14)	1.107±1.995 (11)	1.855±1.955 (49)
site GPP & MODIS faPAR	-0.120±1.276 (14)	-0.142 ±1.366 (11)	0.191±1.852 (45)
BPLUT	-6.230±1.443 (14)	-2.598±2.481 (10)	-4.596±2.396 (44)

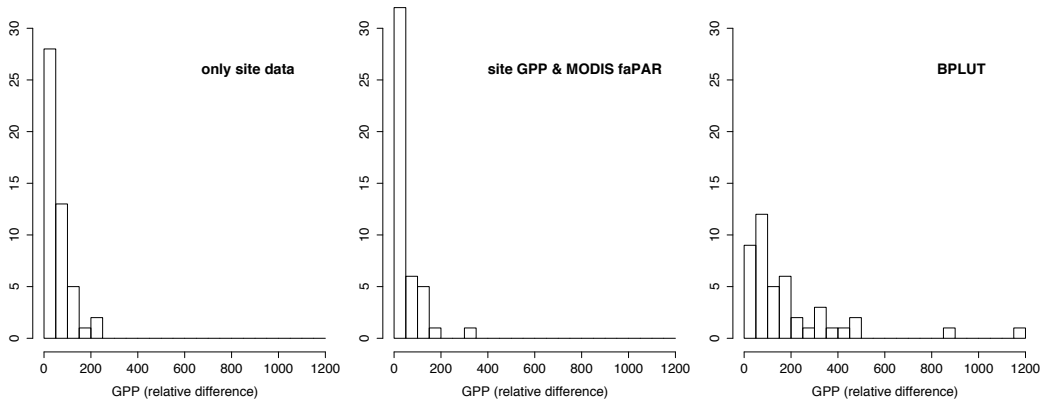

Fig. 3.6: *Relative difference (%) between observed GPP and GPP derived from n light use efficiency models. The LUE for the two leftmost models was estimated from sPRI (reference band 1, no atmospheric correction, SZA 0-10°), based on a regression of the other n-1 sPRI values against LUE estimates. In the right-hand model, LUE is calculated from MODIS biome property look-up table (BPLUT) parameters and site meteorological data.*

3.4 Discussion

3.4.1 Comparing LUEs at different time scales

We demonstrate specifically for a water-limited site that midday LUE on cloud-free days is a good proxy for daily LUE (Fig. 3.2). Other experimental evidence suggests that this relationship might be generally applicable. Sims et al. (2005) report a good relationship between midday and daily LUE on clear days (r = 0.85) for pooled data from a wide range of vegetation types. This was indirectly confirmed for a boreal deciduous forest where Drolet et al. (2005) found low variability in LUE on days useful for MODIS image acquisition. In this case, faPAR for LUE calculation was derived from tower measurements of NDVI. For pooled data from a Canadian boreal forest with different plant functional types and levels of disturbance, Drolet et al. (2008) found a strong relationship between midday and daily LUE (r = 0.96) on clear days (using MODIS faPAR). That we do not find strong differences in the PRI-LUE relationship for different LUE aggregation levels does fit in with this general picture.

The highest 90^{th} percentile of daily LUE per year within the study period amounted to 0.0261 (2002). This compares well with the maximum LUE in other semiarid ecosystems, for instance Sims et al. (2006) reported a maximum daily LUE of 0.02 for a relatively sparse Californian chaparral ecosystem. The site specific maximum LUE is subject to considerable interannual variability (Fig. 3.3). Within the 4 years analysed, the 90^{th} percentile varied by 11%. This indicates that MOD17-like models might improve their performance if parameters were optimised on an annual basis. The operational MOD17 maximum LUE for evergreen broadleaf forests was too low for the Puéchabon forest in the study period. Moreover, the MOD17 biome property look-up table (BPLUT) approach did not simulate the summer depression in LUE, although we used accurate on-site measurements of temperature and VPD. In principle, an optimisation of the MOD17 BPLUT parameters could reduce the discrepancy between modelled and actual LUE. In any case, the error In MOD17 GPP is likely to increase when the constraining environmental factors are extracted from global meteorology datasets. Also, for this particular site the complete water balance needs to be considered to model GPP accurately (unpublished results by Markus Reichstein). Considering soil water content might theoretically improve the situation but retrieving (deep) soil moisture on large spatial scales is not feasible. These results justify the search for alternative LUE estimates.

3.4.2 Strength of relationship between VIs and LUE, aPAR, and GPP

In this study, the red MODIS spectral bands (620-670 nm, 662-672 nm, 673-683 nm) turned out to be the most suitable reference bands for PRI (Fig. 3.4,3.4). The PRI with red reference bands was shown to be clearly more related to LUE than NDVI or EVI. This behaviour is as expected, it has been shown before that using NDVI results in an overestimation of productivity, especially in water limited

sites Running and Nemani (1988). When sampling the total set of satellite data for acquisitions within a narrow range of viewing angles, we found stronger relationships between all versions of PRI and LUE compared to the complete data set. This is especially true for near-nadir viewing angles and viewing zenith angles of 30-40°. Barton and North (2001) showed in a simulation study that the influence of soil background reflectance on PRI is significant for canopies with a leaf area index (LAI) below 3. The relatively sparse vegetation cover in the study area (leaf area index (LAI) just below 3) might thus give rise to a sensitivity of the PRI-LUE relationship to differences in viewing angle. We also need to keep in mind that the PRI, since it is observed from above, represents at best top-of-canopy conditions, not an average over the whole canopy. Some scatter in the LUE-PRI relationship is probably due to this fundamental difference between any optical remote sensing data and the eddy covariance based GPP estimates involved in the evaluation, which integrate over the whole canopy.

For a boreal deciduous forest Drolet et al. (2005) found a strong linear positive relationship between LUE and PRI with reference band 13 calculated from backscatter top-of-atmosphere reflectance(r = 0.87). A weaker relationship was found when using reference band 12 (r = 0.73). They found no significant correlation for the reference bands 1 and 4. Drolet et al. (2008) estimated ecosystem LUE for several Canadian boreal forest sites with different plant functional types and degrees of disturbance with MODIS bands 10, 12, 13, and 14 (488 nm, 551 nm, 667 nm, and 678 nm) as reference bands. Reference band 14 yielded the best correlation with LUE (r^2 = 0.70, pooled data). However, in that study no significant correlation was observed for the individual sites. In our study, PRIs formed with the narrow red bands 13 and 14 have about the same relationship to LUE as a PRI with the broader red band 1 (c.f. Fig. 3.4). Red might be generally useful as a reference band for MODIS based PRI.

Garbulsky et al. (2008) estimated LUE of an Italian *Quercus ilex* forest (leaf area index (LAI) = 3.5) with a MODIS-based PRI. Using at-sensor-radiance and band 12 for reference they found a good correlation (r = 0.78) for all cloud-free image acquisition days. The better performance of reference band 12 and the lower sensitivity to viewing geometry compared to the Puéchabon site might be due to the higher leaf area index (LAI) (3.5 compared to 2.8$\pm$0.4), and maybe also due to generally better water availability (Damm et al., 2002). The performance of the red bands at this closed-canopy stand was not published. For using a satellite-derived PRI at larger spatial scales it will be necessary to find out the optimal reference band under different conditions. If no universally applicable reference band can be identified, we would need to establish stratification rules.

In this study using top-of-atmosphere reflectance data for PRI calculation yielded the highest correlation with LUE for most viewing geometries. In the backscatter constellation, correction with 6S was better, although based on few data. Drolet et al. (2005) reported a similar phenomena. This suggests that the estimates of atmospheric optical thickness provided as MODIS product and/or atmospheric correction with 6S add uncertainty to the small PRI signal. The sampling frequency

and the range of viewing angles used to produce the MODIS atmospheric optical thickness product might be a limiting factor. Integrating data from other satellite missions might mitigate this problem. The simulation study performed by Barton and North (2001) suggests that the index is robust to variation in aerosol as the top-of-atmosphere PRI followed the ground PRI over a range of optical thickness. Their explanation is that the (original) bands are close in wavelength and so unlike Rayleigh scattering the aerosol effects are similar at both 531 and 570 nm. This reasoning is not so convincing when using a red reference band. Currently, we do not have an explanation why using uncorrected red bands gives nevertheless the best results.

3.4.3 Ability of sPRI to track LUE over time

The MODIS-based PRI with one of the reference bands 1, 13, or 14 and no radiance correction applied is able to track the seasonal course of LUE if the observations are constrained to narrow ranges of viewing angles. It is the first time this has been demonstrated for a severely water limited Mediterranean site. The constraints in viewing geometry probably limit the effect of anisotropy in surface reflectance. The remaining temporal variations in the PRI signal in the restricted data sets are better linked with variations in ecosystem LUE. It is likely that not only the xanthophyll-cycle pigment interconversions give raise to the changes in PRI but also seasonal changes in the concentration of xanthophyll cycle pigments. Xanthophyll levels, carotenoid concentrations in general, and chlorophyll levels relate to seasonal changes in vegetation productivity; the PRI signal has been shown to match these variations (Sims and Gamon, 2002; Stylinski et al., 2002; Sims et al., 2006). Filella et al. (2004) state that xanthophyll and carotenoid levels change with environmental conditions and thus also are indicators of photosynthetic downregulation under stress.

The NDVI did not track the decline in LUE as well as the PRI with reference band 1 (Fig. 3.5). Sims et al. (2006) gave one plausible explanation for this: compared to PRI the NDVI seasonal pattern is more sensitive to solar elevation angle effects. The relatively good correspondence between NDVI and LUE in the summer of 2005 compared to previous summers probably results from a caterpillar attack (Allard et al., 2008).

Gamon et al. (1992) tried different reference wavelength for sunflower canopies, 550 nm did not work well with the water stress experiments. Leaves of sclerophylly are less prone to wilting, hence the fraction of soil seen from sensor does not vary (due to wilting, but surely due to changes in viewing angle).

3.4.4 Modelling GPP

In this study, GPP models relying on PRI as an LUE proxy yielded considerably more agreement with observations than the MODIS GPP algorithm, especially

during dry periods. Both approaches were tested with site meteorological data (including incPAR) and MODIS faPAR, hence the differences in performance are not due to the quality of input data. Further research should address the performance of PRI based models with a more universal parameterisation (e.g. for all Mediterranean evergreen needleleaf forests).

Data from optical sensors such as MODIS are often cloud contaminated, temporal aggregations are used to increase the spatial coverage. Sims et al. (2005) documented that the inclusion of cloudy days leads to a large variation of LUE within the aggregation period and thus disturbs the relationship between midday LUE and LUE of the aggregation period. They suggest to estimate midday LUE from satellite data and to compute midday gross carbon fluxes from that. Then rather robust relationships between midday gross carbon flux and eight-day fluxes should be used to extrapolate to longer time periods.

3.4.5 General considerations

Overall, the Puéchabon *Quercus ilex* forest seems to be a suitable test case to study the performance of satellite based PRI in drought-prone areas. For this evergreen forest the PRI signal is not dominated by large seasonal variations in leaf area through senescence or strong wilting. Other semiarid ecosystems, for instance those with brevi-deciduous leaves and sparser canopy structure, can be less suitable for PRI studies (Filella et al., 2004; Sims et al., 2006). But also for the sclerophylly site studied here we can not exclude that the relationship between PRI and LUE in years with excessive drought might differ from years with normal droughts. Sims et al. (2006) observed such changes for a Californian chaparral ecosystem.

3.5 Conclusions

We found that MODIS PRI seems to be a useful estimator of ecosystem LUE, despite the influence of soil and other photosynthetically inactive material on the reflectance signal. This statement is valid during the whole growing season and also times of severe water deficiency. The light use efficiency at times of satellite data acquisition is close to the daily average of light use efficiency, thus PRI can be used to estimate daily LUE. The PRI with either of the three tested red reference bands is correlated best with on-site LUE. Given that the narrow red bands 13 and 14 are prone to saturation in summer and thus provide less useful observations, band 1 seems to be the best reference band for the evergreen oak forest studied here. Since the choice of reference band matters, we recommend to perform an independent careful screening for each new study area, or to look for a universally applicable reference band for MODIS-based PRI. NDVI and EVI were comparatively poor proxies of LUE. The relationship between PRI and LUE improves when the analysis is restricted to small ranges of viewing angles. Near nadir viewing

angles yield the best results. In the end, this study also demonstrates that GPP models relying on PRI as a LUE proxy correspond considerably better with observations than the MODIS GPP algorithm, especially when water is scarce.

CHAPTER 4

Remote sensing of light use efficiency in diverse ecosystems with MODIS-based PRI

Contents

Chapter summary

Several studies sustained the possibility that a photochemical reflectance index (PRI) directly obtained from satellite data can be used as a proxy for ecosystem light use efficiency (LUE) in diagnostic models of gross primary productivity. This modelling approach would avoid the complications that are involved in using meteorological data as constraints for a fixed maximum LUE. However, no unifying model predicting LUE across climate zones and time based on MODIS PRI has

been published to date. In this study, we evaluate the effectiveness with which MODIS-based PRI can be used to estimate ecosystem light use efficiency at study sites of different plant functional types and vegetation densities. Our objective is to examine if known limitations such as dependence on viewing and illumination geometry can be overcome and a single PRI-based model of LUE (i.e. based on the same reference band) can be applied under a wide range of conditions. Furthermore, we were interested in the effect of using different fraction of absorbed photosynthetically active radiation (faPAR) products on the in-situ LUE used as ground truth and thus on the whole evaluation exercise. We found that estimating LUE at site-level based on PRI reduces uncertainty compared to the approaches relying on a maximum LUE reduced by minimum temperature and vapour pressure deficit. Despite the advantages of using PRI to estimate LUE at site-level, we could not establish an universally applicable light use efficiency model based on MODIS PRI. Models that were optimised for a pool of data from several sites did not perform well.

4.1 Introduction

Sound estimates of gross primary productivity (GPP) are essential for an accurate quantification of the global carbon cycle and an understanding of its variability (Schulze, 2006). Many diagnostic models of primary productivity are based on a light use efficiency approach (Running et al., 2000; Yuan et al., 2007; Beer et al., 2010, e.g.).

All light use efficiency models represent photosynthetic assimilation of vegetation as a function of the amount of photosynthetically active radiation absorbed by plants (aPAR) (Monteith, 1972; Running et al., 2000). In these models, all environmental and biophysical constraints on the conversion of photo energy to plant biomass are aggregated in the term light use efficiency (LUE). GPP is thus calculated as:

$$\mathrm{GPP} = \mathrm{LUE} \times \mathrm{aPAR} \tag{4.1}$$

$$\mathrm{aPAR} = \mathrm{faPAR} \times \mathrm{PAR} \tag{4.2}$$

where faPAR is the fraction of absorbed photosynthetically active radiation . The simplicity of this approach, with little need for ancillary data, makes it possible to base these models on remote sensing products and meteorological fields (Hilker et al., 2008b; McCallum et al., 2009). Thus, an important prerequisite for application on the global scale is fulfilled.

It should be noted, although the definition of aPAR is clear, faPAR and incident PAR derived from different sources and can differ substantially (e.g. McCallum et al., 2010).

LUE is influenced by many factors and thus varies in space and time. Factors lim-

iting LUE include plant water availability and atmospheric water demand as well as temperature and plant nutrition. LUE is usually modelled by constraining a certain maximum LUE according to a set of environmental conditions (e.g. Running et al., 2000; Yuan et al., 2007; Horn and Schulz, 2010). The determinants of LUE and on which time-scales they act are only partially resolved. Among the main difficulties on the daily to annual time-scales are finding a suitable surrogate for ecosystem water limitation (Garbulsky et al., 2010) and the accuracy of the available meteorological data (Heinsch et al., 2006).

It is thus attractive to derive LUE directly from just one kind of satellite data, without relying on estimates of different meteorological variables. Two types of remotely sensed data are candidates for this: fluorescence and the photochemical reflectance index (PRI).

While studies using airborne fluorescence measurements had promising results, the signal-to-noise ratio needs to be improved to be useful for satellite-based observations; efforts are ongoing (Meroni et al., 2009b). The PRI combines reflectance at 531 nm (ρ_{531}) with a reference wavelength insensitive to short-term changes in light energy conversion efficiency (ρ_{ref}) and normalises it (Gamon et al., 1992; Peñuelas et al., 1995):

$$\mathrm{PRI} = (\rho_{531} - \rho_{\mathrm{ref}}) \,/\, (\rho_{531} + \rho_{\mathrm{ref}}) \tag{4.3}$$

The original PRI formulation by Gamon et al. (1992) used 550 nm as the primary reference band since, according to a study on sunflowers, it seemed least affected by changes in green canopy structure. It also had 531 nm and reference wavelength swapped compared to recent use (c.f. Eq. 4.3). Later studies noted that for leaf-level reflectance, 570 nm appears to normalise best for confounding effects like pigment content and chloroplast movement (Gamon et al., 1993a, 1995). Thus, 570 nm became the most widely used PRI reference band. Recently, Middleton et al. (2009) showed for a douglas fir forest that reference bands in the ranges 540–574 nm, 480–515 nm and 670–680 nm have a high correlation with foliage LUE. An overview on protocols used for PRI studies can be found in a review by Garbulsky et al. (2011).

PRI can be a useful proxy for LUE because changes in reflectance at 531 nm are a side effect of mechanisms that protect the photosynthetic system in the leaves from excess light by down-regulating carbon assimilation (for an extensive summary, see Middleton et al., 2009; Coops et al., 2010). PRI also correlates with the total content of carotenoid pigments (Stylinski et al., 2002), this needs to be considered when looking at seasonal changes in PRI.

At site level, PRI has been shown to give good estimates of LUE when derived from field spectrometers (Gamon et al., 1992), but also from airborne sensors (Nichol et al., 2000, 2002; Rahman et al., 2001). Recently, the MODIS sensor on TERRA and AQUA has also been used successfully at ecosystem scale (Rahman et al., 2004; Drolet et al., 2005, 2008; Garbulsky et al., 2008; Goerner et al., 2009; Xie et al., 2009). MODIS provides a useful temporal resolution, a band around 531 nm,

but not the reference band at 570 nm. Thus, the MODIS PRI has been based on several alternative reference bands. However, the PRI has some well known limitations (Grace et al., 2007). Multiple studies showed that the PRI signal is affected by the viewing and illumination geometry, including the fraction of sunlit and shaded leaves seen by the sensor, canopy structure, and background reflectance (Barton and North, 2001; Nichol et al., 2002; Suárez et al., 2008; Sims and Gamon, 2002; Louis et al., 2005; Drolet et al., 2008; Hilker et al., 2009; Middleton et al., 2009).

These difficulties, along with data access problems, might have hindered the evaluation of an LUE model based on MODIS PRI across space and time. So far it is unclear if one model can be applied at multiple sites. Also, the question remains whether one MODIS PRI reference band can be recommended for all sites, or if different reference bands have to be used depending on for example plant functional type and vegetation density.

Despite the fluctuations in illumination geometry, dimension of the surface area sensed by each instantaneous field-of-view and background reflectance at every site, the site level models based on MODIS PRI published so far yielded good agreement with observed LUE. That considerable potential exists for mapping LUE with a common model has also been shown by Drolet et al. (2008), who found a unifying model for eight sites in central Saskatchewan. These boreal sites are close to each other (within the confines of one satellite scene), hence they can be simultaneously monitored instead of by comparing data from different image acquisitions. The viewing geometry and atmospheric disturbance of the satellite signal is therefore similar. Consequentially, the next step is to evaluate PRI based models across sites and satellite scenes.

In this study, we evaluate the effectiveness with which MODIS-based PRI can be used to estimate ecosystem light use efficiency (LUE) at study sites of four distinct plant functional types and different vegetation densities. Our objective is to find out if the limitations can be overcome and a single PRI-based model of LUE (i.e. based on the same reference band) can be applied under a wide range of conditions. Furthermore, we were interested in how different faPAR products affect the in-situ LUE estimates which are used as ground truth.

4.2 Data and methods

4.2.1 Selection of study sites

To be able to properly evaluate the PRI-based LUE estimates, we conducted this study at a selection of sites from the FLUXNET LaThuile data set that provides the necessary gross primary productivity and site meteorology data (`www.fluxdata.org`).

Here, we focus on non-boreal forest/savanna sites with water stress during part of the year. Some sites have to be excluded because of too few valid PRI data. Such

Tab. 4.1: *Overview of the sites used in this study.*

Site code	Site name	Lat, Lon (flux tower)	Data used	PFT (dominant species)	LAI	References
ZA-Kru	Skukuza, Kruger National Park (South Africa)	−25.0197, 31.4969	2001–2003	Savanna (Combretum apiculatum, Sclerocarya birrea, Acacia nigrescens)	1 (area avg. trees, max.), 3 (within tree canopy, max.), 1 (herbaceous layer, avg.)	Scholes et al. (2001); Kutsch et al. (2008)
FR-Pue	Puechabon (France)	43.7414, 3.59583	2000–2006	evergreen broad-leaved forest (Quercus ilex L)	2.8 ± 0.4	Allard et al. (2008)
IT-Cpz	Castelporziano (Italy)	41.7052, 12.3761	2000–2006	evergreen broad-leaved forest (Quercus ilex L.)	3.2–3.8	Tirone et al. (2003)
US-MMS	Morgan Monroe State Forest (US)	39.3231, −86.4131	2000–2005	deciduous broad-leaved forest (sugar maple, tulip poplar, sassafras, white and red oak)	4.8	Schmid et al. (2000)
US-Me2	Metolius – intermediate aged ponderosa pine (US)	44.4523, −121.557	2003–2005	evergreen needle-leaved forest (Pinus ponderosa)	2.8 (overstorey), 0.2 (understorey)	Thomas et al. (2009)

data scarcity can be caused by frequent cloud cover or saturation of the satellite signal at sparsely vegetated sites. The largest limitation on the number of relevant sites is the size of the targeted ecosystem surrounding the flux tower. It must be large enough to contain the footprint of a $\geq 1 \times 1$ km MODIS pixel so that the flux tower footprint is representative of the remotely sensed footprint.

We thus conducted our analysis on 5 sites: two dry-summer subtropical evergreen broad-leaved forests, a site with vegetation typical for tropical savanna, a humid-subtropical deciduous forest and a dry-summer subtropical evergreen needle-leaved forest (see Fig. 4.1). A sixth site (Mitra) fulfilled the homogeneity criteria mentioned above but had to be discarded because to few satellite data were available, a consequence of frequent sensor saturation due the sparseness of vegetation. All years for which eddy covariance and MODIS data are available simultaneously were analysed (Table 4.1). Castelporziano is a borderline case regarding the extension of the target ecosystem. For this site, we discarded satellite scenes in which the pixel containing the flux tower is partially made of non-forest.

4.2.2 In-situ LUE

We define LUE as the effectiveness with which an ecosystem uses absorbed photosynthetically active radiation (aPAR) to produce photosynthates (recorded as

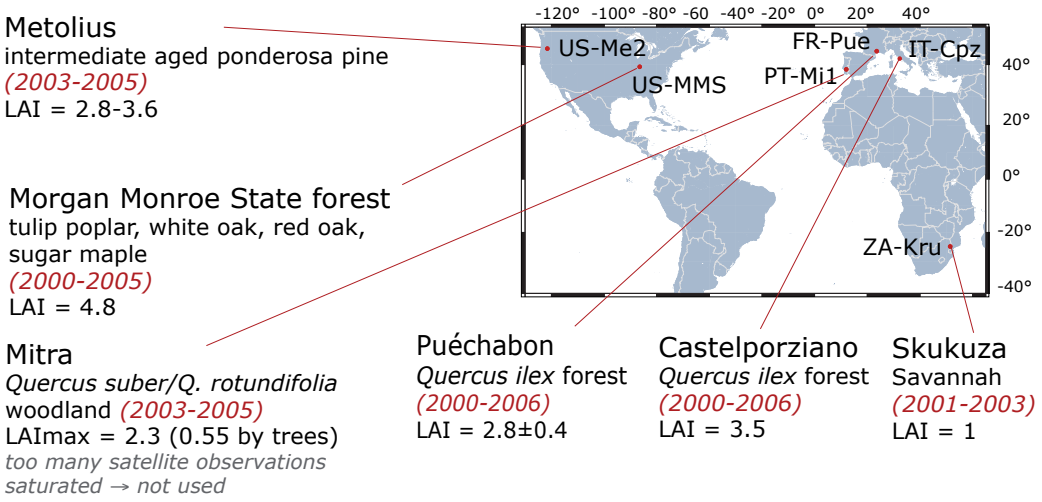

Fig. 4.1: *Map of non-boreal, drought-influenced sites from the FLUXNET La Thuille dataset, where the 1x1 km MODIS pixel including the tower is homogeneous.*

gross primary productivity, GPP):

$$\mathrm{LUE} = \frac{\mathrm{GPP}}{\mathrm{faPAR} \times \mathrm{PAR}} \tag{4.4}$$

We used daily and half-hourly GPP data derived from eddy covariance measurements, in-situ PAR measurements from the Fluxnet LaThuile data base, and different satellite based faPAR data sets. The eddy covariance data were processed using the standardised methodology described in Papale et al. (2006); Reichstein et al. (2005). We calculated aPAR as the product of available photosynthetically active radiation (PAR, here in the form of average daylight photosynthetic photon flux density—μmol m^{-2} s^{-1}) and the fraction of PAR that is actually absorbed by the vegetation (faPAR).

Since representative in-situ faPAR measurements are scarce, and considering potential application of the PRI model to a larger area, we used satellite based faPAR data to calculate aPAR. Readymade faPAR products are known to differ from each other (McCallum et al., 2010). To test the impact of product choice on the evaluation of the PRI-models we used three different faPAR sets: the MODIS collection 5 MOD15A2 and MYD15A2 products (`https://lpdaac.usgs.gov/lpdaac/products/modis_products_table/leaf_area_index_fraction_of_photosynthetically_active_radiation/8_day_l4_global_1km/mod15a2`) (2000–2006, 8-days-composite), the SeaWiFS-based faPAR of the Joint Research Centre (`http://fapar.jrc.ec.europa.eu`) (2000–2006, although much of the 2006 data were discarded because of poor quality flags, 10-days-composite) and the SPOT-Vegetation based Cyclopes faPAR product (Baret et al., 2007) (only available for 2000–2003, 10-days-composite). The faPAR data were quality checked and linearly interpolated to daily time steps, except for periods where no good data were recorded for longer than 19 days (equal to 1 missing value in

the aggregated SeaWiFS and Cyclopes products) or 23 days (equal to 2 missing values in the aggregates MODIS product). The light use efficiency calculated with these faPAR data is denoted as LUE_{MODIS}, $LUE_{SeaWiFS}$ and $LUE_{Cyclopes}$. For the US-Me2 site, no valid aPAR is contained in the Cyclopes data set throughout the study period.

4.2.3 Modelling LUE from MODIS based PRI

4.2.3.1 Acquisition and processing of MODIS reflectance data

For the study on multiple sites the pre-processing described in section 2.2.1 has been slightly changed. Instead of downloading the MOD35 cloud product the information needed for an initial cloud cover screening was taken from the MOD/MYD04 aerosol product.

Light reaching a satellite sensor after traveling trough the atmosphere is inevitably affected by scattering and absorption. In addition, natural surfaces reflect light differently subject to the viewing geometry. Ideally, data recorded by a satellite sensor should be corrected for these wavelength-dependent effects to make the reflectances computed from these records comparable. Albeit, from the pilot study (see chapter 3, Goerner et al., 2009) and preliminary experiments we know that correcting MODIS reflectances with bidirectional reflectance distribution function (BRDF) parameters from existing data bases either has no effect on the PRI signal (when using POLDER/PARASOL based parameters (Bacour and Bréon, 2005), see Fig. 2.2) or only seems to increase noise in the PRI signal (when using the MODIS MOD43 product, see Fig. 2.3). Additional doubt about the usefulness of correcting reflectance data for this study using ready made products is caused by the unavailability of a BRDF model and atmospheric parameters at the exact acquisition time and spatial resolution of the radiance data and some of the spectral bands listed in Table 1.2. Because the need for synchronous estimates of atmospheric parameters flagged as high quality also reduces the number of available observations, we chose not to correct specifically for atmospheric or surface anisotropy effects. To some degree, a correction is inherent in a ratio made of reflectances that are not too far apart in the visible part of the solar spectrum.

The MODIS cloud mask does not allow the detection of cloud cover or cloud shadows with absolute certainty. To rule out cloudiness, we visually checked for each day if the daily course of incident PAR (measured in-situ as Photosynthetic Photon Flux Density on half-hourly basis) follows an ideal curve. Acquisition dates at which the measured PAR at the flux towers notably differs from the PAR pattern during cloud free days at the same time of year were excluded from further analysis (see Fig. 2.1 for example).

Tab. 4.2: *Overview of abbreviations used for "in-situ" light use efficiency and for LUE modelled from vegetation indices (The models denoted with * were established for each site (for all MODIS viewing angles and also specifically for viewing angles $<10°$) as well as for all evergreen sites combined and the two evergreen oak sites combined.)*

Abbreviation	Explanation
LUE used for evaluation	
LUE_{MODIS}	light use efficiency calculated from site GPP, site PAR, and MODIS faPAR
$LUE_{SeaWiFS}$	light use efficiency calculated from site GPP, site PAR, and Joint Research Center (JRC) SeaWiFS faPAR
$LUE_{Cyclopes}$	light use efficiency calculated from site GPP, site PAR, and Cyclopes faPAR
*LUE modelled from vegetation indices, general scheme**	
$LUE_{PRI_{X,\ Y}}$	LUE modelled from regression between PRI_X (i.e. with reference band X) and LUE_Y
LUE modelled from vegetation indices, example	
$LUE_{PRI_1,\ SeaWiFS}$	LUE modelled from regression between PRI_1 and $LUE_{SeaWiFS}$
LUE_{PRI}	LUE modelled from regression between PRI and observed LUE (summary term for multiple models)
$LUE_{NDVI,\ MODIS}$	LUE modelled from regression between NDVI and LUE_{MODIS}
LUE calculated using look-up table and site meteorology	
LUE_{MOD17}	LUE calculated from biome specific MOD17 parameters and site Tmin, VPD
$LUE_{MOD17,\ opt}$	LUE calculated from optimised biome specific MOD17 parameters and site Tmin, VPD

4.2.3.2 Preparation of vegetation indices

The standard configuration of the PRI (Eq. 4.3) has to be adapted to the spectral bands available on MODIS (Drolet et al., 2005). The MODIS band 11 is centred at 531 nm (cf. Table 1.2). As the MODIS-sensor is not equipped with a spectral band centred at 570 nm, we tested bands 1 (620–670 nm), 4 (545–565 nm), and 12 (546–556 nm) as potential reference bands, in accordance with the proposition of Drolet et al. (2005, 2008). A modification of PRI has been computed from top-of-atmosphere reflectances for each of the 4 reference bands, denoted by PRI_1, PRI_4. PRI_{10}, and PRI_{12}. We compared the performance of the PRI as a proxy of LUE against what can be achieved with a well known broadband vegetation index. The NDVI is known to respond to changes in biomass, but also chlorophyll content as well as leaf water stress (Myneni et al., 1995; Treitz and Howarth, 1999). The

index is hence useful to see which part of the variation in LUE can be explained already by factors other then changes in the composition of xanthophyll pigments. We calculated the NDVI (Tucker, 1979) from reflectance data:

$$\mathrm{NDVI} = \frac{\rho_{\mathrm{NIR}} - \rho_{\mathrm{red}}}{\rho_{\mathrm{NIR}} + \rho_{\mathrm{red}}} = \frac{\rho_{\mathrm{bd2}} - \rho_{\mathrm{bd1}}}{\rho_{\mathrm{bd2}} + \rho_{\mathrm{bd1}}} \tag{4.5}$$

4.2.3.3 Empirical PRI-based LUE models

Exponential relationships between observed LUE ($\mathrm{LUE}_{\mathrm{MODIS}}$, $\mathrm{LUE}_{\mathrm{SeaWiFS}}$, $\mathrm{LUE}_{\mathrm{Cyclopes}}$) and PRI were explored with Bayesian hierarchical models. Models were established separately for each version of PRI with data binned as follows:

- observations from all evergreen sites combined (i.e. FR-Pue, IT-Cpz, US-Me2; separate models for NDVI, PRI_1, PRI_2. PRI_{10} and PRI_{12}),
- observations from the two evergreen broad-leaved sites combined (i.e. FR-Pue, IT-Cpz; also separate models for each vegetation index),
- one site specific model (for sensor viewing zenith angles $\leq 40°$), this results in five models per vegetation index,
- separate bins for each range of viewing zenith angles (0–10°, 10–20°, 20–30°, 30–40°) for each site, this results in 20 models per vegetation index.

Results for all those viewing angle bins are listed in the appendix. In the following we will only show outcomes for the complete range of viewing angles and near-nadir observations (0–10°). The variance explained with models fitted to the other bins lies in between those two. Table 4.2 gives an overview of how observed and modelled light use efficiencies are denoted in this study.

4.2.4 LUE modelled from Tmin, VPD and plant functional type

For benchmarking the performance of vegetation index-based LUE proxies, we also calculated the LUE in the way it is operationally used in the MODIS GPP algorithm (Heinsch et al., 2003). In this approach, a biome-specific maximum light use efficiency is reduced by a vapour pressure deficit scalar and a minimum temperature scalar. These attenuation scalars are calculated from daily daylight VPD and Tmin based on linear ramp functions, the parameters of which are contained in the biome property look-up table (BPLUT).

$$\mathrm{LUE}_{\mathrm{MOD17}} = \mathrm{LUE}_{\mathrm{max,\ BLUT}} \times \mathrm{f}(\mathrm{VPD}) \times \mathrm{f}\,(Tmin) \tag{4.6}$$

We computed $\mathrm{LUE}_{\mathrm{MOD17}}$ using the standard MOD17 parameters and $\mathrm{LUE}_{\mathrm{MOD17.opt}}$ using parameters that have been optimised per site and year by Enrico Tomelleri (see section on LUE models in the Supplement of Beer et al., 2010).

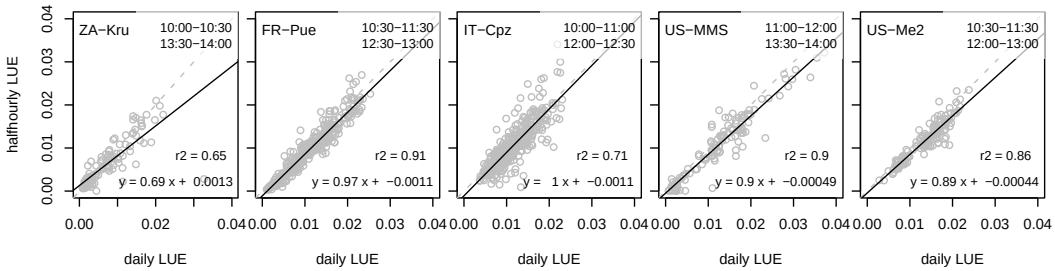

Fig. 4.2: *Comparing daily and half-hourly light use efficiency (based on MODIS faPAR) for all the cloud free times where MODIS PRI is available. The times of MODIS overpass are given in the upper right corner of each* panel.

As this study is concerned with the site level, we use for both $\mathrm{LUE}_{\mathrm{MOD17}}$ and $\mathrm{LUE}_{\mathrm{MOD17.opt}}$ site measurements of VPD and Tmin from the Fluxnet LaThuile data set instead of the 1° by 1.25° NASA Data Assimilation Office (DAO) data routinely fed into the MODIS GPP algorithm.This way we also exclude uncertainties in the DAO meteorology as an additional source of error.

4.3 Results

4.3.1 Are LUEs at times of MODIS overpass representative for the whole day?

The MODIS sensors operate sun-synchronous, i.e. images are only acquired within a certain window of local time (morning through midday on the Terra platform, midday through afternoon on the Aqua satellite). As a first step in our analysis, we checked if the LUE at time of satellite overpass is representative for the whole day. For the five sites in this study, half-hourly $\mathrm{LUE}_{\mathrm{MODIS}}$ during the time of MODIS overpass can explain 65% (ZA-Kru) through 92% (FR-Pue) of the variability in daily $\mathrm{LUE}_{\mathrm{MODIS}}$ (c.f. Fig. 4.2). The slope of the regression line between half-hourly and daily LUE for ZA-Kru has the strongest deviation from the 1:1 line. Midday LUE at ZA-Kru is lower compared to other sites, while LUE in the late afternoon and evening is on average higher than at the other sites (c.f. Fig. 4.4). This might be due to differences in moisture limitation. The atmospheric moisture demand increases during middays stronger than at the other study sites (c.f. Fig. 4.3).

The relationship between halfhourly and daily LUE remains the same when using other faPAR products. This justifies the use of PRI “snapshots” to estimate daily LUE.

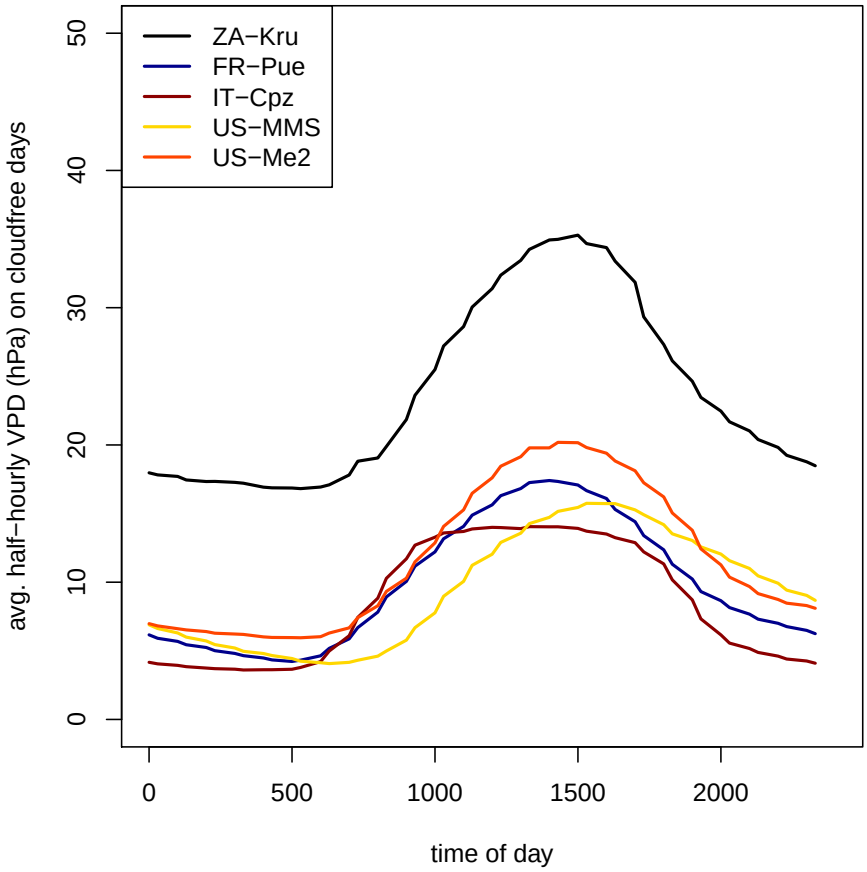

Fig. 4.3: *Average diurnal course of vapour pressure deficit (VPD) at the study sites.*

4.3.2 Which MODIS-PRI version suits which setting?

In the next step of our analysis, we only use $\text{LUE}_{\text{MODIS}}$ to evaluate the different modelled LUEs and to figure out which PRI configuration is most useful for which site. Afterwards, the effect of using different faPAR products is scrutinised using only the best suited PRI reference bands.

As an example for the relationship between PRI and LUE, Fig. 4.5 shows PRI_1 and $\text{LUE}_{\text{MODIS}}$ for all five studies sites as well as for the combined evergreen and oak models (c.f. Sect. 4.2.3.3). We chose exponential functions to avoid negative modelled LUEs. The divergences between the fitted models become already apparent in this example. Taking into account the known uncertainties introduced by flux data processing—in this case by comparing two different flux partitioning methods does not change this pattern (see Fig. 4.6 & section 2.1.2).

For all LUE modelled site-specific based on PRI and NDVI, the correspondence with $\text{LUE}_{\text{MODIS}}$ is better for near-nadir observations than for all observations together (c.f. R^2s in Fig. 4.7).

$\text{LUE}_{\text{MODIS}}$ can be modelled properly based on PRI for the savanna site ZA-Kru

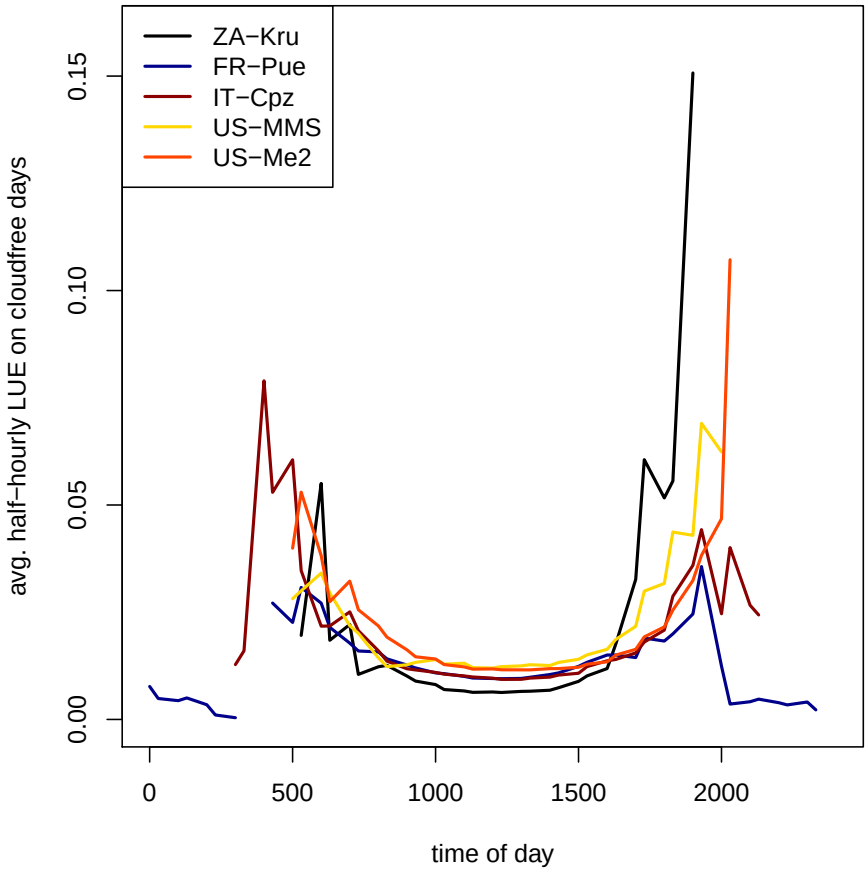

Fig. 4.4: *Average diurnal course of light use efficiency (LUE) at the study sites.*

(R^2 for near nadir observations [R^2_{nadir}] = 0.78, R^2 for all observations [R^2_{all}] = 0.49) and for the deciduous broad-leaved forest site US-MMS ($R^2_{\text{nadir}} = 0.71$, $R^2_{\text{all}} = 0.46$). $\text{LUE}_{\text{MODIS}}$ can be reasonably well modelled for the two evergreen oak forest sites (FR-Pue: $R^2_{\text{nadir}} = 0.57$, $R^2_{\text{all}} = 0.45$; IT-Cpz: $R^2_{\text{nadir}} = 0.43$, $R^2_{\text{all}} = 0.44$). The modelling of $\text{LUE}_{\text{MODIS}}$ for the evergreen needle-leaved forest US-Me2 is less successful using PRI ($R^2_{\text{nadir}} = 0.37$, $R^2_{\text{all}} = 0.2$, see also the table in the Supplement).

The optimal reference band for the PRI differs between sites. For three sites with completely different characteristics, $\text{LUE}_{\text{PRI}_1,\ \text{MODIS}}$ with a site-specific model explains most of the variability in daily $\text{LUE}_{\text{MODIS}}$ (ZA-Kru, FR-Pue, US-MMS). PRI_4 is most suitable for modelling LUE at IT-Cpz. $\text{LUE}_{\text{PRI}_{12},\ \text{MODIS}}$ works best at the US-Me2 site.

4.3.3 Can LUE estimation from MODIS-PRI be generalised?

Ideally, a model of light use efficiency would be parameterised once for all possible cases, or for well defined categories, and could then be applied to other location in the same range of environmental conditions. When applying the model that

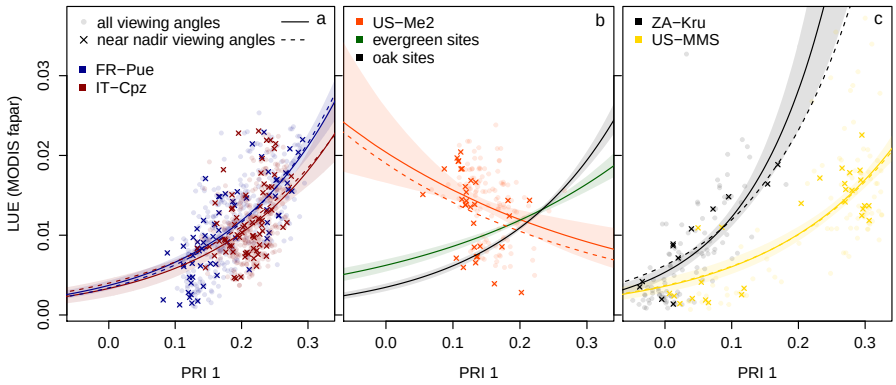

Fig. 4.5: *Light use efficiency (based on MODIS faPAR) versus PRI based on reference band 1 with exponential models fitted to the observations. The shaded areas represent the 95% Bayesian confidence interval. For each site, two different models were calculated. One is using all available observations (solid lines) and the other only observations with near nadir sensor viewing angles (0–10°, dashed lines). In addition, the combined models for evergreen sites (FR-Pue, IT-Cpz, US-Me2) and oak sites (FR-Pue, IT-Cpz) are shown (panel c).*

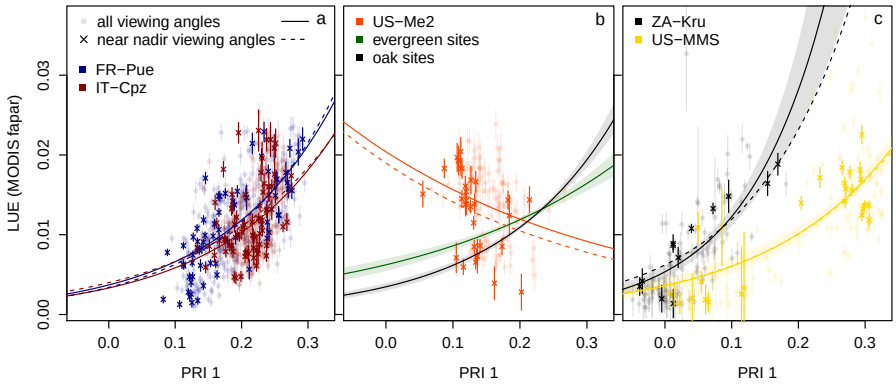

Fig. 4.6: *Corresponds to Fig. 4.5. The error bars represent twice the mean difference in LUE between partitioning based on nighttime or daytime data (c.f. section 2.1.2).*

has been established for the pooled evergreen-site observations at site level, the correspondence with observed LUE values is low (c.f. Figs. 4.5b, 4.7, 4.8) as it can be expected for sites of different plant functional type and location. Even when parameterising a model for the two evergreen broad-leaved forest sites with the same dominant species, the explained variability is low.

4.3.4 How does LUE modelled from MODIS-PRI compare to other LUE models?

Of course, estimating LUE from PRI would not be justified if the same or a better accuracy can be achieved with models/data that are already operational.

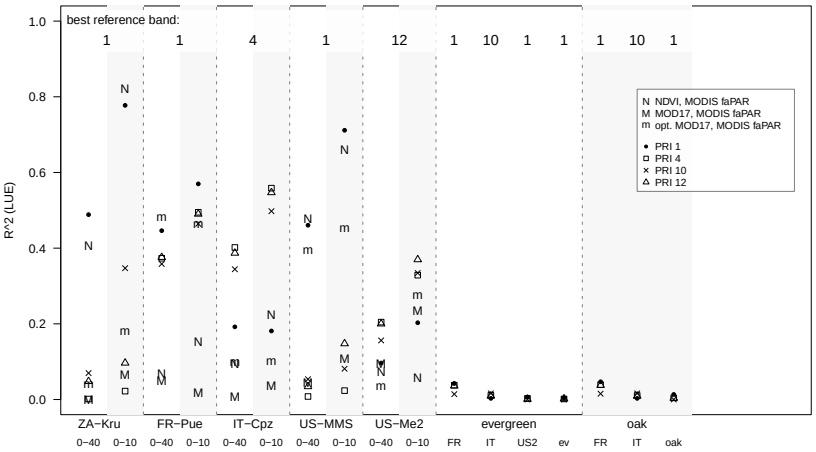

Fig. 4.7: R^2 *of modelled LUE vs.* LUE_{MODIS} *for two ranges of sensor viewing zenith angle: 0–40° and 0–10°. The most suitable reference band for each site is displayed at the top. The same pattern appears when using the root mean square error (not shown).*

$LUE_{NDVI,\ MODIS}$ resulted only for the two sites with high deciduousness in a slightly better agreement with observed LUE: for near-nadir observations in ZA-Kru, and when using all observations in US-MMS. The differences in R^2 to the best LUE_{PRI} are only 0.03% and 0.2% (c.f. Fig. 4.7, Table in the Supplement).

For the sites we have studied, LUE_{MOD17} has in every setting much less agreement with observations than LUE_{PRI}. $LUE_{MOD17,\ opt.}$ performs much better, though not superior to LUE_{PRI} except at FR-Pue with MODIS viewing angles ranging from 0–40°. The agreement between $LUE_{MOD17.opt}$ and the reference LUE increases slightly (without changing any of the statements above) when using faPAR from MODIS collection 4 instead of 5 to calculate LUE_{MOD17} because the MOD17 parameters have been optimised based on collection 4 data (not shown). Note that, while benchmarking with LUE_{MOD17} and $LUE_{MOD17.opt}$ provides an additional point of reference, the main evaluation is performed with in-situ LUE.

4.3.5 Which influence does the choice of an faPAR product have on PRI evaluation?

For the deciduous forest site (US-Me2), the choice of faPAR product does not influence the relationship between observed and modelled LUE. The temporal dynamics of both the MODIS and SeaWiFS faPAR are very similar, Cyclopes faPAR is not available for this site.

The strongest faPAR induced difference in fit between models and observations occurs at the deciduous broad-leaved US-MMS forest. There, using MODIS faPAR results in the best fit. Cyclopes faPAR for US-MMS shows a too gradual decrease in autumn/winter and a too early (but at the same time too slow) increase in spring. In contrast, the SeaWiFS faPAR seems to have too steep increases and decreases and the beginning and end of the growing seasons (data not shown).

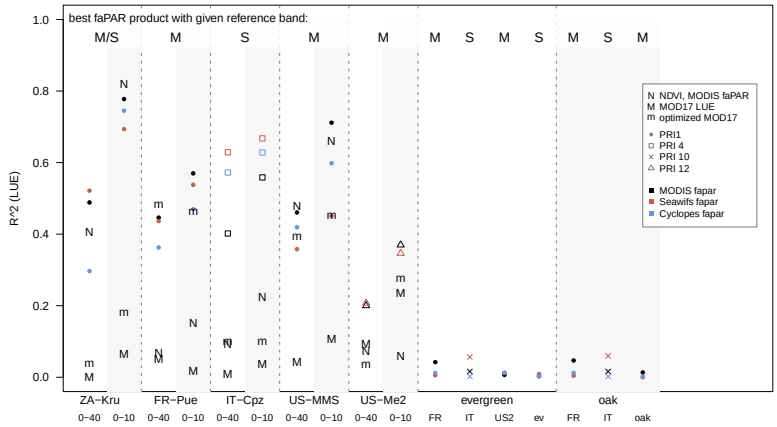

Fig. 4.8: R^2 *of modelled vs. observed LUE using PRI with the best reference band for each site to find out the most suitable faPAR product for each setting. At each site, two ranges of sensor viewing zenith angle are shown: 0–40° and 0-10°. The best faPAR product for a given reference band is denoted with M (MODIS MOD15) and S (JRC SeaWiFS faPAR).*

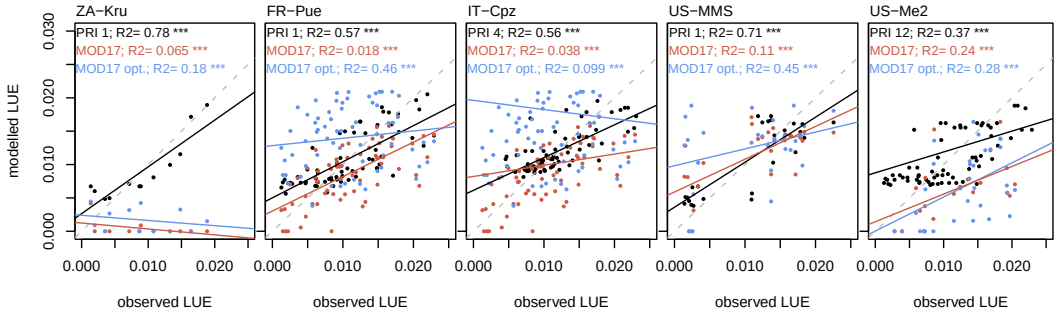

Fig. 4.9: *LUE modelled from PRI (black), from MOD17 parameters (red), and from optimised MOD17 parameters (blue) versus ecosystem LUE calculated from fluxes and MODIS faPAR. Shown are only points for which a near-nadir PRI observation exists for the respective study site. Significance codes: p value* $\leq$ *0.001:* $\star\star\star$*; p value* $\leq$ *0.01:* $\star\star$

In contrast with the other two faPAR products, Cyclopes faPAR at the ZA-Kru savanna site has a lower amplitude and does not seem to track the beginning and end of the growing season properly (concluded from comparing faPAR and GPP time series, data not shown). This might be the reason of the poor agreement between model and observation for the Cyclopes based LUE. SeaWiFS faPAR captures the length of the growing season for this savanna site well, which might be the reason for the higher agreement when using this faPAR product.

At the FR-Pue evergreen oak forest, both the MODIS and the SeaWiFS faPAR product show hardly any seasonality. This is probably why, despite MODIS faPAR having higher absolute values, choosing one or the other faPAR product has no influence on model fit. Cyclopes faPAR for the FR-Pue site has higher values in winter. The model fit is worse when LUE is based on Cyclopes faPAR.

At the other evergreen oak forest, IT-Cpz, using SeaWiFS faPAR instead of the other faPAR products to calculate in-situ LUE results in a higher agreement with

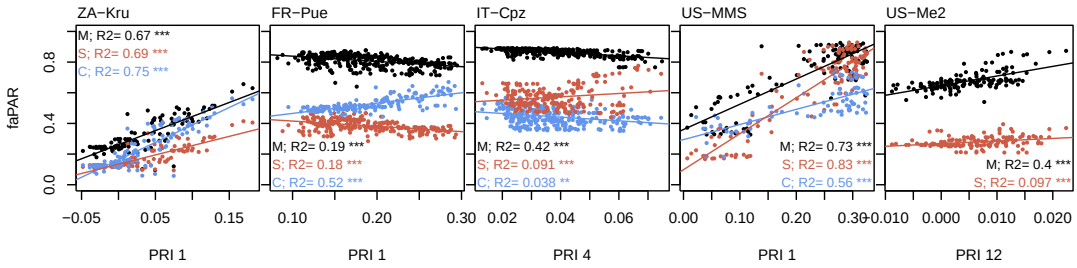

Fig. 4.10: *Scatterplots with R^2 of faPAR from different products (Black: MODIS – M), Red: SeaWiFS – S, Blue: Cyclopes – C) vs. PRI with site-specific most suitable reference band. Significance codes: p value $\leq$0.001: $***$; p value $\leq$0.01:$**$*

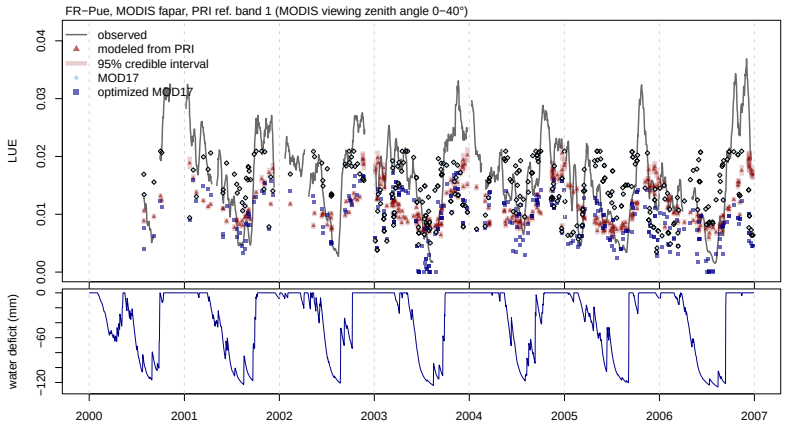

Fig. 4.11: *Top: Time series of observed LUE as 14-day moving average (based on MODIS faPAR) and modelled LUEs (exponential model based on PRI with reference band 1, MOD17, and optimised MOD17) at the FR-Pue site. Bottom: Water deficit in mm (calculated from field capacity and in-situ soil water content measurements).*

LUE_{PRI} (c.f. Fig. 4.8). A reason might be that the MODIS faPAR algorithm depends on proper biome classification and biome-specific canopy structures and soil patterns (McCallum et al., 2010).

4.3.6 Influence of vegetation structure on the PRI signal

For the deciduous sites (ZA-Kru and US-MMS), the MODIS photochemical reflectance index can be estimated from faPAR (see Fig. 4.10). The intra-annual changes in MODIS PRI are related to the temporal dynamics of total leaf area.

The fraction of PAR absorbed by the vegetation at the evergreen sites shows little seasonal variation compared to the changes in PRI. Thus, for these sites the changes in PRI cannot be explained by variation in faPAR. This suggests that the changes in PRI in those evergreen sites are more a result of changes in leaf pigment composition rather than structural changes.

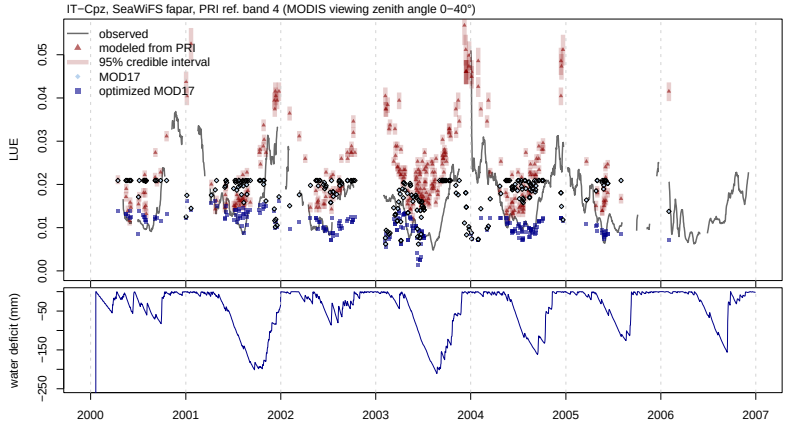

Fig. 4.12: *Top: Time series of observed LUE as 14-day moving average (based on SeaWiFS faPAR) and modelled LUEs (exponential model based on PRI with reference band 4, MOD17, and optimised MOD17) at the IT-Cpz site. Bottom: Water deficit in mm (calculated from water balance).*

4.3.7 Sensitivity of the different modelled LUEs to seasonal and interannual variability

The modelling approaches detailed in this study (c.f. Sects. 4.2.3.3, 4.2.4) differ in how well they are capable of reproducing annual and interannual variations in LUE.

At the evergreen oak site FR-Pue, $\mathrm{LUE}_{\mathrm{PRI}_1}$ does capture the seasonal dynamics, including the decline in LUE during summer drought, but not the interannual variability (c.f. Fig. 4.11). The observed LUE decline in summer is more pronounced during the 2003 heat wave, while the $\mathrm{LUE}_{\mathrm{PRI}_1}$ amplitude is similar to other years.

$\mathrm{LUE}_{\mathrm{MOD17}}$ is less capable of capturing the summer depression than the PRI based model. $\mathrm{LUE}_{\mathrm{MOD17.opt}}$ reproduces the minimum of summer depression well, but the modelled summer depression is much longer than observed.

At the other evergreen oak site, IT-Cpz, no distinct interannual variability is observed. The seasonal cycle is captured well by $\mathrm{LUE}_{\mathrm{PRI}_4}$ (c.f. Fig. 4.12). Depending on the faPAR product used for the in-situ LUE, LUE is severely over- or underestimated by $\mathrm{LUE}_{\mathrm{MOD17}}$, the seasonal cycle is not well reproduced. $\mathrm{LUE}_{\mathrm{MOD17.opt}}$ shows a dampened seasonal cycle and in general underestimates LUE.

At US-MMS the time series has gaps during cloud cover in winter time, but there are still enough observations and PRI data to estimate the annual minimum in LUE. There is a peak in observed LUE in summer 2002 that is not reproduced by $\mathrm{LUE}_{\mathrm{PRI}_1}$, otherwise the seasonality is tracked well (not shown). $\mathrm{LUE}_{\mathrm{MOD17}}$ does not match the LUE observations in spring and autumn, while $\mathrm{LUE}_{\mathrm{MOD17.opt}}$ underestimates the LUE peak in summer.

The evergreen needle-leaf site (US-Me2) possesses a low seasonal variability of LUE. The small fluctuations that are observed are neither well simulated by

LUE_{PRI}, nor by LUE_{MOD17} or $LUE_{MOD17.opt}$ (not shown).

The short LUE time series of the savanna site is mimicked well by the PRI model, apart from an overestimation in 2002 and some missed nuances (not shown). LUE_{MOD17} and LUE_{MOD17} values underestimate LUE observations, except for the southern-hemisphere winter in 2002, when the observed LUE is low compared to other years.

4.4 Discussion and conclusions

We conclude that in general estimating LUE at site-level based on PRI reduces uncertainty compared to the other approaches we tested. There is only one set of LUE observations which can be slightly better approximated by an LUE model based on VPD and Tmin than by LUE_{PRI}: the 0–40° viewing zenith angle FRPUE data (c.f. Figs. 4.7, 4.8). Note that this LUE is not derived from the standard MOD17 parameters, but from parameters that have been optimised per site and year. This indicates that, at site level, MODIS-based PRI is very competitive as a proxy for light use efficiency.

It is apparent that fine-tuning maximum light use efficiency as well as the VPD and Tmin parameters improves the performance of MOD17 type models of LUE (and ultimately GPP). However, our results support the growing body of evidence suggesting that Tmin and VPD alone are not sufficient to characterise temporal LUE (and hence GPP) dynamics due to i.e. drought stress (Kanniah et al., 2009b; Maselli et al., 2009; Garbulsky et al., 2010). Soil water availability determines stomatal conductance (Rambal et al., 2003) and hence productivity to a large extent and must be considered in LUE models that constrain a maximum LUE with environmental variables. Soil water estimates are difficult to obtain over larger regions. Estimates derived from remote sensing data are still poor, especially for forests (Guglielmetti et al., 2008). Surrogates of soil water content based on evapotranspiration and precipitation could be a viable alternative Leuning et al. (2005); Coops et al. (2007). Remotely sensed indices of vegetation water content such as the land surface water index (Xiao et al., 2005) or surface temperature might also help to obtain the seasonal variations of LUE in models that determine photosynthetic efficiency from environmental stresses (Hilker et al., 2008b). For these approaches, constraints due to different image acquisition geometries must also be considered.

For the South-African savanna site and the humid subtropical deciduous broadleafed forest (US-MMS), the accuracy of LUE modelled from NDVI is comparable to that of LUE_{PRI}. At both sites, vegetation greenness and faPAR (as well as leaf area) are intrinsically linked to CO_2 exchange. Hence NDVI and faPAR display similar seasonal dynamics as light use efficiency (Garbulsky et al., 2011). The PRI signal in general is influenced both by changes in vegetation structure and by changes in pigment composition. Unsurprisingly, the gain in accuracy through using PRI instead of NDVI or faPAR is highest for evergreen sites where changes in

LUE are largely unrelated to greenness and changes in leaf area simply because there is little change in greenness over time while LUE varies significantly (see also Running and Nemani, 1988; Gamon et al., 1992; Garbulsky et al., 2011).

Despite the advantages of using PRI to estimate LUE at site-level, we found no universally applicable light use efficiency model based on MODIS PRI. Models that are optimised for a pool of data from several sites do not perform well.

Plant functional type, even dominant species is not a sufficient criterion to generalise PRI based models. The two sites that are dominated by Quercus ilex, FR-Pue and IT-Cpz, seem to have a very different spectral response at comparable LUE levels since their optimal reference bands are 1 (red) and 4 (green). The different behaviour at IT-Cpz might be brought about by a different stand structure, as for example manifested in a higher LAI (c.f. Table 4.1), as well as higher ground water levels due to the closeness of the sea and hence less water stress (Valentini et al., 1992).

The optimal reference bands we determined (MODIS bands 1, 4, 12) fall within the spectral regions identified by Middleton et al. (2009); Cheng et al. (2009) as useful PRI reference wavelengths in a study on foliar LUE in a Douglas fir stand. Middleton et al. (2009) also showed that a PRI based on the relatively broad spectral bands of MODIS (10 nm) correlates well with PRI values derived from 3 nm wide bands. The results of our analysis suggest that the usability of different reference wavelength might depend on species composition and stand structure. The first study on PRI by Gamon et al. (1992) pointed out that no single reference wavelength suited all purposes equally well (e.g. tracking LUE in unstressed and water stressed sunflowers). The review by Garbulsky et al. (2011) points out that the optical properties of the canopy are influenced – apart from species and environmental conditions – by the fraction of dead and woody biomass, vegetation density and spectral properties of the soil, all of which can affect the suitability of reference bands. The present study adds to the body of knowledge showing that 570 nm is not the only reference bands suitable for PRI. A data base encompassing more sites with a diversity of functional and structural traits would be desirable to arrive at a final conclusion in this regard.

In summary, when calibrated at site level a model based on MODIS PRI gives better or at least as good estimates of ecosystem light use efficiency as the other approaches we tested. In this study, an universally applicable model relating LUE to MODIS PRI across different sites could not be found.

CHAPTER 5

Outlook

To increase the amount of data useful for a parameter estimation, it would be helpful to include more heterogeneous sites in future analysis. A footprint climatology assessment such as described by Chen et al. (2009) in combination with multi-angular high spectral resolution measurements (Hilker et al., 2008a) would be valuable for optimising model parameters in these cases. The impact of the sun's position on the PRI-LUE relationships in this study should be limited by the similar data acquisition times (c.f. Fig. 4.2). Nevertheless, a follow on-study should consider the sensor angle relative to the position of the sun to obtain certainty on the influence of the image acquisition geometry on the PRI-LUE relationship.

Using only PRI values for near-nadir satellite observations does improve the accuracy of LUE predictions compared to using the whole range of viewing angles, or observations binned in off-nadir 10° wide bands of viewing zenith angle. In a boreal setting, modelling LUE only based on PRI derived from backscatter reflectance also explained LUE_{obs} variance better than when using observations combined (Drolet et al., 2005, 2008). This is an indirect way of tackling the dependence of reflectance on viewing geometry. When looking from different angles, different fractions of e.g. tree canopy, understorey/grass, and soil will be visible to the sensor and result in a variation of surface reflection. Excluding off-nadir observations reduces this effect. For example, the validity of the more densely vegetated and homogeneous FR-Pue site is less effected by viewing angle then the savanna site where the contribution of trees to the signal by MODIS is more dependent on viewing angle. Another reason why near nadir data might have a better correspondence with in-situ LUE is a smaller atmospheric effect on PRI/NDVI due to the shorter Earth surface-satellite distance at small viewing zenith angles. The drawback of excluding part of the data is of course that the temporal coverage might become inadequate. Hilker et al. (2009) found that most of the directional effects on the LUE-PRI relationship can be attributed to atmospheric scattering. The standard single orbit algorithms such as 6S (Vermote et al., 1997) cannot compensate for this atmospheric disturbance. MAIAC, a generic aerosol-surface retrieval algorithm recently developed for MODIS (Lyapustin and Wang, 2009) showed promising results for detecting subtle changes in narrow waveband indices such as PRI (Hilker et al., 2009).

Another promising approach seems to be the consideration of shadow fraction in PRI-based estimations of PRI. Ground-based pilot studies have been very successful in doing so (Hall et al., 2008; Hilker et al., 2009). The fraction of shaded/sunlit parts of the canopy has an important influence on the light use effi-

ciency of vegetation and not just the PRI signal. However, which fraction of sunlit leaves is seen by a satellite depends on the position of the sensor relative to the canopy and the sun as well as the canopy structure. If the vegetation structure is not well known, uncertainty remains whether changes in PRI are due to a different position of the sensor or due to actual changes in LUE. For space-borne PRI studies, multi-angular acquisitions, taken within a short time period in which LUE is constant, are necessary (Coops et al., 2010).

Future research directions to improve the knowledge on PRI could include the development of physically-based models that predict reflectance changes at 531 nm. Innovations in this regard must allow leaf optical properties to vary with leaf-level illumination conditions and base the computation of reflectance changes on down-regulation of photosynthesis (Coops et al., 2010).

Acronyms

ANN artificial neural networks . . . 12
AOGCM Atmosphere–Ocean General Circulation Models . . . 6
aPAR absorbed photosynthetically active radiation . . . iv
bcPAR below canopy photosynthetically active radiation . . . 38
BPLUT biome property look-up table . . . 13
BRDF bidirectional reflectance distribution function . . . 21
DAO Data Assimilation Office . . . 15
EVI enhanced vegetation index . . . 20
faPAR fraction of absorbed photosynthetically active radiation . . . iv
GPP gross primary productivity . . . iii
GMAO Global Modeling and Assimilation Office . . . 15
incPAR Incident PAR . . . 36
JRC Joint Research Center . . . 62
LAI leaf area index . . . 14
LUE light use efficiency . . . iii
MODIS Moderate-resolution Imaging Spectroradiometer . . . iii
MTE model tree ensemble . . . 12
NDVI normalised difference vegetation index . . . 15
NEE net ecosystem exchange . . . 28
NEP net ecosystem productivity . . . 3
NPP net primary productivity . . . 2
PAR photochemically active radiation . . . 4
PPFD photosynthetic photon flux density . . . 29
PRI photochemical reflectance index . . . iii
R_a autotrophic respiration . . . 2
R_{eco} total ecosystem respiration . . . 3
R_g global radiation . . . 29
R_h heterotrophic respiration . . . 3
R_n net radiation . . . 29
RuBP Ribulose-1,5-bisphosphate . . . 4
RUE radiation use efficiency . . . 9
Rubisco ribulose-bisphosphate carboxylase-oxygenase . . . 4
SeaWiFS Sea-viewing Wide Field-of-view Sensor
SPOT Satellite Pour l'Observation de la Terre
sPRI scaled photochemical reflectance index . . . iv
Tmin minimum daily temperature . . . iv
u* friction velocity . . . 28
UMD University of Maryland . . . 14
VI vegetation index . . . iv
VPD vapour pressure deficit . . . iv
WUE water use efficiency . . . 12

APPENDIX A

Appendix

A.1 MOD17 GPP model

Tab. A.1: *The biome property look-up table (BPLUT) for MOD17 collection 5 (Heinsch et al., 2003)*

Biome type	Parameter				
	LUE_{max} (kg C MJ^{-1})	$Tmin_{min}$ (°C)	$Tmin_{max}$ (°C)	VPD_{min} (Pa)	VPD_{max} (Pa)
Evergreen needle forest	0.001008	-8.0	8.31	650	2500
Evergreen broadleaf forest	001159	-8.0	9.09	1100	3900
Deciduous needle forest	0.001103	-8.0	10.44	650	3100
Deciduous broadleaf forest	0.001044	-8.0	7.94	650	2500
Mixed forest	0.001116	-8.0	8.5	650	2500
Grassy woodland	0.000800	-8.0	11.39	930	3100
Wooded grassland	0.000768	-8.0	11.39	650	3100
Closed shrubland	0.000888	-8.0	8.61	650	3100
Open shrubland	0.000774	-8.0	8.80	650	3600
Grass	0.000680	-8.0	12.02	650	3500
Crop	0.000680	-8.0	12.02	650	4100

A.2 LUE modelled from PRI

			MODIS faPAR																SeaWiFS faPAR												Cyclopes faPAR												MODIS faPAR					
			NDVI			PRI 1			PRI 4			PRI 10			PRI 12			PRI 1			PRI 4			PRI 10			PRI 12			PRI 1			PRI 4			PRI 10			PRI 12			MOD17			MOD17 opt.		
Model	Site	VZA	r2	sl.	int.	r2	sl.	int.	r2	sl.	int.	r2	sl.	int.	r2	sl.	int.	r2	sl.	int.	r2	sl.	int.	r2	sl.	int.	r2	sl.	int.	r2	sl.	int.	r2	sl.	int.	r2	sl.	int.	r2	sl.	int.	r2	sl.	int.	r2	sl.	int.
site spec.	ZA-Kru	0-40°	0.41	0.39	0	0.49	0.44	0	n.s.	n.s.	n.s.	0.07	0.07	0.01	0.05	0.05	0.01	0.52	0.47	0.01	n.s.	n.s.	n.s.	0.06	0.05	0.01	0.05	0.05	0.01	0.3	0.24	0.01	n.s.	n.s.	n.s.	n.s.	n.s.	n.s.	n.s.	n.s.	n.s.	n.s.	n.s.	n.s.	0.04	-0.04	0
		0-10°	0.82	0.65	0	0.78	0.7	0	n.s.	n.s.	n.s.	0.35	0.13	0.01	n.s.	n.s.	n.s.	0.69	0.6	0.01	n.s.	n.s.	n.s.	n.s.	n.s.	n.s.	n.s.	n.s.	n.s.	0.75	0.45	0	n.s.	n.s.	n.s.	0.37	0.04	0.01	n.s.	n.s.	n.s.	n.s.	n.s.	n.s.	n.s.	n.s.	n.s.
		10-20°	0.59	0.48	0	0.78	0.65	0	n.s.	n.s.	n.s.	n.s.	n.s.	n.s.	n.s.	n.s.	n.s.	0.76	0.61	0.01	n.s.	n.s.	n.s.	n.s.	n.s.	n.s.	n.s.	n.s.	n.s.	0.66	0.22	0.01	n.s.	n.s.	n.s.	n.s.	n.s.	n.s.	n.s.	n.s.	n.s.	n.s.	n.s.	n.s.	n.s.	n.s.
		20-30°	n.s.	n.s.	n.s.	0.18	0.16	0.01	n.s.	n.s.	n.s.	n.s.	n.s.	n.s.	n.s.	n.s.	n.s.	0.31	0.26	0.01	n.s.	n.s.	n.s.	n.s.	n.s.	n.s.	n.s.	n.s.	n.s.	n.s.	n.s.	n.s.	n.s.	n.s.	n.s.	n.s.	n.s.	n.s.	n.s.	n.s.	n.s.	n.s.	n.s.	n.s.	n.s.	n.s.
		30-40°	0.63	0.55	0	0.57	0.5	0	n.s.	n.s.	n.s.	0.12	0.06	0.01	n.s.	n.s.	n.s.	0.53	0.46	0.01	n.s.	n.s.	n.s.	n.s.	n.s.	n.s.	n.s.	n.s.	n.s.	0.44	0.26	0.01	n.s.	n.s.	n.s.	n.s.	n.s.	n.s.	n.s.	n.s.	n.s.	n.s.	n.s.	n.s.	n.s.	n.s.
	FR-Pue	0-40°	0.07	0.07	0.01	0.45	0.43	0.01	0.37	0.36	0.01	0.36	0.28	0.01	0.38	0.36	0.01	0.44	0.42	0.02	0.43	0.41	0.02	0.43	0.42	0.02	0.44	0.42	0.02	0.36	0.35	0.01	0.32	0.3	0.01	0.38	0.26	0.01	0.32	0.31	0.01	0.05	0.19	0.01	0.48	0.53	0
		0-10°	0.15	0.11	0.01	0.57	0.54	0.01	0.49	0.47	0.01	0.46	0.34	0.01	0.49	0.47	0.01	0.54	0.52	0.01	0.56	0.54	0.01	0.52	0.5	0.01	0.54	0.53	0.01	0.47	0.37	0.01	0.42	0.4	0.01	0.41	0.3	0.01	0.39	0.37	0.01	n.s.	n.s.	n.s.	0.46	0.52	0
		10-20°	n.s.	n.s.	n.s.	0.34	0.33	0.01	0.27	0.26	0.01	0.28	0.21	0.01	0.29	0.27	0.01	0.45	0.43	0.02	0.44	0.42	0.02	0.43	0.42	0.02	0.48	0.47	0.01	0.38	0.32	0.01	0.36	0.36	0.01	0.38	0.28	0.01	0.41	0.39	0.01	n.s.	n.s.	n.s.	0.34	0.39	0
		20-30°	0.05	0.05	0.01	0.45	0.43	0.01	0.37	0.34	0.01	0.32	0.25	0.01	0.37	0.35	0.01	0.5	0.48	0.01	0.44	0.41	0.02	0.45	0.42	0.02	0.45	0.43	0.01	0.42	0.34	0.01	0.36	0.34	0.01	0.42	0.26	0.01	0.35	0.32	0.01	0.12	0.29	0.01	0.6	0.61	0
		30-40°	0.1	0.1	0.01	0.45	0.43	0.01	0.38	0.35	0.01	0.39	0.27	0.01	0.38	0.35	0.01	0.35	0.32	0.02	0.37	0.34	0.02	0.41	0.39	0.02	0.39	0.36	0.02	0.27	0.24	0.01	0.22	0.22	0.01	0.33	0.21	0.01	0.24	0.22	0.01	0.05	0.19	0.01	0.46	0.54	0
	IT-Cpz	0-40°	0.09	0.09	0.01	0.19	0.2	0.01	0.4	0.4	0.01	0.34	0.3	0.01	0.39	0.39	0.01	0.18	0.19	0.02	0.63	0.64	0.01	0.56	0.58	0.01	0.6	0.62	0.01	0.2	0.19	0.01	0.57	0.57	0.01	0.48	0.44	0.01	0.53	0.54	0.01	n.s.	n.s.	n.s.	0.1	0.2	0.01
		0-10°	0.22	0.18	0.01	0.18	0.16	0.01	0.56	0.49	0.01	0.5	0.39	0.01	0.55	0.51	0.01	0.14	0.14	0.02	0.67	0.63	0.01	0.57	0.53	0.01	0.64	0.62	0.01	0.18	0.13	0.02	0.63	0.5	0.01	0.62	0.46	0.01	0.63	0.56	0.01	n.s.	n.s.	n.s.	0.1	0.17	0.01
		10-20°	0.07	0.05	0.01	0.23	0.23	0.01	0.52	0.47	0.01	0.4	0.33	0.01	0.48	0.47	0.01	0.09	0.09	0.02	0.56	0.53	0.01	0.5	0.49	0.01	0.52	0.51	0.01	0.3	0.21	0.01	0.57	0.47	0.01	0.48	0.4	0.01	0.5	0.47	0.01	n.s.	n.s.	n.s.	0.09	0.19	0.01
		20-30°	0.05	0.04	0.01	0.12	0.12	0.01	0.26	0.25	0.01	0.21	0.18	0.01	0.24	0.23	0.01	0.31	0.3	0.02	0.7	0.71	0.01	0.6	0.59	0.01	0.67	0.68	0.01	0.21	0.15	0.02	0.65	0.55	0.01	0.53	0.43	0.01	0.62	0.58	0.01	n.s.	n.s.	n.s.	0.05	0.16	0.01
		30-40°	0.09	0.09	0.01	0.25	0.26	0.01	0.42	0.38	0.01	0.39	0.29	0.01	0.41	0.38	0.01	0.14	0.14	0.02	0.57	0.55	0.01	0.59	0.57	0.01	0.56	0.55	0.01	0.2	0.17	0.02	0.45	0.33	0.01	0.37	0.3	0.01	0.41	0.34	0.01	n.s.	n.s.	n.s.	0.14	0.23	0.01
	US-MMS	0-40°	0.48	0.46	0.01	0.46	0.42	0.01	n.s.	n.s.	n.s.	0.05	0.05	0.01	0.03	0.03	0.01	0.36	0.34	0.01	n.s.	n.s.	n.s.	n.s.	n.s.	n.s.	n.s.	n.s.	n.s.	0.42	0.38	0.01	n.s.	n.s.	n.s.	n.s.	n.s.	n.s.	n.s.	n.s.	n.s.	0.04	0.12	0.01	0.39	0.29	0.01
		0-10°	0.66	0.62	0	0.71	0.67	0	n.s.	n.s.	n.s.	n.s.	n.s.	n.s.	0.15	0.11	0.01	0.45	0.42	0.01	n.s.	n.s.	n.s.	n.s.	n.s.	n.s.	n.s.	n.s.	n.s.	0.6	0.49	0.01	n.s.	n.s.	n.s.	n.s.	n.s.	n.s.	n.s.	n.s.	n.s.	n.s.	n.s.	n.s.	0.45	0.49	0.01
		10-20°	0.4	0.35	0.01	0.39	0.35	0.01	n.s.	n.s.	n.s.	n.s.	n.s.	n.s.	n.s.	n.s.	n.s.	0.31	0.28	0.01	n.s.	n.s.	n.s.	n.s.	n.s.	n.s.	n.s.	n.s.	n.s.	n.s.	n.s.	n.s.	n.s.	n.s.	n.s.	n.s.	n.s.	n.s.	n.s.	n.s.	n.s.	n.s.	n.s.	n.s.	n.s.	0.37	0.27	0.01
		20-30°	0.41	0.35	0.01	0.36	0.33	0.01	n.s.	n.s.	n.s.	n.s.	n.s.	n.s.	n.s.	n.s.	n.s.	0.26	0.23	0.01	n.s.	n.s.	n.s.	n.s.	n.s.	n.s.	n.s.	n.s.	n.s.	0.39	0.34	0.01	n.s.	n.s.	n.s.	n.s.	n.s.	n.s.	n.s.	n.s.	n.s.	n.s.	n.s.	n.s.	n.s.	0.45	0.23	0.01
		30-40°	0.55	0.47	0.01	0.5	0.43	0.01	n.s.	n.s.	n.s.	n.s.	n.s.	n.s.	n.s.	n.s.	n.s.	0.53	0.41	0.01	n.s.	n.s.	n.s.	n.s.	n.s.	n.s.	n.s.	n.s.	n.s.	0.49	0.33	0.02	n.s.	n.s.	n.s.	n.s.	n.s.	n.s.	n.s.	n.s.	n.s.	n.s.	n.s.	n.s.	n.s.	0.43	0.29	0.01
	US-Me2	0-40°	0.07	0.06	0.01	0.1	0.08	0.01	0.2	0.18	0.01	0.16	0.14	0.01	0.2	0.2	0.01	0.1	0.1	0.03	0.21	0.2	0.03	0.2	0.19	0.03	0.21	0.2	0.03																0.09	0.34	0	n.s.	n.s.	n.s.
		0-10°	n.s.	n.s.	n.s.	0.2	0.11	0.01	0.33	0.21	0.01	0.33	0.26	0.01	0.37	0.31	0.01	0.19	0.14	0.03	0.31	0.25	0.02	0.34	0.31	0.02	0.35	0.31	0.02																0.24	0.51	0	0.28	0.41	0
		10-20°	0.14	0.05	0.01	0.18	0.06	0.01	0.23	0.12	0.01	n.s.	n.s.	n.s.	0.22	0.17	0.01	n.s.	n.s.	n.s.	n.s.	n.s.	n.s.	n.s.	n.s.	n.s.	n.s.	n.s.	n.s.																n.s.	n.s.	n.s.	n.s.	n.s.	n.s.
		20-30°	0.11	0.08	0.01	0.2	0.08	0.01	0.25	0.12	0.01	0.2	0.14	0.01	0.23	0.17	0.01	0.16	0.09	0.03	0.24	0.19	0.03	0.28	0.25	0.03	0.27	0.23	0.03																0.14	0.44	0	n.s.	n.s.	n.s.
		30-40°	0.1	0.04	0.01	0.1	0.05	0.01	0.21	0.13	0.01	0.14	0.11	0.01	0.21	0.18	0.01	0.14	0.1	0.03	0.25	0.22	0.03	0.25	0.22	0.03	0.26	0.24	0.02																n.s.	n.s.	n.s.	n.s.	n.s.	n.s.
evergreen	FR-Pue					0.04	-0.1	0.01	0.04	-0.08	0.01	0.01	-0.04	0.01	0.04	-0.08	0.01	n.s.	n.s.	n.s.	n.s.	n.s.	n.s.	n.s.	n.s.	n.s.	n.s.	n.s.	n.s.	n.s.	n.s.	n.s.	n.s.	n.s.	n.s.	n.s.	n.s.	n.s.	n.s.	n.s.	n.s.	n.s.						
	IT-Cpz					n.s.	n.s.	n.s.	0.01	0.05	0.01	0.02	0.05	0.01	n.s.	n.s.	n.s.	0.06	0.06	0.03	0.06	0.12	0.02	0.06	0.08	0.03	0.05	0.11	0.02	n.s.	n.s.	n.s.	n.s.	n.s.	n.s.	n.s.	n.s.	n.s.	n.s.	n.s.	n.s.	n.s.						
	US-Me2					n.s.	n.s.	n.s.	n.s.	n.s.	n.s.	n.s.	n.s.	n.s.	n.s.	n.s.	n.s.	n.s.	n.s.	n.s.	0.12	0.19	0.02	0.08	0.07	0.03	0.11	0.2	0.02																				
	combined					0.04	-0.1	0.01	0.04	-0.08	0.01	0.01	-0.04	0.01	0.04	-0.08	0.01	n.s.	n.s.	n.s.	n.s.	n.s.	n.s.	n.s.	n.s.	n.s.	n.s.	n.s.	n.s.	n.s.	n.s.	n.s.	n.s.	n.s.	n.s.	n.s.	n.s.	n.s.	n.s.	n.s.	n.s.	n.s.						
oak	FR-Pue					0.05	-0.16	0.01	0.04	-0.11	0.01	0.02	-0.05	0.01	0.04	-0.1	0.01	n.s.	n.s.	n.s.	n.s.	n.s.	n.s.	n.s.	n.s.	n.s.	n.s.	n.s.	n.s.	n.s.	n.s.	n.s.	n.s.	n.s.	n.s.	n.s.	n.s.	n.s.	n.s.	n.s.	n.s.	n.s.						
	IT-Cpz					n.s.	n.s.	n.s.	0.01	0.07	0.01	0.02	0.07	0.01	n.s.	n.s.	n.s.	0.06	0.13	0.02	0.06	0.16	0.02	0.06	0.14	0.02	0.05	0.15	0.02	n.s.	n.s.	n.s.	n.s.	n.s.	n.s.	n.s.	n.s.	n.s.	n.s.	n.s.	n.s.	n.s.						
	combined					0.05	-0.16	0.01	0.04	-0.11	0.01	0.02	-0.05	0.01	0.04	-0.1	0.01	n.s.	n.s.	n.s.	n.s.	n.s.	n.s.	n.s.	n.s.	n.s.	n.s.	n.s.	n.s.	n.s.	n.s.	n.s.	n.s.	n.s.	n.s.	n.s.	n.s.	n.s.	n.s.	n.s.	n.s.	n.s.						

Tab. A.2: *R^2, slope and intercept of the regression line between modelled LUE and observed LUE. 'n.s.' means that the R^2 between both LUEs is not significant at the 5% level.*

Bibliography

Allard, V., J. M. Ourcival, S. Rambal, R. Joffre, and A. Rocheteau. 2008. Seasonal and annual variation of carbon exchange in an evergreen Mediterranean forest in southern France. *Global Change Biology* **14**, 714–725. 38, 52, 59

Allen, C. D., A. K. Macalady, H. Chenchouni, D. Bachelet, N. McDowell, M. Vennetier, T. Kitzberger, A. Rigling, D. D. Breshears, and E. T. Hogg. 2010. A global overview of drought and heat-induced tree mortality reveals emerging climate change risks for forests. *Forest Ecology and Management* **259**, 660–684. 6

Ananyev, G., Z. S. Kolber, D. Klimov, P. G. Falkowski, J. A. Berry, U. Rascher, R. Martin, and B. Osmond. 2005. Remote sensing of heterogeneity in photosynthetic efficiency, electron transport and dissipation of excess light in Populus deltoides stands under ambient and elevated CO2 concentrations, and in a tropical forest canopy, using a new laser-induced fluoresc. *Global Change Biology* **11**, 1195–1206. 17

Andrade, F. H., S. A. Uhart, and A. Cirilo. 1993. Temperature affects radiation use efficiency in maize. *Field Crops Research* **32**, 17–25. 10

Asner, G. P., D. Nepstad, G. Cardinot, and D. Ray. 2004. Drought stress and carbon uptake in an Amazon forest measured with spaceborne imaging spectroscopy.. *Proceedings of the National Academy of Sciences of the United States of America* **101**, 6039–44. 20, 22

Asner, G. P., K. Carlson, and R. Martin. 2005. Substrate age and precipitation effects on Hawaiian forest canopies from spaceborne imaging spectroscopy. *Remote Sensing of Environment* **98**, 457–467. 22

Atlas, R. M., and R. Lucchesi. 2000. File Specification for GEOS-DAS Gridded Output. 15

Aubinet, M., A. Grelle, A. Ibrom, U. Rannik, J. B. Moncrieff, T. Foken, A. S. Kowalski, P. H. Martin, P. Berbigier, C. Bernhofer, R. Clement, J. Elbers, A. Granier, T. Grünwald, K. Morgenstern, K. Pilegaard, C. Rebmann, W. Snijders, R. Valentini, and T. Vesala. 2000. Estimates of the annual net carbon and water exchange of forests: the EUROFLUX methodology. *Advances in Ecological Research*. 8, 9, 27, 28

Aubinet, M., B. Heinesch, and M. Yernaux. 2003a. Horizontal and vertical co 2 advection in a sloping forest. *Boundary-Layer Meteorology* **108**, 397–417. 28

Aubinet, M., P. Berbigier, C. Bernhofer, a. Cescatti, C. Feigenwinter, a. Granier, T. Grünwald, K. Havrankova, B. Heinesch, B. Longdoz, B. Marcolla, L. Montagnani, and P. Sedlak. 2005. Comparing CO2 Storage and Advection Conditions at Night at Different Carboeuroflux Sites. *Boundary-Layer Meteorology* **116**, 63–93. 28

Aubinet, M., R. Clement, J. Elbers, T. Foken, A. Grelle, A. Ibrom, J. Moncrieff, K. Pilegaard, U. Rannik, and C. Rebmann. 2003b. *Methodology for data acquisition, storage and treatment*. Springer-Verlag, Berlin. 8

Bacour, C., and F.-M. Bréon. 2005. Variability of biome reflectance directional signatures as seen by POLDER. *Remote Sensing of Environment* **98**, 80–95. 32, 61

Bacour, C., F. Baret, D. Beal, M. Weiss, and K. Pavageau. 2006. Neural network estimation of LAI, fAPAR, fCover and LAIxCab, from top of canopy MERIS reflectance data: Principles and validation. *Remote Sensing of Environment* **105**, 313–325. 41

Baker, N. R. 2008. Chlorophyll fluorescence: a probe of photosynthesis in vivo.. *Annual review of plant biology* **59**, 89–113. 17

Baldocchi, D. D. 2003. Assessing the eddy covariance technique for evaluating carbon dioxide exchange rates of ecosystems: past, present and future. *Global Change Biology* **9**, 479–492. 7

Baldocchi, D. D. 2008. TURNER REVIEW No. 15. 'Breathing' of the terrestrial biosphere: lessons learned from a global network of carbon dioxide flux measurement systems. *Australian Journal of Botany* **56**, 1. 8, 28

Baldocchi, D. D., and J. S. Amthor. 2001. *Canopy Photosynthesis: History, Measurements, and Models*. In: 2. Pp. 9–32. Academic Press, San Diego. 3, 11

Baldocchi, D. D., B. B. Hincks, and T. P. Meyers. 1988. Measuring Biosphere-Atmosphere Exchanges of Biologically Related Gases with Micrometeorological Methods. *Ecology* **69**, 1331–1340. 8, 28

Baret, F., J. Morissette, R. A. Fernandes, J. Champeaux, R. B. Myneni, J. Chen, S. Plummer, M. Weiss, C. Bacour, S. Garrigues, and J. Nickeson. 2006. Evaluation of the representativeness of networks of sites for the global validation and intercomparison of land biophysical products: proposition of the CEOS-BELMANIP. *IEEE Transactions on Geoscience and Remote Sensing* **44**, 1794–1803. 15

Baret, F., O. Hagolle, B. Geiger, P. Bicheron, B. Miras, M. Huc, B. Berthelot, F. Nino, M. Weiss, and O. Samain. 2007. LAI, fAPAR and fCover CYCLOPES global products derived from VEGETATION Part 1: Principles of the algorithm. *Remote Sensing of Environment* **110**, 275–286. 60

Barford, C. C., S. C. Wofsy, M. L. Goulden, J. W. Munger, E. H. Pyle, S. P. Urbanski, L. Hutyra, S. R. Saleska, D. Fitzjarrald, and K. Moore. 2001. Factors controlling long- and short-term sequestration of atmospheric CO2 in a mid-latitude forest.. *Science* **294**, 1688–91. 28

Barton, C. V. M., and P. R. J. North. 2001. Remote sensing of canopy light use efficiency using the photochemical reflectance index - Model and sensitivity analysis. *Remote Sensing of Environment* **78**, 264 – 273. 21, 23, 51, 52, 58

Beer, C., M. Reichstein, E. Tomelleri, P. Ciais, M. Jung, N. Carvalhais, C. Rodenbeck, M. A. Arain, D. D. Baldocchi, G. B. Bonan, A. Bondeau, A. Cescatti, G. Lasslop, A. Lindroth, M. Lomas, S. Luyssaert, H. Margolis, K. W. Oleson, O. Roupsard, E. Veenendaal, N. Viovy, C. Williams, F. I. Woodward, and D. Papale. 2010. Terrestrial Gross Carbon Dioxide Uptake: Global Distribution and Covariation with Climate. *Science*. 3, 5, 11, 12, 56, 63

Beer, C., M. Reichstein, P. Ciais, G. D. Farquhar, and D. Papale. 2007. Mean annual GPP of Europe derived from its water balance. *Geophysical Research* **34**, 101029/. 12

Beer, C., P. Ciais, M. Reichstein, D. D. Baldocchi, B. E. Law, D. Papale, J.-F. Soussana, C. Ammann, N. Buchmann, D. Frank, G. D. Farquhar, D. Giannelle, I. A. Janssens, A. Knohl, N. Buchmann, B. Köstner, E. Moors, J.-F. Soussana, O. Roupsard, H. Verbeek, T. Vesala, J. C. Williams, G. Wohlfahrt, D. Gianelle, B. Köstner, E. Moors, O. Roupsard, H. Verbeeck, T. Vesala, C. A. Williams, and G. Wohlfahrt. 2009. Temporal and among-site variability of inherent water use efficiency at the ecosystem level. *Global Biogeochemical Cycles* **23**, 1–13. 12

Bilger, W., O. Björkman, and S. S. Thayer. 1989. Light-induced spectral absorbance changes in relation to photosynthesis and the epoxidation state of xanthophyll cycle components in cotton leaves. *Plant Physiology* **91**, 542–551. 18

Bloom, S., A. da Silva, D. Dee, M. Bosilovich, J.-D. Chern, S. Pawson, S. Schubert, M. Sienkiewicz, I. Stajner, W.-W. Tan, and M.-L. Wu. 2005. Documentation and Validation of the Goddard Earth Observing System (GEOS) Data Assimilation System ‚Äì Version 4. *Technical Report Series on Global Modeling and Data Assimilation* **26**, 165. 15

Bouchet, R. J. 1963. Evapotranspiration reelle evapotranspiration potentielle, signification climatique.. *International Association of Scientific Hydrology. General Assembly of Berkeley, Transactions, vol. 2, Evaporation.*. Berkley, California. Pp. 134–142. 13

Canadell, J. G., H. A. Mooney, D. D. Baldocchi, J. A. Berry, J. R. Ehleringer, C. B. Field, S. T. Gower, D. Y. Hollinger, J. E. Hunt, R. B. Jackson, S. W. Running, G. R. Shaver, W. Steffen, S. E. Trumbore, R. Valentini, and B. Y. Bond. 2000. Carbon Metabolism of the Terrestrial Biosphere: A Multitechnique Approach for Improved Understanding. *Ecosystems* **3**, 115–130. 2, 11

Canadell, J. G., P. Ciais, P. Cox, and M. Heimann. 2004. Quantifying, understanding and managing the carbon cycle in the next decades. *Climatic Change* **67**, 147–160. 11

Chapin, F. S., G. M. Woodwell, J. T. Randerson, E. B. Rastetter, G. M. Lovett, D. D. Baldocchi, D. A. Clark, M. E. Harmon, D. S. Schimel, R. Valentini, C. Wirth, J. D. Aber, J. J. Cole, M. L. Goulden, J. W. Harden, M. Heimann, R. W. Howarth, P. A. Matson, A. D. McGuire, J. M. Melillo, H. A. Mooney, J. C. Neff, R. A. Houghton, M. L. Pace, M. G. Ryan, S. W. Running, O. E. Sala, W. H. Schlesinger, and E.-D.

Schulze. 2006. Reconciling Carbon-cycle Concepts, Terminology, and Methods. *Ecosystems* **9**, 1041–1050. 3

Chapin, F. S., P. A. Matson, and H. A. Mooney. 2002. *Carbon input to terrestrial ecosystems*. In: 5. Pp. 97–122. Springer, New York. 4, 9

Chapin III, F. S., J. McFarland, A. D. McGuire, E. S. Euskirchen, R. W. Ruess, and K. Kielland. 2009. The changing global carbon cycle : linking plant ‚Äì soil carbon dynamics to global consequences. *Journal of Ecology* **97**, 840–850. 2

Chen, B., T. A. Black, N. C. Coops, T. Hilker, J. A. T. Trofymow, and K. Morgenstern. 2009. Assessing tower flux footprint climatology and scaling between remotely sensed and eddy covariance measurements. *Boundary-Layer Meteorology* **130**, 137–167. 75

Cheng, Y.-B., E. M. Middleton, T. Hilker, N. C. Coops, T. A. Black, and P. Krishnan. 2009. Dynamics of spectral bio-indicators and their correlations with light use efficiency using directional observations at a Douglas-fir forest. *Measurement Science and Technology* **20**, 095107. 73

Christensen, J., B. Hewitson, A. Busuioc, A. Chen, X. Gao, I. Held, R. Jones, R. Kolli, W.-T. Kwon, R. Laprise, V. M. n. Rueda, L. Mearns, C. Menéndez, J. Räisänen, A. Rinke, A. Sarr, and P. Whetton. 2007. *Regional Climate Projections*. In: 11. Pp. 847–939. Cambridge University Press, Cambridge, United Kingdom and New York, NY, USA. 6, 23

Ciais, P., M. Reichstein, N. Viovy, A. Granier, J. Ogée, V. Allard, M. Aubinet, N. Buchmann, C. Bernhofer, A. Carrara, F. Chevallier, N. De, Noblet, A. Friend, P. Friedlingstein, T. Grünwald, B. Heinesch, P. Keronen, A. Knohl, G. Krinner, D. Loustau, G. Manca, G. Matteucci, F. Miglietta, J. Ourcival, D. Papale, K. Pilegaard, M. Rautiainen, G. Seufert, J. Soussana, M. Sanz, E.-D. Schulze, T. Vesala, and R. Valentini. 2005. Europe-wide reduction in primary productivity caused by the heat and drought in 2003.. *Nature* **437**, 529–33. 11

Clark, D. a., S. Brown, D. W. Kicklighter, J. Q. Chambers, J. R. Thomlinson, and J. Ni. 2001. Measuring Net Primary Production in Forests: Concepts and Field Methods. *Ecological Applications* **11**, 356–370. 6

Clausi, D. A. 2002. An analysis of co-occurrence texture statistics as a function of grey level quantization. *Canadian Journal of Remote Sensing* **28**, 45–62. 38

Cohen, W. B., T. K. Maiersperger, Z. Yang, S. T. Gower, D. P. Turner, W. D. Ritts, M. Berterretche, and S. W. Running. 2003. Comparisons of land cover and LAI estimates derived from ETM+ and MODIS for four sites in North America: a quality assessment of 2000/2001 provisional MODIS products. *Remote Sensing of Environment* **88**, 233–255. 15

Coops, N. C., R. Jassal, R. Leuning, A. T. Black, and K. Morgenstern. 2007. Incorporation of a soil water modifier into MODIS predictions of temperate Douglas-fir gross primary productivity: Initial model development. *Agricultural and Forest Meteorology* **147**, 99–109. 72

Coops, N. C., T. Hilker, F. G. Hall, C. J. Nichol, and G. G. Drolet. 2010. Estimation of Light-use Efficiency of Terrestrial Ecosystems from Space: A Status Report. *BioScience* **60**, 788–797. 57, 76

Dall'Osto, L., C. Lico, J. Alric, G. Giuliano, M. Havaux, and R. Bassi. 2006. Lutein is needed for efficient chlorophyll triplet quenching in the major LHCII antenna complex of higher plants and effective photoprotection in vivo under strong light.. *BMC plant biology* **6**, 32. 21

Damm, A., J. Elbers, A. Erler, B. Gioli, K. Hamdi, R. Hutjes, M. Kosvancova, M. Meroni, F. Miglietta, A. Moersch, J. Moreno, A. Schickling, R. Sonnenschein, T. Udelhoven, S. Van Der Linden, P. Hostert, and U. Rascher. 2002. Severe drought effects on ecosystem CO2 and H2O fluxes at three mediterranean evergreen sites: Revision of current hypotheses. *Global Change Biology* **8**, 999–1017. 23, 51

Damm, A., J. Elbers, A. Erler, B. Gioli, K. Hamdi, R. Hutjes, M. Kosvancova, M. Meroni, F. Miglietta, A. Moersch, J. Moreno, A. Schickling, R. Sonnenschein, T. Udelhoven, S. Van Der Linden, P. Hostert, and U. Rascher. 2010. Remote sensing of sun-induced fluorescence to improve modeling of diurnal courses of gross primary production (GPP). *Global Change Biology* **16**, 171–186. 18

Davidson, Malcolm, M. Berger, I. Moya, J. Moreno, T. Laurila, M.-P. Stoll, and J. Miller. 2003. Mapping photosynthesis from space - a new vegetation-fluorescence technique. *ESA Bulletin (ISSN 0376-4265)*. 18

De Wit, C. 1959. Potential photosynthesis of crop surfaces. *Netherlands Journal of Agricultural Science* **7**, 141–149. 9

DeLucia, E. H., J. E. Drake, R. B. Thomas, and M. Gonzales-Meler. 2007. Forest carbon use efficiency: is respiration a constant fraction of gross primary production?. *Global Change Biology* **13**, 1157–1167. 11

Demmig-Adams, B. 1990. Carotenoids and photoprotection in plants: A role for the xanthophyll zeaxanthin. *Biochimica et Biophysica Acta (BBA) - Bioenergetics* **1020**, 1–24. 5

Demmig-Adams, B., and W. W. Adams. 2006. Photoprotection in an ecological context: the remarkable complexity of thermal energy dissipation.. *The New Phytologist* **172**, 11–21. 4, 37

Demmig, B., K. Winter, A. Krüger, and F.-C. Czygan. 1987. Photoinhibition and Zeaxanthin Formation in Intact Leaves: A Possible Role of the Xanthophyll Cycle in the Dissipation of Excess Light Energy. *Plant Physiology* **84**, 218–224. 5, 37

Denman, K., G. Brasseur, A. Chidthaisong, P. Ciais, P. Cox, R. Dickinson, D. Hauglustaine, C. Heinze, E. Holland, D. Jacob, U. Lohmann, S. Ramachandran, P. D. S. Dias, S. Wofsy, and X. Zhang. 2007. *Couplings Between Changes in the Climate System and Biogeochemistry*. In: 7. Pp. 500–587. Cambridge University Press, Cambridge, United Kingdom and New York, NY, USA. 2, 11

Drolet, G., E. M. Middleton, K. F. Huemmrich, F. G. Hall, B. Amiro, A. Barr, T. Black, J. McCaughey, and H. Margolis. 2008. Regional mapping of gross light-use efficiency using MODIS spectral indices. *Remote Sensing of Environment* **112**, 3064–3078. 22, 24, 42, 50, 51, 57, 58, 62, 75

Drolet, G. G., K. F. Huemmrich, F. G. Hall, E. M. Middleton, T. A. Black, T. Black, A. Barr, A. A. Barr, and H. Margolis. 2005. A MODIS-derived photochemical reflectance index to detect inter-annual variations in the photosynthetic light-use efficiency of a boreal deciduous forest. *Remote Sensing of Environment* **98**, 212–224. 22, 31, 41, 42, 50, 51, 57, 62, 75

Falge, E. 2001. Gap filling strategies for defensible annual sums of net ecosystem exchange. *Agricultural and Forest Meteorology* **107**, 43–69. 28

Farquhar, G. D., and M. L. Roderick. 2003. Atmospheric science. Pinatubo, diffuse light, and the carbon cycle.. *Science* **299**, 1997–8. 21

Feigenwinter, C., C. Bernhofer, and R. Vogt. 2004. The influence of advection on the short term CO2 - budget in and above a forest canopy. *Boundary-Layer Meteorology* **113**, 201–224. 28

Feigenwinter, C., C. Bernhofer, U. Eichelmann, B. Heinesch, M. Hertel, D. Janous, O. Kolle, F. Lagergren, a. Lindroth, and S. Minerbi. 2008. Comparison of horizontal and vertical advective CO2 fluxes at three forest sites. *Agricultural and Forest Meteorology* **148**, 12–24. 28

Filella, I., A. Porcar-Castell, S. Munne-Bosch, J. Back, M. F. Garbulsky, and J. Penuelas. 2009. PRI assessment of long-term changes in carotenoids/chlorophyll ratio and short-term changes in de-epoxidation state of the xanthophyll cycle. *International Journal of Remote Sensing* **30**, 4443–4455. 21, 24

Filella, I., J. Peñuelas, L. Llorens, and M. Estiarte. 2004. Reflectance assessment of seasonal and annual changes in biomass and CO2 uptake of a Mediterranean shrubland submitted to experimental warming and drought. *Remote Sensing of Environment* **90**, 308–318. 21, 38, 52, 53

Filella, I., T. Amaro, J. L. Araus, and J. Peñuelas. 1996. Relationship between photosynthetic radiation-use efficiency of barley canopies and the photochemical reflectance index. *Physiologia Plantatum* **96**, 211–216. 19

Finnigan, J. 2008. An introduction to flux measurements in difficult conditions.. *Ecological applications* **18**, 1340–50. 28

Finnigan, J. J. 2004. A re-evaluation of long-term flux measurement techniques, part 2: Coordinate systems. *Boundary-Layer Meteorology* **113**, 1–41. 28

Finnigan, J. J., R. Clement, Y. Malhi, R. Leuning, and H. A. Cleugh. 2003. A re-evaluation of long-term flux measurement techniques, part 1: averaging and coordinate rotation. *Boundary-Layer Meteorology* **107**, 1–48. 27, 28

Flexas, J., J. M. Escalona, S. Evain, J. Gulías, I. Moya, C. B. Osmond, and H. Medrano. 2002. Steady-state chlorophyll fluorescence (Fs) measurements as a tool to follow variations of net CO2 assimilation and stomatal conductance during water-stress in C3 plants.. *Physiologia plantarum* **114**, 231–240. 17 *FLUXNET project*

FLUXNET project *2010. 9*

Frank, H., and G. Brudvig. 2004. Redox Functions of Carotenoids in Photosynthesis. Biochemistry **43***, 8607–8615. 21*

Galmés, J., H. Medrano, and J. Flexas. 2007. Photosynthetic limitations in response to water stress and recovery in Mediterranean plants with different growth forms.. The New phytologist **175***, 81–93. 36*

Gamon, J. A., C. B. Field, M. L. Goulden, and K. L. Griffin. 1995. Relationships Between NDVI, Canopy Structure, and Photosynthesis in Three Californian Vegetation Types. Ecological Society of America **5***, 28–41. 37, 57*

Gamon, J. A., I. Filella, and J. Peñuelas. 1993a. The dynamic 531-Nanometer Delta reflectance signal: a survey of twenty angiosperm species*. Pp. 172–177. American Society of Plant Physiologists. 18, 19, 20, 22, 57*

Gamon, J. A., J. Peñuelas, and C. Field. 1992. A narrow-waveband spectral index that tracks diurnal changes in photosynthetic efficiency. Remote Sensing of Environment **41***, 35–44. 18, 19, 22, 24, 37, 42, 52, 57, 73*

Gamon, J. A., J. Peñuelas, C. B. Field, O. Björkman, W. Bilger, and A. L. Fredeen. 1990. Remote sensing of the xanthophyll cycle and fluorescence in sunflower leaves and canopies. Oecologia **85***, 1–7. 19, 37*

Gamon, J. A., L. Serrano, and J. S. Surfus. 1997. The photochemical reflectance index: an optical indicator of photosynthetic radiation use efficiency across species, functional types, and nutrient levels. Oecologia **112***, 492–501. 18, 19*

Gamon, J. A., S. L. Ustin, C. Field, R. Valentini, and D. Roberts. 1993b. Functional patterns in an annual grassland during an AVIRIS overflight,òÜ,òÜ,òÜ. Remote Sensing of Environment **44***, 239–253. 20*

Garbulsky, M. F., J. Peñuelas, D. Papale, and I. Filella. 2008. Remote estimation of carbon dioxide uptake by a Mediterranean forest. Global Change Biology **14***, 2860–2867. 22, 23, 51, 57*

Garbulsky, M. F., J. Peñuelas, D. Papale, J. Ardö, M. L. Goulden, G. Kiely, A. D. Richardson, E. Rotenberg, E. M. Veenendaal, and I. Filella. 2010. Patterns and controls of the variability of radiation use efficiency and primary productivity across terrestrial ecosystems. Global Ecology and Biogeography **19***, 253–267. 10, 57, 72*

Garbulsky, M. F., J. Peñuelas, J. A. Gamon, Y. Inoue, and I. Filella. 2011. The photochemical reflectance index (PRI) and the remote sensing of leaf, canopy

and ecosystem radiation use efficiencies: A review and meta-analysis. Remote Sensing of Environment **115**, *281–297. 19, 57, 72, 73*

Gaudinski, J. B., M. S. Torn, W. J. Riley, T. E. Dawson, J. D. Joslin, and H. Majdi. 2010. Measuring and modeling the spectrum of fine-root turnover times in three forests using isotopes, minirhizotrons, and the Radix model. Global Biogeochemical Cycles **24**, *1–17. 7*

Giorgi, F. 2006. Climate change hot-spots. Geophysical Research Letters **33**, *1–4. 23*

Gitelson, A. A., and M. N. Merzlyak. 1994. Spectral reflectance changes associate with autumn senescence of Aesculus hippocastanum L., and Acer platanoides L. leaves. Journal of Plant Physiology **143**, *286–292. 21*

Göckede, M., T. Foken, M. Aubinet, M. Aurela, J. Banza, C. Bernhofer, J. M. Bonnefond, Y. Brunet, A. Carrara, R. Clement, E. Dellwik, J. Elbers, W. Eugster, J. Fuhrer, A. Granier, T. Grünwald, B. Heinesch, I. A. Janssens, A. Knohl, R. Koeble, T. Laurila, B. Longdoz, G. Manca, M. V. Marek, T. Markkanen, J. A. Mateus, G. Matteucci, M. Mauder, M. Migliavacca, S. Minerbi, J. B. Moncrieff, L. Montagnani, E. Moors, J.-M. Ourcival, D. Papale, J. a. S. Pereira, K. Pilegaard, G. Pita, S. Rambal, C. Rebmann, A. Rodrigues, E. Rotenberg, M. J. Sanz, P. Sedlak, G. Seufert, L. Siebicke, J.-F. Soussana, R. Valentini, T. Vesala, H. Verbeeck, and D. Yakir. 2008. Quality control of CarboEurope flux data ‚Äì Part 1: Coupling footprint analyses with flux data quality assessment to evaluate sites in forest ecosystems. Biogeosciences **5**, *433–450. 30, 38*

Goerner, A., M. Reichstein, and S. Rambal. 2009. Tracking seasonal drought effects on ecosystemlight use efficiency with satellite-based PRI in a Mediterranean forest. Remote Sensing of Environment **113**, *1101–1111. i, 57, 61*

Goerner, A., M. Reichstein, E. Tomelleri, N. Hanan, S. Rambal, D. Papale, D. Dragoni, and C. Schmullius. 2011. Remote sensing of ecosystem light use efficiency with MODIS-based PRI. Biogeosciences **8**, *189–202. i*

Goetz, S. J., and S. D. Prince. 1999. Modelling terrestrial carbon exchange and storage: evidence and implications of functional convergence in light-use efficiency. Advances in Ecological Research **28**, *57–92. 36*

Goulden, M. L., J. W. Munger, S.-M. Fan, B. C. Daube, and S. C. Wofsy. 1996. Measurements of carbon sequestration eddy covariance: methods and a critical accuracy by long-term evaluation of accuracy. Global Change Biology **2**, *169–182. 28*

Gower, S. T., C. J. Kucharik, and J. M. Norman. 1999. Direct and Indirect Estimation of Leaf Area Index, fAPAR, and Net Primary Production of Terrestrial Ecosystems. Remote Sensing of Environment **70**, *20–51. 6, 7, 10, 40*

Grace, J., C. J. Nichol, M. Disney, P. Lewis, T. Quaife, and P. Bowyer. 2007. Can we measure terrestrial photosynthesis from space directly, using spectral re-

flectance and fluorescence?. Global Change Biology **13**, *1484–1497. 9, 17, 18, 23, 36, 58*

Granger, R., and D. Gray. 1989. Evaporation form natural nonsaturated surfaces. Journal of Hydrology **111**, *21–29. 13*

Green, S. D. 2003. Foliar morphology and canopy nitrogen as predictors of light-use efficiency in terrestrial vegetation. Agricultural and Forest Meteorology **115**, *163–171. 36*

Gu, L. 2002. Advantages of diffuse radiation for terrestrial ecosystem productivity. Journal of Geophysical Research. *21*

Gu, L., E. M. Falge, T. Boden, D. D. Baldocchi, T. A. Black, S. R. Saleska, T. Suni, S. B. Verma, T. Vesala, and S. C. Wofsy. 2005. Objective threshold determination for nighttime eddy flux filtering. Agricultural and Forest Meteorology **128**, *179–197. 28*

Gu, L., J. D. Fuentes, H. H. Shugart, R. M. Staebler, and T. a. Black. 1999. Responses of net ecosystem exchanges of carbon dioxide to changes in cloudiness: Results from two North American deciduous forests. Journal of Geophysical Research **104**, *31421–31434. 21*

Guanter, L., L. Alonso, L. Gómez-Chova, J. Amorós-López, J. Vila, and J. Moreno. 2007. Estimation of solar-induced vegetation fluorescence from space measurements. Geophysical Research Letters **34**, *1–5. 18*

Guglielmetti, M., M. Schwank, C. Matzler, C. Oberdorster, J. Vanderborght, and H. Fluhler. 2008. FOSMEX: Forest Soil Moisture Experiments With Microwave Radiometry. IEEE Transactions on Geoscience and Remote Sensing **46**, *727–735. 72*

Guo, J., and C. M. Trotter. 2004. Estimating photosynthetic light-use efficiency using the photochemical reflectance index: variations among species. Functional Plant Biology **31**, *255. 19, 21*

Hall, F. G., T. Hilker, N. C. Coops, A. Lyapustin, K. F. Huemmrich, E. M. Middleton, H. A. Margolis, G. G. Drolet, and T. A. Black. 2008. Multi-angle remote sensing of forest light use efficiency by observing PRI variation with canopy shadow fraction. Remote Sensing of Environment **112**, *3201–3211. 19, 75*

Hansen, M. C., R. S. Defries, J. R. G. Townshend, and R. Sohlberg. 2000. Global land cover classification at 1 km spatial resolution using a classification tree approach. International Journal of Remote Sensing **21**, *1331–1364. 14*

Haxeltine, A., and I. C. Prentice. 1996. A General Model for the Light-Use Efficiency of Primary Production. Functional Ecology **10**, *551–561. 12*

Heimann, M. 2009. Searching out the sinks. Nature Geoscience **2**, *3–4. 11*

Heinsch, F. A., M. Reeves, P. Votava, S. Kang, C. Milesi, M. Zhao, J. Glassy, W. M. Jolly, R. Loehman, C. F. Bowker, J. S. Kimball, R. R. Nemani, and S. W. Running.

2003. User,Äôs Guide GPP and NPP (MOD17A2/A3) Products NASA MODIS Land Algorithm. 13, 14, 15, 16, 41, 63, 79

Heinsch, F. A., M. Zhao, S. W. Running, J. S. Kimball, R. R. Nemani, K. J. Davis, P. V. Bolstad, B. D. Cook, A. R. Desai, D. M. Ricciuito, B. E. Law, W. C. Oechel, H. J. Kwon, H. Luo, S. C. Wofsy, A. L. Dunn, J. W. Munger, D. D. Baldocchi, L. Xu, D. Y. Hollinger, A. D. Richardson, P. C. Stoy, M. B. Siqueira, R. K. Monson, S. P. Burns, and L. B. Flanagan. 2006. Evaluation of remote sensing based terrestrial productivity from MODIS using regional tower eddy flux network observations. IEEE Transactions on Geoscience and Remote Sensing **44**, *1908–1925.* 13, 14, 15, 16, 37, 57

Hilker, T., A. Lyapustin, F. G. Hall, Y. Wang, N. C. Coops, G. G. Drolet, and T. A. Black. 2009. An assessment of photosynthetic light use efficiency from space: Modeling the atmospheric and directional impacts on PRI reflectance. Remote Sensing of Environment **113**, *24632475.* 58, 75

Hilker, T., N. C. Coops, F. G. Hall, T. A. Black, B. Chen, P. Krishnan, M. A. Wulder, P. J. Sellers, E. M. Middleton, and K. F. Huemmrich. 2008a. A modeling approach for upscaling gross ecosystem production to the landscape scale using remote sensing data. Journal of Geophysical Research **113**, *1–15.* 75

Hilker, T., N. C. Coops, T. A. Black, M. A. Wulder, and R. D. Guy. 2008b. The use of remote sensing in light use efficiency based models of gross primary production: A review of current status and future requirements. Science of the Total Environment **404**, *411–423.* 21, 56, 72

Horn, J. E., and K. Schulz. 2010. Identification of a general light use efficiency model for gross primary production. Biogeosciences Discussions **7**, *7673–7726.* 57

Huemmrich, K. F., J. L. Privette, M. Mukelabai, R. B. Myneni, and Y. Knyazikhin. 2005. Time-series validation of MODIS land biophysical products in a Kalahari woodland, Africa. International Journal of Remote Sensing **26**, *4381–4398.* 15

Huete, A. R., H. Q. Liu, K. Batchily, and W. van Leeuwen. 1997. A comparison of vegetation indices over a global set of TM images for EOS-MODIS. Remote Sensing of Environment **59**, *440–451.* 43

Hwang, T., S. Kang, J. Kim, Y. Kim, D. Lee, and L. Band. 2008. Evaluating drought effect on MODIS Gross Primary Production (GPP) with an eco-hydrological model in the mountainous forest, East Asia. Global Change Biology **14**, *1037–1056.* 16

Inoue, Y., J. Peñuelas, A. Miyata, and M. Mano. 2008. Normalized difference spectral indices for estimating photosynthetic efficiency and capacity at a canopy scale derived from hyperspectral and CO2 flux measurements in rice. Remote Sensing of Environment **112**, *156–172.* 19

Janssen, P., and P. Heuberger. 1995. Calibration of process-oriented models. Ecological Modelling **83**, *55–66.* 43

Jung, M., M. Reichstein, and A. Bondeau. 2009. Towards global empirical upscaling of FLUXNET eddy covariance observations: validation of a model tree ensemble approach using a biosphere model. Biogeosciences **6**, *2001–2013. 12*

Kanniah, K., J. Beringer, L. Hutley, N. Tapper, and X. Zhu. 2009a. Evaluation of Collections 4 and 5 of the MODIS Gross Primary Productivity product and algorithm improvement at a tropical savanna site in northern Australia. Remote Sensing of Environment **113**, *1808–1822. 16*

Kanniah, K., J. Beringer, L. Hutley, N. Tapper, and X. Zhu. 2009b. Evaluation of Collections 4 and 5 of the MODIS Gross Primary Productivity product and algorithm improvement at a tropical savanna site in northern Australia. Remote Sensing of Environment **113**, *1808–1822. 72*

King, M. D., J. Closs, S. Spangler, R. Greenstone, S. Wharton, and M. Myers. 2004. EOS Data Products Handbook Volume 1. *Vol. 1, Greenbelt, MD 20771. 15*

Kiniry, J. R., J. A. Landivar, M. Witt, T. J. Gerik, J. Cavero, and L. J. Wade. 1998. Radiation-use efficiency response to vapor pressure deficit for maize and sorghum. Field Crops Research **56**, *265–270. 10*

Knohl, A., and D. D. Baldocchi. 2008. Effects of diffuse radiation on canopy gas exchange processes in a forest ecosystem. Journal of Geophysical Research **113**, *1–17. 16*

Kolber, Z., D. Klimov, G. Ananyev, U. Rascher, J. Berry, and B. Osmond. 2005. Measuring photosynthetic parameters at a distance: laser induced fluorescence transient (LIFT) method for remote measurements of photosynthesis in terrestrial vegetation.. Photosynthesis research **84**, *121–9. 17*

Kolber, Z., O. Prasil, and P. Falkowski. 1998. Measurements of variable chlorophyll fluorescence using fast repetition rate techniques: defining methodology and experimental protocols. Biochimica et biophysica acta **1367**, *88–106. 17*

Kumar, M., and J. Monteith. 1981. Remote sensing of crop growth. *Pp. 133–144. Academic Press, New York. 36*

Kutsch, W. L., N. P. Hanan, B. Scholes, I. Mchugh, W. Kubheka, H. Eckhardt, and C. Williams. 2008. Response of carbon fluxes to water relations in a savanna ecosystem in South Africa. Biogeosciences **5**, *1797–1808. 59*

Lacaze, B., S. Rambal, and T. Winkel. 1994. Identifying spatial patterns of Mediterranean landscapes from geostatistical analysis of remotely-sensed data. International Journal of Remote Sensing **15**, *2337–2350. 38*

Lacaze, R., E. Fédèle, and F.-M. Bréon. 2009. POLDER-3 / PARASOL BRDF Databases User Manual. 32

Landsberg, J., and R. Waring. 1997. A generalised model of forest productivity

using simplified concepts of radiation-use efficiency, carbon balance and partitioning. Forest Ecology and Management **95**, *209–228. 10*

Lasslop, G., M. Reichstein, D. Papale, A. D. Richardson, A. Arneth, A. G. Barr, P. Stoy, and G. Wohlfahrt. 2010. Separation of net ecosystem exchange into assimilation and respiration using a light response curve approach: critical issues and global evaluation. Global Change Biology **16**, *187–208. 28, 29*

Lauvaux, T., B. Gioli, C. Sarrat, P. J. Rayner, P. Ciais, F. Chevallier, J. Noilhan, F. Miglietta, Y. Brunet, E. Ceschia, H. Dolman, J. A. Elbers, C. Gerbig, R. Hutjes, N. Jarosz, D. Legain, and M. Uliasz. 2009. Bridging the gap between atmospheric concentrations and local ecosystem measurements. Geophysical Research Letters **36**, *1–5. 11*

Lee, X. 1998. On micrometeorological observations of surface-air exchange over tall vegetation. Agricultural and Forest Meteorology **91**, *39–49. 27*

Leuning, R., H. Cleugh, S. Zegelin, and D. Hughes. 2005. Carbon and water fluxes over a temperate forest and a tropical wet/dry savanna in Australia: measurements and comparison with MODIS remote sensing estimates. Agricultural and Forest Meteorology **129**, *151–173. 16, 37, 72*

Lieth, H., and R. H. Whittaker. 1975. Primary productivity of the biosphere. *Ecological studies ; 14. Springer. 12*

Loescher, H. W., B. E. Law, L. Mahrt, D. Y. Hollinger, J. Campbell, and S. C. Wofsy. 2006. Uncertainties in, and interpretation of, carbon flux estimates using the eddy covariance technique. Journal of Geophysical Research **111**, *1–19. 28*

Lohse, K. A., P. D. Brooks, J. C. McIntosh, T. Meixner, and T. E. Huxman. 2009. Interactions Between Biogeochemistry and Hydrologic Systems. Annual Review of Environment and Resources **34**, *65–96. 3*

Louis, J., M. Aurela, a. Ounis, J. Ducruet, S. Evain, T. Laurila, T. Thum, G. Wingsle, L. Alonso, and R. Pedros. 2005. Remote sensing of sunlight-induced chlorophyll fluorescence and reflectance of Scots pine in the boreal forest during spring recovery. Remote Sensing of Environment **96**, *37–48. 21, 58*

Luyssaert, S., M. Reichstein, E.-D. Schulze, I. A. Janssens, B. E. Law, D. Papale, D. Dragoni, M. L. Goulden, A. Granier, W. L. Kutsch, S. Linder, G. Matteucci, E. Moors, J. W. Munger, K. Pilegaard, M. Saunders, and E. M. Falge. 2009. Toward a consistency cross-check of eddy covariance flux ‚Äì based and biometric estimates of ecosystem carbon balance. Global Biogeochemical Cycles **23**, *1–13. 3, 6, 28*

Lyapustin, A., and Y. Wang. 2009. The Time Series Technique for Aerosol Retrievals Over Land from MODIS. *In: 3. Pp. 69–99. Springer, Berlin Heidelberg. 75*

Macatangay, R., T. Warneke, C. Gerbig, S. Körner, R. Ahmadov, M. Heimann, and

J. Notholt. 2008. A framework for comparing remotely sensed and in-situ CO 2 concentrations. Atmospheric Chemistry and Physics **8**, *2555–2568. 11*

Majdi, H., K. Pregitzer, A.-S. Morén, J.-E. Nylund, and G. I. Ågren. 2005. Measuring Fine Root Turnover in Forest Ecosystems. Plant and Soil **276**, *1–8. 7*

Mäkelä, A., M. Pulkkinen, P. Kolari, F. Lagergren, P. Berbigier, A. Lindroth, D. Loustau, E. Nikinmaa, T. Vesala, and P. Hari. 2008. Developing an empirical model of stand GPP with the LUE approach: analysis of eddy 2 covariance data at five contrasting conifer sites in Europe. Global Change Biology **14**, *92 – 108. 10, 13*

Martel, M.-C., H. A. Margolis, C. Coursolle, F. J. Bigras, F. A. Heinsch, and S. W. Running. 2005. Decreasing photosynthesis at different spatial scales during the late growing season on a boreal cutover.. Tree physiology **25**, *689–99. 37*

Maselli, F., D. Papale, N. Puletti, G. Chirici, and P. Corona. 2009. Combining remote sensing and ancillary data to monitor the gross productivity of water-limited forest ecosystems. Remote Sensing of Environment **113**, *657–667. 72*

Mauder, M., T. Foken, R. Clement, J. Elbers, W. Eugster, T. Grünwald, B. Heusinkveld, and O. Kolle. 2008. Quality control of CarboEurope flux data? Part II: Inter-comparison of eddy-covariance software. Biogeosciences **5**, *451–462. 29*

McCallum, I., W. Wagner, C. Schmullius, A. Shvidenko, M. Obersteiner, S. Fritz, and S. Nilsson. 2009. Satellite-based terrestrial production efficiency modeling.. Carbon balance and management **4**, *8. 13, 56*

McCallum, I., W. Wagner, C. Schmullius, A. Shvidenko, M. Obersteiner, S. Fritz, and S. Nilsson. 2010. Comparison of four global FAPAR datasets over Northern Eurasia for the year 2000. Remote Sensing of Environment **114**, *941–949. 56, 60, 70*

McMillen, R. T. 1988. An eddy correlation technique with extended applicability to non-simple terrain. Boundary-Layer Meteorology **43**, *231–245. 28*

Meehl, G., T. Stocker, W. Collins, P. Friedlingstein, A. Gaye, J. Gregory, A. Kitoh, R. Knutti, J. Murphy, A. Noda, S. Raper, I. Watterson, A. Weaver, and Z.-C. Zhao. 2007. Global Climate Projections*. Cambridge University Press, Cambridge, United Kingdom and New York, NY, USA. 7*

Meroni, M., C. Panigada, M. Rossini, V. Picchi, S. Cogliati, and R. Colombo. 2009a. Using optical remote sensing techniques to track the development of ozone-induced stress. Environmental Pollution **157**, *1413–1420. 20*

Meroni, M., M. Rossini, L. Guanter, L. Alonso, U. Rascher, R. Colombo, and J. Moreno. 2009b. Remote sensing of solar-induced chlorophyll fluorescence: Review of methods and applications. Remote Sensing of Environment **113**, *2037–2051. 17, 18, 57*

Meroni, M., M. Rossini, V. Picchi, C. Panigada, S. Cogliati, C. Nali, and R. Colombo. 2008. Assessing Steady-state Fluorescence and PRI from Hyperspectral Proxi-

mal Sensing as Early Indicators of Plant Stress: The Case of Ozone Exposure. Sensors **8**, *1740–1754. 18, 37*

Méthy, M. 2000. Analysis of photosynthetic activity at the leaf and canopy levels from reflectance measurements: a case study. Photosynthetica **38**, *505–512. 19, 20*

Middleton, E. M., Y.-B. Cheng, T. Hilker, T. A. Black, P. Krishnan, N. C. Coops, and K. F. Huemmrich. 2009. Linking foliage spectral responses to canopy-level ecosystern photosynthetic light-use efficiency at a Douglas-fir forest in Canada. Canadian Journal of Remote Sensing **35**, *166–188. 57, 58, 73*

MODIS Land Team 2009. MODIS C6 Reprocessing Proposed Changes to the Science Algorithms. 16

Moffat, A., E. G. Union, D. Papale, P. Ciais, W. Cramer, A. Richardson, R. Valentini, D. Hollinger, M. Reichstein, A. Barr, G. Churkina, C. Beckstein, A. Desai, and B. Braswell. 2007. Comprehensive comparison of gap-filling techniques for eddy covariance net carbon fluxes. Agricultural and Forest Meteorology **147**, *209–232. 28*

Monsi, M., and T. Saeki. 2005. On the factor light in plant communities and its importance for matter production. 1953.. Annals of botany **95**, *549–67. 9*

Monteith, J., and C. Moss. 1977. Climate and the Efficiency of Crop Production in Britain. Philosophical Transactions of the Royal Society of London. Series B, Biological Sciences **281**, *277–294. 9, 10, 36*

Monteith, J. L. 1972. Solar Radiation and Productivity in Tropical Ecosystems. Journal of Applied Ecology **9**, *747–766. 9, 10, 12, 36, 39, 56*

Morton, F. I. 1983. Operational estimates of areal evapotranspiration and their significance to the science and practice of hydrology. Journal of Hydrology **66**, *1–76. 13*

Mu, Q., F. A. Heinsch, M. Zhao, and S. W. Running. 2007a. Regional evaporation estimates from flux tower and MODIS satellite data. Remote Sensing of Environment **106**, *285–304. 13*

Mu, Q., M. Zhao, F. A. Heinsch, M. Liu, H. Tian, and S. W. Running. 2007b. Evaluating water stress controls on primary production in biogeochemical and remote sensing based models. Journal of Geophysical Research **112**, *1–13. 13*

Myneni, R. B., F. G. Hall, P. J. Sellers, and A. L. Marshak. 1995. The interpretation of spectral vegetation indexes. IEEE Transactions on Geoscience and Remote Sensing **33**, *0–5. 62*

Myneni, R. B., S. Hoffman, Y. Knyaszikhin, J. L. Privette, J. Glassy, Y. Tian, Y. Wang, X. Song, Y. Zhang, G. R. Smith, A. Lotsch, M. Friedl, J. T. Morisette, P. Votava, and R. R. Nemani. 2002. Global products of vegetation leaf area and fraction absorbed PAR from year one of MODIS data. Remote Sensing of Environment **83**, *214–213. 14, 15, 40*

Naumann, J. C., D. R. Young, and J. E. Anderson. 2008a. Leaf chlorophyll fluorescence, reflectance, and physiological response to freshwater and saltwater flooding in the evergreen shrub, Myrica cerifera. Environmental and Experimental Botany **63**, *402–409. 20, 37*

Naumann, J. C., J. E. Anderson, and D. R. Young. 2008b. Linking physiological responses, chlorophyll fluorescence and hyperspectral imagery to detect salinity stress using the physiological reflectance index in the coastal shrub, Myrica cerifera. Remote Sensing of Environment **112**, *3865–3875. 20*

Nemani, R. R., C. D. Keeling, H. Hashimoto, W. M. Jolly, S. C. Piper, C. J. Tucker, R. B. Myneni, and S. W. Running. 2003. Climate-Driven Increases in Global Terrestrial Net Primary Production from 1982 to 1999. Science **300**, *1560–1563. 5*

Nichol, C. J., J. Lloyd, O. Shibistova, A. Arneth, C. Roser, A. Knohl, S. Matsubara, and J. Grace. 2002. Remote sensing of photosynthetic-light-use efficiency of a Siberian boreal forest. Tellus B **54**, *677–687. 20, 22, 37, 57, 58*

Nichol, C. J., K. F. Huemmrich, T. A. Black, P. G. Jarvis, C. L. Walthall, J. Grace, and F. G. Hall. 2000. Remote sensing of photosynthetic-light-use efficiency of boreal forest. Agricultural and Forest Meteorology **101**, *131–142. 20, 22, 37, 57*

Nobel, P. S. 2005. Physicochemical and Environmental Plant Physiology*. 3 ed. Elsevier Academic Press, Amsterdam. 3*

Ollinger, S. V., A. D. Richardson, M. E. Martin, D. Y. Hollinger, S. E. Frolking, P. B. Reich, L. C. Plourde, G. G. Katul, J. W. Munger, R. Oren, P. V. Bolstad, B. D. Cook, M. C. Day, T. A. Martin, R. K. Monson, and H. P. Schmid. 2008. Canopy nitrogen, carbon assimilation, and albedo in temperate and boreal forests: Functional relations and potential climate feedbacks. PNAS*. 10*

Panigada, C., M. Rossini, M. Meroni, R. Marzuoli, G. Gerosa, and R. Colombo. 2009. Indicators of ozone effects on Fagus sylvatica L. by means of spectroradiometric measurements. Italian Journal of Remote Sensing **41**, *3–20. 20*

Papageorgiou, G. C., and Govindjee. (Eds.) 2005. Chlorophyll a Fluorescence : A Signature of Photosynthesis (Advances in Photosynthesis and Respiration)*. Springer. 17*

Papale, D., and R. Valentini. 2003. A new assessment of European forests carbon exchanges by eddy fluxes and artificial neural network spatialization. Global Change Biology **9**, *525–535. 12*

Papale, D., M. Reichstein, M. Aubinet, E. Canfora, C. Bernhofer, W. L. Kutsch, B. Longdoz, S. Rambal, R. Valentini, T. Vesala, and D. Yakir. 2006. Towards a standardized processing of Net Ecosystem Exchange measured with eddy covariance technique: algorithms and uncertainty estimation. Biogeosciences **3**, *571–583. 8, 29, 38, 60*

Peñuelas, J., and Y. Inoue. 2000. Reflectance assessment of canopy CO2 uptake. International Journal of Remote Sensing **21**, *3353–3356. 20*

Peñuelas, J., I. Filella, and J. A. Gamon. 1995. Assessment of Photosynthetic Radiation-Use Efficiency with Spectral Reflectance. New Phytologist **131**, *291–296. 18, 19, 21, 37, 57*

Peguero-Pina, J. J., F. Morales, J. Flexas, E. Gil-Pelegrín, and I. Moya. 2008. Photochemistry, remotely sensed physiological reflectance index and de-epoxidation state of the xanthophyll cycle in Quercus coccifera under intense drought.. Oecologia **156**, *1–11. 20*

Plummer, S. 2006. On validation of the MODIS gross primary production product. IEEE Transactions on Geoscience and Remote Sensing **44**, *1936–1938. 15, 16*

Polley, H. W., R. L. Phillips, A. B. Frank, J. A. Bradford, P. L. Sims, J. A. Morgan, and J. R. Kiniry. 2010. Variability in Light-Use Efficiency for Gross Primary Productivity on Great Plains Grasslands. Ecosystems. *10*

Poorter, H., C. Remkes, and H. Lambers. 1990. Carbon and Nitrogen Economy of 24 Wild Species Differing in Relative Growth Rate. Plant Physiology **94**, *621–627. 11*

Potter, C. S., S. A. Klooster, and V. Brooks. 1999. Interannual Variability in Terrestrial Net Primary Production: Exploration of Trends and Controls on Regional to Global Scales. Ecosystems **2**, *36–48. 13*

Quézel, P., and F. Médail. 2003. Ecologie et Biogéographie des Forêts du Bassin Méditerranéen. *Elsevier, Paris. 38*

Rahman, A. F., J. A. Gamon, D. A. Fuentes, D. A. Roberts, and D. Prentis. 2001. Modeling spatially distributed ecosystem flux of boreal forest using hyperspectral indices from AVIRIS imagery. Journal of Geophysical Research **106**, *33579–33591. 20, 57*

Rahman, A. F., V. D. Cordova, J. A. Gamon, H. P. Schmid, and D. A. Sims. 2004. Potential of MODIS ocean bands for estimating CO2 flux from terrestrial vegetation: A novel approach. Geophysical Research Letters. *22, 42, 57*

Rambal, S. 1993. The differential role of mechanisms for drought resistance in a Mediterranean evergreen shrub: a simulation approach. Plant, Cell and Environment **16**, *35–44. 38*

Rambal, S., J.-M. Ourcival, R. Joffre, F. Mouillot, Y. Nouvellon, M. Reichstein, and A. Rocheteau. 2003. Drought controls over conductance and assimilation of a Mediterranean evergreen ecosystem: scaling from leaf to canopy. Global Change Biology **9**, *1813–1824. 72*

Rascher, U., and R. Pieruschka. 2008. Spatio-temporal variations of photosynthesis: the potential of optical remote sensing to better understand and scale light use efficiency and stresses of plant ecosystems. Precision Agriculture **9**, *355–366. 17*

Rebmann, C., M. Göckede, T. Foken, M. Aubinet, M. Aurela, P. Berbigier, C. Bernhofer, N. Buchmann, A. Cescatti, R. Ceulemans, R. Clement, J. A. Elbers, A. Granier, T. Grünwald, D. Guyon, Havráankováa, B. Heinesch, A. Knohl, T. Laurila, B. Longdoz, B. Marcolla, T. Markkanen, F. Miglietta, J. B. Moncrieff, L. Montagnani, E. Moors, M. Nardino, J.-M. Ourcival, S. Rambal, U. Rannik, E. Rotenberg, P. Sedlak, G. Unterhuber, T. Vesala, and D. Yakir. 2005. Quality analysis applied on eddy covariance measurements at complex forest sites using footprint modelling. Theoretical and Applied Climatology **80**, *121–141. 22*

Reichstein, M., D. Papale, R. Valentini, M. Aubinet, C. Bernhofer, A. Knohl, T. Laurila, A. Lindroth, E. Moors, K. Pilegaard, and G. Seufert. 2007. Determinants of terrestrial ecosystem carbon balance inferred from European eddy covariance flux sites. Geophysical Research Letters **34**, *1–5. 11*

Reichstein, M., E. Falge, D. D. Baldocchi, D. Papale, M. Aubinet, P. Berbigier, C. Bernhofer, N. Buchmann, T. Gilmanov, A. Granier, T. Grünwald, K. Havránková, H. Ilvesniemi, D. Janous, A. Knohl, T. Laurila, A. Lohila, D. Loustau, G. Matteucci, T. Meyers, F. Miglietta, J.-M. Ourcival, J. Pumpanen, S. Rambal, E. Rotenberg, M. J. Sanz, J. D. Tenhunen, G. Seufert, F. Vaccari, T. Vesala, D. Yakir, and R. Valentini. 2005. On the separation of net ecosystem exchange into assimilation and ecosystem respiration: review and improved algorithm. Global Change Biology **11**, *1424–1439. 28, 29, 38, 60*

Reichstein, M., R. Valentini, S. W. Running, and J. Tenhunen. 2004. Improving remote-sensing based GPP estimates (MODIS-MOD17I through inverse parameter estimation with carboeurope eddy covariance flux data. Geophysical Research Abstracts, EGU General Assembly 2004. *Vol. 6. Nice. 16*

Reynolds, O. 1985. On the Dynamical Theory of Incompressible Viscous Fluids and the Determination of the Criterion. Philosophical Transactions of the Royal Society of London A **186**, *123–164. 8*

Rienecker, M., M. Suarez, R. Todling, J. Bacmeister, L. Takacs, H.-C. Liu, W. Gu, M. Sienkiewicz, R. Koster, R. Gelaro, I. Stajner, and J. Nielsen. 2008. The GEOS-5 Data Assimilation System ‚Äî Documentation of Versions 5.0.1, 5.1.0, and 5.2.0. Technical Report Series on Global Modeling and Data Assimilation **27**, *101. 16*

Ritts, W. D., D. P. Turner, A. L. Dunn, S. W. Running, S. Kurc, S. Wofsy, and E. Small. 2006. Assessing interannual variation in MODIS-based estimates of gross primary production. IEEE Transactions on Geoscience and Remote Sensing **44**, *1899–1907. 16*

Robinson, S. A. 2001. Plant Light Stress. Encyclopedia of Life Sciences *Pp. 1–5. 4, 5, 17*

Rödenbeck, C., S. Houweling, M. Gloor, and M. Heimann. 2003. CO2 flux history 1982‚Äì2001 inferred from atmospheric data using a global inversion of atmospheric transport. Atmospheric Chemistry and Physics **3**, *1919–1964. 11*

Roy, J., and B. Saugier. 2001. Terrestrial Primary Productivity: Definitions and Milestones. *In: 1. Pp. 1–8. Academic Press, San Diego. 11*

Ruimy, A., and B. Saugier. 1994. Methodology for the estimation of terrestrial net primary production from remotely sensed data. Journal of Ge **99**, *5263–5283. 10, 36*

Ruimy, A., L. Kergoat, A. Bondeau, and The Participants Of The Potsdam NPP Model Intercomparison. 1999. Comparing global models of terrestrial net primary productivity (NPP): analysis of differences in light absorption and light-use efficiency. Global Change Biology **5**, *56–64. 12*

Ruiz-Barradas, A., and S. Nigam. 2005. Warm Season Rainfall Variability over the U.S. Great Plains in Observations, NCEP and ERA-40 Reanalyses, and NCAR and NASA Atmospheric Model Simulations. Journal of Climate **18**, *1808–1830. 16*

Running, S. W. 1999. A Global Terrestrial Monitoring Network Integrating Tower Fluxes, Flask Sampling, Ecosystem Modeling and EOS Satellite Data. Remote Sensing of Environment **70**, *108–127. 9*

Running, S. W., and R. R. Nemani. 1988. Relating seasonal patterns of the AVHRR vegetation index to simulated photosynthesis and transpiration of forests in different climates. Remote Sensing of Environment **24**, *347–367. 13, 20, 24, 51, 73*

Running, S. W., P. E. Thornton, R. R. Nemani, and J. M. Glassy. 2000. Global terrestrial gross and net primary productivity from the Earth Observing System. *Pp. 44–57. Springer, New York. 12, 14, 56, 57*

Running, S. W., R. R. Nemani, F. A. Heinsch, M. Zhao, M. Reeves, and H. Hashimoto. 2004. A continuous satellite-derived measure of global terrestrial primary productivity. BioScience **54**, *547–560. 13*

Runyon, J., R. H. Waring, S. N. Goward, and J. M. Welles. 1994. Environmental Limits on Net Primary Production and Light-Use Efficiency Across the Oregon Transect. Ecological Applications **4**, *226–237. 36*

Schmid, H. P. 1994. Source areas for scalars and scalar fluxes. Boundary-Layer Meteorology **67**, *293–318. 7*

Schmid, H. P., S. B. Grimmond, F. Cropley, B. Offerle, and H.-B. Su. 2000. Measurements of CO2 and energy fluxes over a mixed hardwood forest in the mid-western United States. Agricultural and Forest Meteorology **103**, *357–374. 59*

Scholes, R. J., N. Gureja, M. Giannecchinni, D. Dovie, B. Wilson, N. Davidson, K. Piggott, C. McLoughlin, K. Van Der Velde, A. Freeman, S. Bradlay, R. Smart, and S. Ndala. 2001. The environment and vegetation of the flux measurement site near Skukuza, Kruger National Park. Koedoe **44**, *73–83. 59*

Schulze, E.-D. 2006. Biological control of the terrestrial carbon sink. Biogeosciences **3**, *147–166. 56*

Schulze, E.-D., E. Beck, and K. Müller-Hohenstein. 2005. Plant Ecology*. Vol. 12. Springer, Berlin - Heidelberg. 2, 3*

Schwalm, C. R., L. B. Flanagan, H. A. Margolis, T. A. Black, B. D. Amiro, M. A. Arain, A. G. Barr, A. L. Dunn, P. M. Lafleur, J. H. Mccaughey, A. L. Orchansky, and S. C. Wofsy. 2006. Photosynthetic light use efficiency of three biomes across an east,Äìwest continental-scale transect in Canada. Agricultural and Forest Meteorology **140***, 269–286. 9, 37*

Siciliano, D., K. Wasson, D. C. Potts, and R. Olsen. 2008. Evaluating hyperspectral imaging of wetland vegetation as a tool for detecting estuarine nutrient enrichment. Remote Sensing of Environment **112***, 4020–4033. 20*

Sims, D. A., A. F. Rahman, V. D. Cordova, D. D. Baldocchi, L. B. Flanagan, A. H. Goldstein, D. Y. Hollinger, L. Misson, R. K. Monson, H. P. Schmid, S. C. Wofsy, and L. Xu. 2005. Midday values of gross CO flux and light use efficiency during satellite overpasses can be used to directly estimate eight-day mean flux. Agricultural and Forest Meteorology **131***, 1–12. 10, 50, 53*

Sims, D. A., and J. A. Gamon. 2002. Relationships between leaf pigment content and spectral reflectance across a wide range of species, leaf structures and developmental stages. Remote Sensing of Environment **81***, 337–354. 21, 37, 52, 58*

Sims, D. A., H. Luo, S. Hastings, S. Hastings, W. A. C. Oechel, A. F. Rahman, and J. A. Gamon. 2006. Parallel adjustments in vegetation greenness and ecosystem CO2 exchange in response to drought in a Southern California chaparral ecosystem. Remote Sensing of. Remote Sensing of Environment **103***, 289–303. 38, 50, 52, 53*

Sinclair, T. R., and R. C. Muchow. 1999. Radiation use efficiency. Advances in Agronomy*. 10*

Solomon, S., D. Qin, M. Manning, R. B. Alley, T. Berntsen, N. L. Bindoff, Z. Chen, A. Chidthaisong, G. C. Hegerl, J. M. Gregory, M. Heimann, G. C. Hegerl, M. Heimann, B. Hewitson, B. J. Hoskins, F. Joos, J. Jouzel, V. Kattsov, U. Lohmann, T. Matsuno, M. Molina, N. Nicholls, J. Overpeck, G. Raga, V. Ramaswamy, J. Ren, M. Rusticucci, R. Somerville, T. F. Stocker, P. Whetton, and R. A. Wood. 2007. Technical Summary*. Cambridge University Press, Cambridge, United Kingdom and New York, NY, USA. 1*

Solomon, S., G.-K. Plattner, R. Knutti, and P. Friedlingstein. 2009. Irreversible climate change due to carbon dioxide emissions.. Proceedings of the National Academy of Sciences of the United States of America **106***, 1704–9. 6, 7*

Song, C., C. E. Woodcock, K. C. Seto, M. P. Lenney, and S. A. Macomber. 2001. Classification and Change Detection Using Landsat TM Data When and How to Correct Atmospheric Effects?. Remote Sensing of Environment **75***, 230–244. 42*

Still, C. J., J. T. Randerson, and I. Y. Fung. 2004. Large-scale plant light-use

efficiency inferred from the seasonal cycle of atmospheric CO2. Global Change Biology **10**, *1240–1252. 10*

Stylinski, C. D., J. A. Gamon, and W. C. Oechel. 2002. Seasonal patterns of reflectance indices, carotenoid pigments and photosynthesis of evergreen chaparral species. Oecologia **131**, *366–374. 19, 21, 37, 52, 57*

Suárez, L., P. J. Zarco-Tejada, G. Sepulcre-Cantó, O. Pérez-Priego, J. C. Jiménez-Muñoz, J. R. Miller, and J. Sobrino. 2008. Assessing canopy PRI for water stress detection with diurnal airborne imagery. Remote Sensing of Environment **112**, *560–575. 20, 21, 37, 58*

Suárez, L., P. J. Zarco-Tejada, V. González-Dugo, J. Berni, R. Sagardoy, F. Morales, and E. Fereres. 2010. Detecting water stress effects on fruit quality in orchards with time-series PRI airborne imagery. Remote Sensing of Environment **114**, *286–298. 20*

Sun, J., S. Burns, a. Delany, S. Oncley, a. Turnipseed, B. Stephens, D. Lenschow, M. Lemone, R. Monson, and D. Anderson. 2007. CO2 transport over complex terrain. Agricultural and Forest Meteorology **145**, *1–21. 28*

Sun, P., a. Grignetti, S. Liu, R. Casacchia, R. Salvatori, F. Pietrini, F. Loreto, and M. Centritto. 2008. Associated changes in physiological parameters and spectral reflectance indices in olive (Olea europaea L.) leaves in response to different levels of water stress. International Journal of Remote Sensing **29**, *1725–1743. 20*

Tambussi, E. A., J. Casadesus, S. Munné-Bosch, and J. L. Araus. 2002. Photoprotection in water-stressed plants of durum wheat (Triticum turgidum var. durum): changes in chlorophyll fluorescence, spectral signature and photosynthetic pigments. Functional Plant Biology **29**, *35–44. 20*

Telfer, A. 2005. Too much light? How b-carotene protects the photosystem II reaction centre. Photochemical & Photobiological Sciences **4**, *950–956. 21*

Terradas, J. 1999. Holm oak and holm oak forests: An introduction. *Pp. 3–14. Vol. 137. Springer, Berlin. 38*

Thenot, F., M. Méthy, and T. Winkel. 2002. The Photochemical Reflectance Index (PRI) as a water-stress index. International Journal of Remote Sensing **23**, *5135–5139. 20*

Thomas, V., J. McCaughey, P. Treitz, D. Finch, T. Noland, and L. Rich. 2009. Spatial modelling of photosynthesis for a boreal mixedwood forest by integrating micrometeorological, lidar and hyperspectral remote sensing data. Agricultural and Forest Meteorology **149**, *639–654. 59*

Tirone, G., S. Dore, G. Matteucci, S. Greco, and R. Valentini. 2003. Evergreen Mediterranean Forests. Carbon and Water Fluxes, Balances, Ecological and Ecophysiological Determinants. *In: 7. Springer, Heidelberg. 59*

Toller, G. N., A. Isaacman, and J. Kuyper. 2005. MODIS Level 1B Product User's Guide - For Level 1B Version 5.06 (Terra) and Version 5.07 (Aqua). 31

Treitz, P. M., and P. J. Howarth. 1999. Hyperspectral remote sensing for estimating biophysical parameters of forest ecosystems. Progress in Physical Geography **23**, *359–390.* 62

Trotter, G. M., D. Whitehead, and E. J. Pinkney. 2002. The photochemical reflectance index as a measure of photosynthetic light use efficiency for plants with varying foliar nitrogen contents. International Journal of Remote Sensing **23**, *1207–1212.* 19

Trumbore, S. E., and J. B. Gaudinski. 2003. The Secret Lives of Roots. Science **302**, *1344–1345.* 7

Tucker, C. J. 1979. Red and photographic infrared linear combinations for monitoring vegetation. Remote Sensing of Environment **8**, *127–150.* 43, 63

Turner, D. P. 2002. Effects of spatial variability in light use efficiency on satellite-based NPP monitoring. Remote Sensing of Environment **80**, *397–405.* 37

Turner, D. P. 2003. Scaling Gross Primary Production (GPP) over boreal and deciduous forest landscapes in support of MODIS GPP product validation. Remote Sensing of Environment **88**, *256–270.* 10, 16

Turner, D. P., W. D. Ritts, W. B. Cohen, T. K. Maeirsperger, S. T. Gower, A. A. Kirschbaum, S. W. Running, M. Zhao, S. C. Wofsy, A. L. Dunn, B. E. Law, J. L. Campbell, W. C. Oechel, H. J. Kwon, T. P. Meyers, E. E. Small, S. A. Kurc, and J. A. Gamon. 2005. Site-level evaluation of satellite-based global terrestrial gross primary production and net primary production monitoring. Global Change Biology **11**, *666–684.* 10, 16, 37

Turner, D. P., W. Ritts, W. B. Cohen, S. T. Gower, S. W. Running, M. Zhao, M. H. Costa, A. A. Kirschbaum, J. M. Ham, S. R. Saleska, and D. E. Ahl. 2006. Evaluation of MODIS NPP and GPP products across multiple biomes. Remote Sensing of Environment **102**, *282–292.* 37

Valentini, R., G. E. Scarascia Mugnozza, and J. R. Ehleringer. 1992. Hydrogen and Carbon Isotope Ratios of Selected Species of a Mediterranean Macchia Ecosystem. Functional Ecology **6**, *627–631.* 73

Valentini, R., J. G. Canadell, S. T. Gower, D. D. Baldocchi, D. Y. Hollinger, S. W. Running, H. A. Mooney, J. a. Berry, J. R. Ehleringer, C. B. Field, J. E. Hunt, R. B. Jackson, G. R. Shaver, W. Steffen, S. E. Trumbore, and B. Y. Bond. 2000. Commentary: Carbon Metabolism of the Terrestrial Biosphere: A Multitechnique Approach for Improved Understanding. Ecosystems **3**, *115–130.* 9

van der Werf, G. R., J. T. Randerson, L. Giglio, N. Gobron, and a. J. Dolman. 2008. Climate controls on the variability of fires in the tropics and subtropics. Global Biogeochemical Cycles **22**, *1–13.* 5

Vermote, E. F., C. Justice, and F. Breon. 2009. Towards a generalized approach for correction of the BRDF effect in MODIS directional reflectances. IEEE Transactions on Geoscience and Remote Sensing **47**, *898–908. 32*

Vermote, E. F., D. Tanre, J. L. Deuzé, M. Herman, and J.-J. Morcrette. 1997. Second simulation of the satellite signal in the solar spectrum, 6S: An overview. IEEE Transactions on Geoscience and Remote Sensing **35**, *675–686. 41, 75*

Weng, J.-H., T.-S. Liao, M.-Y. Hwang, C.-C. Chung, C.-P. Lin, and C.-H. Chu. 2006. Seasonal variation in photosystem II efficiency and photochemical reflectance index of evergreen trees and perennial grasses growing at low and high elevations in subtropical Taiwan.. Tree Physiology **26**, *1097–1104. 37*

Westerling, A. L., H. G. Hidalgo, D. R. Cayan, and T. W. Swetnam. 2006. Warming and earlier spring increase western U.S. forest wildfire activity.. Science **313**, *940–3. 5*

Wofsy, S. C., M. L. Goulden, J. W. Munger, S.-M. Fan, P. S. Bakwin, B. C. Daube, L. Bassow, and F. A. Bazzaz. 1993. Net exchange of CO2 in a mid-latitude forest. Science **260**, *1314–1317. 9*

Wolfe, R. E., D. P. Roy, and E. F. Vermote. 1998. MODIS land data storage, gridding, and compositing methodology: Level 2 grid. IEEE Transactions on Geoscience and Remote Sensing **36**, *1324–1338. 22, 31*

Woodward, F. I., T. M. Smith, and W. R. Emanuel. 1995. A global land primary productivity and phytogeography model. Global Biogeochemical Cycles **9**, *471. 10*

Xiao, X., Q. Zhang, D. Hollinger, J. Aber, and B. Moore. 2005. Modeling Gross Primary Production of an Evergreen Needleleaf Forest Using Modis and Climate Data. Ecological Applications **15**, *954–969. 72*

Xie, X., Z. Gao, and W. Gao. 2009. Estimating photosynthetic light-use efficiency of Changbai Mountain by using MODIS-derived photochemical reflectance index. Proceedings of SPIE **7454**, *745415–745415–7. 22, 57*

Yi, C., D. E. Anderson, A. A. Turnipseed, S. P. Burns, J. P. Sparks, D. I. Stannard, and R. K. Monson. 2008. The contribution of advective fluxes to net ecosystem exchange in a high-elevation subalpine forest. Ecological Applications **18**, *1379–1390. 28*

Yuan, W., D. D. Baldocchi, S. Liu, C. Bernhofer, G. Zhou, L. Tieszen, H. Gholz, a. Goldstein, and M. Goulden. 2007. Deriving a light use efficiency model from eddy covariance flux data for predicting daily gross primary production across biomes. Agricultural and Forest Meteorology **143**, *189–207. 13, 37, 56, 57*

Zhao, M., and S. W. Running. 2010. Drought-Induced Reduction in Global Terrestrial Net Primary Production from 2000 Through 2009. Science **329**, *940–943. 5*

Zhao, M., S. W. Running, F. A. Heinsch, and R. R. Nemani. 2005. Improvements of the MODIS terrestrial gross and net primary production global data set. Remote Sensing of Environment **95**, *164–176. 14, 15*

Zusammenfassung

Die Erforschung des globalen Kohlenstoffkreislaufs ist Teil der Bestrebungen, das Erdsystem einschließlich der Wechselwirkungen zwischen seinen Komponenten Atmosphäre, Biosphäre, Hydrosphäre und Geosphäre zu verstehen. Aufgrund der deutlichen Beinflussung des Kohlenstoffkreislaufes - und indirekt anderer Stoff- und Energieflüsse - durch menschliche Aktivitäten ist das Interesse an diesem Wissenschaftsfeld nicht nur akademischer Natur.

Gesicherte Erkenntnisse über die Funktionsweise des globalen Kohlenstoffkreislaufes können nur durch die geschickte und möglichst vielseitige Kombinationen von Erdsystemmodellen mit Messungen erzielt werden. Ein wichtiger Teilbereich sind hierbei Modelle der Primärproduktivität, also der Assimilierung von Kohlenstoff durch die Vegetation, denn dies ist die wichtigste Senke von CO_2 abgesehen von (auf anderen Zeitskalen relevanten) geologischen Vorgängen.

Ein guter Teil der diagnostischen Modelle, welche die aktuelle Produktivität der Vegetation quantifizieren, basieren auf dem Konzept der Lichtausnutzungseffizienz (*light use efficiency*, LUE): die von den Pflanzen absorbierte Lichtenergie wird mit einem bestimmten Wirkungsgrad in chemische Energie umgewandelt. Die Lichtausnutzungseffizienz hängt vom Vegetationstyp, biotischen und abiotischen Standortbedingungen ab. In globalen Modellen wird LUE häufig abstrahiert, indem eine (eventuell biom-spezifische) maximale Lichtausnutzungseffizienz festgelegt wird, aus der die tatsächliche LUE als Funktion leicht zu quantifizierender Umweltfaktoren ermittelt wird. Im Fall des operativ betriebenen MOD17-Models der Nettoprimärproduktion sind die limitierenden Faktoren die Tagesminimumtemperatur und das Sättigungsdefizit von Wasserdampf in der Atmosphäre. Schwächen dieses Models sind strukturelle Defizite, z.B. die ungenügende Berücksichtigung des Bodenwassergehaltes, und durch die Verwendung globaler meteorologischer Datensätze bedingte Ungenauigkeiten. Diese Schwierigkeiten machen sich besonders für immergrüne Vegetation unter Trockenstress bemerkbar, wenn die photosynthetische Aktivität trotz relativ konstanter Lichtabsorbtion stark sinkt.

Der Photochemische Reflexionsindex (*photochemical reflectance index*, PRI) hat sich in zahlreichen Studien an einzelnen Blättern bis hin zur Ökosystemebene als Schätzer der Lichtausnutzungseffizient bewährt und ist daher auch für globale Produktivitätsmodelle als Alternative zur Berechnung der photosynthetischen Effizienz aus meteorologischen Daten und einem fixen Maximalwert interessant. Der spektrale Index nutzt aus, dass eine Verringerung der photosynthetischen Effizienz mit einem veränderten Reflexionsverhalten im Bereich um 531 nm einher geht. Dieses Signal wird durch die in einem von diesen Mechanismen nicht beeinflussten Spektralbereich gemessene Reflexion normalisiert. Bisher wurde noch kein Model veröffentlicht, das aus satellitengestützen PRI-Messungen Lichtausnutzungseffizenz allgemeingültig für mehrere funktionelle Pflanzentypen und Klimazonen berechnet.

In dieser Arbeit wurde an mehreren Standorten mit zeitweiligem Trockenstress untersucht, welches PRI-Referenzband und welcher Aufnahmewinkel sich am besten für die Ableitung der Lichtausnutzungseffizienz auf Ökosystemebene eignet. Die Anwendbarkeit einer Vielzahl von denkbaren Produktivitätsmodelen auf der Grundlage von MODIS-PRI wurde für verschiedenartige funktionelle Pflanzentypen mit unterschiedlichen Vegetationsdichten geprüft. Eine Kernfrage der Arbeit ist, ob trotz bekannter Einschränkungen wie zum Beispiel der Abhängigkeit des PRI von der Aufnahmegeometrie, mit vorhandenen Mitteln ein unter unterschiedlichen Bedingungen universell anwendbares PRI-basiertes Model der Lichtausnutzungseffizienz entwickelt werden kann. Diese von PRI abgeleitete LUE wurde mit der Lichtausnutzungseffizienz aus dem konventionellen MOD17-Modell und der LUE aus einem mit lokalen Meteorologischen Daten optimierten MOD17-Modell verglichen.

Es wurde außerdem betrachtet, welchen Einfluss die Wahl verschiedener fernerkundlicher faPAR-Produkte auf die als Referenz verwendete in-situ Lichtausnutzungseffizienz hat. faPAR (d.h. der relative Anteil absorbierter photosynthetisch aktiver Strahlung) ist zur Berechnung der insgesamt von der Vegetation absorbierten Energie unabdingbar und beeinflusst daher die gesamte Evaluierung.

Ein Ergebnis der vorliegenden Arbeit ist, dass ein für einzelne Standorte kalibriertes PRI-gestütztes Produktivitätsmodell genauer ist als das mit lokal gemessenen meteorologischen Daten betriebene MOD17-Modell. Es konnte jedoch kein PRI-LUE-Modell gefunden werden, dass für mehrere Standorte Gültigkeit hat. Neben den Modelparametern unterscheiden sich auch die jeweils best-geeigneten Referenzbänder zwischen verschiedenen Standorten. Somit kann der lokal erzielte Genauigkeitsgewinn nicht für größere und damit heterogeneres Gebiete genutzt werden.

Diese Arbeit stellt durch den methodischen Vergleich zahlreicher Einflussfaktoren einen wertvollen Beitrag zur fernerkundlichen Messung der Lichtausnutzungseffizienz und damit zur Verbesserung von globalen Modellen der Ökosystemproduktivität dar.

Selbständigkeitserklärung

Ich erkläre, dass ich die vorliegende Arbeit selbständig und unter Verwendung der angegebenen Hilfsmittel, persönlichen Mitteilungen und Quellen angefertigt habe.

.....	.....	.....
Ort	Datum	Unterschrift der Verfasserin